NUMERICAL AND EXPERIMENTAL STUDY OF TAPERED LAMINATES WITH PLY DROPS

116 213

A THESIS SUBMITTED TO
THE GRADUTE SCHOOL OF NATURAL AND APPLIED SCIENCES
OF
THE MIDDLE EAST TECHNICAL UNIVERSITY

BY

ULAÇ MURAT ÜNLÜ

IN PARTIAL FULFILLMENT OF THE REQUIREMENTS FOR THE DEGREE OF
MASTER OF SCIENCE
IN
THE DEPARTMENT OF AERONAUTICAL ENGINEERING

116213

SEPTEMBER 2001

T.C. YÜKSEKÖĞRETİM KURULU
DOKÜMANTASYON MERKEZİ

Approval of the Graduate School of Natural and Applied Sciences

Prof. Dr. Tayfur ÖZTÜRK
Director

I certify that this thesis satisfies all the requirements as a thesis for the degree of Master of Science.

Prof. Dr. Nafiz ALEMDAROĞLU
Chairman of Department

This is to certify that we have read this thesis and that in our opinion it is fully adequate in scope and quality, as a thesis for the degree of Master of Science.

Prof. Dr. Mehmet A. AKGÜN
Supervisor

Examining Committee Members:

Prof. Dr. Nuri AKKAŞ

Prof. Dr. Süha ORAL

Prof. Dr. Yalçın MENGİ

Prof. Dr. Mehmet A. AKGÜN

Assoc. Prof. Dr. İsmail H. TUNCER

ABSTRACT

NUMERICAL AND EXPERIMENTAL STUDY OF TAPERED LAMINATES WITH PLY DROPS

Ünlü, Ulaç Murat

M.S. Department of Aeronautical Engineering

Supervisor: Prof. Dr. Mehmet A. AKGÜN

September 2001, 164 pages

In this study, the effects of ply-drops on the stress state of tapered fiber-reinforced composite laminates in tension were investigated. Preliminary studies were conducted to determine a suitable element aspect ratio for the finite element model and to investigate the effect of interply resin layers. A three-dimensional finite element model was constructed with interply resin layers surrounding the ply-drops. Equivalent von Mises stress in the interply resin layer was used to predict the location of delamination onset. Two failure criteria were used to predict delamination onset load. The average stress concept was applied to interlaminar stresses and used with a delamination failure criterion, which was a modification of Tsai-Wu failure criterion. Maximum stress criterion was additionally used as the second failure criterion. Seven different layups for tapered laminates were analyzed with finite element method and five different layups were analyzed experimentally. Flat laminates

representing the thin section of the tapered laminates were also manufactured and tested to serve as a reference.

Experimental observations and the finite element analysis results indicate that interlaminar shear stress in the upper interply resin layer is the dominant stress state and mainly responsible for delamination onset. The delamination was found to initiate at the end of the last ply drop. Delamination onset stress was altered by changing the orientation of plies. Longitudinal stiffness of dropped plies has an important role on the delamination onset stress. Considerable difficulty was encountered in establishing the delamination onset stresses experimentally. The consistency of the finite element analysis results with the experimental delamination onset values depended on specimen configuration and varied between -1.33% and 11.5%.

Keywords: Composite, Taper, Ply-Drop, Interlaminar Stresses, Delamination, Finite Element Analysis (FEA), Experimental Study.

ÖZ

KAT DÜŞÜMLÜ DEĞİŞKEN KESİTLİ KOMPOZİT LAMİNATLARIN NÜMERİK VE DENEYSEL ÇALIŞMASI

Ünlü, Ulaç Murat
Yüksek Lisans, Havacılık Mühendisliği Bölümü
Tez Yöneticisi: Prof. Dr. Mehmet A. AKGÜN

Eylül 2001, 164 sayfa

Bu çalışmada, kat düşümlerinin değişken kesitli elyaf takviyeli kompozit laminatlar üzerindeki gerilim durumuna etkisi araştırılmıştır. Sonlu eleman modeli için uygun eleman en/boy oranı belirlenmesi ve katlar arası reçine katmanlarının etkisinin incelenmesi için ön çalışmalar yaplmıştır. Kat düşümlerini çevreleyen reçine katmanları dahil edilerek üç boyutlu bir sonlu eleman modeli yapılmıştır. Katmanlar arası ayrışma yeri eşdeğer von Mises gerilimi kullanılarak bulunmuştur. Katmanlar arası ayrışma yükünü bulmak için iki işgörmezlik kıstası kullanılmıştır. Ortalama gerilim kavramı tabakalar arası gerilimlere uygulanmış ve Tsai-Wu işgörmezlik kıstasının bir modifikasyonu olan ayrışma kıstasında kullanılmıştır. Ek olarak, maksimum gerilme kıstası ikinci işgörmezlik kıstası olarak kullanılmıştır. Yedi farklı kat dizilimli değişken kesitli laminat, sonlu eleman metodu ile analiz edilmiş ve beş farklı kat dizilimli değişken kesitli laminat üretilip test edilmiştir. Değişken kesitli laminatların ince kısımlarını temsil eden düz laminatlar referans oluşturmak amacıyla üretilip test edilmiştir.

Deneysel gözlemler ve sonlu eleman analiz sonuçları, üst reçine katmanındaki katlar arası kesme gerilmesinin, baskın gerilme olduğunu göstermiştir. Ayrışma başlangıcı, son kat düşümünün bitiminde bulunmuştur. Ayrışma başlangıç gerilmesi katların farklı açısal dizilimiyle değiştirilmiştir. Kat düşümlerinin, boylamasına elastikiyetlerinin ayrışma başlangıç gerilmeleri üzerinde önemli bir etkisi olduğu görülmüştür. Deneysel olarak ayrışma gerilmesi bulunmasında önemli zorluklarla karşılaşılmıştır. Sonlu eleman anlizinin sonuçlarının deneysel sonuçlarla tutarlılığı, konfigurasyona bağlı olarak, -1.33% ve 11.5% arasında değişkenlik göstermiştir.

Anahtar Kelimeler: Kompozit, Değişken Kesit, Kat Düşümü, Katlar Arası Gerilim, Ayrışma, Sonlu Eleman Analizi, Deneysel Çalışma.

To My Family

ACKNOWLEDGMENTS

I would like to express my sincere thanks to Prof. Dr. Mehmet A. AKGÜN for his constant guidance, supervision and motivation.

Many thanks to my friends, Gökçe, Faruk, Semih and Cengiz, in Roketsan, Engineering Development Department for their support and encouragement.

I express sincere appreciation to my sweet rabbit, for her endless patience and moral supports and sincere thanks to my mother, for her sacrifices throughout my career.

TABLE OF CONTENTS

CHAPTER 1

INTRODUCTION

1.1 Composite Materials

The phrase "composite material" refers to a material that is formed by combining two or more materials on a macroscopic scale. Structures made of such materials are called composite structures [49]. Composite materials are fabricated to have better engineering properties than the conventional materials. Some of the properties that can be improved by forming a composite material are stiffness, strength, weight, corrosion resistance, thermal properties, fatigue life and wear resistance. Most man-made composite materials are made from two materials: a reinforcement material supported by a binder (matrix) material. Thus, composites typically have a discontinuous fiber or particle phase that is stiffer and stronger than the continuous matrix phase [48].

Composites can be divided into classes in various manners. One simple classification scheme is to separate them according to reinforcement forms as particulate reinforced composites, which are composed of particles in a matrix, fibrous reinforced composites, which consist of fibers in matrix, and laminated composites, which consists of layers of various materials.

Composite materials have a long history of usage. Their beginnings are unknown, but all recorded history contains references to some form of

composite materials. For example, straw was used by the Israelites to strengthen mud bricks. More recently composite materials are finding applications in a variety of systems including aircraft and submarine structures, space structures, automobiles, sports equipment, medical prosthetic devices and electronic circuit boards. They are most suitable in applications that require high strength-to-weight and stiffness-to-weight ratios. With the increased use of fiber-reinforced composites in structural components, studies involving the behaviour of components made of composites are receiving considerable attention. Functional requirements and economic considerations of design are forcing engineers to seek reliable and accurate yet economical methods of determining static and dynamic characteristics of structural components [48].

Currently, almost every aerospace company is developing products made with fiber-reinforced composite materials. Military aircraft designers were among the first to realize the tremendous potential of composites with high specific strength and high specific stiffness since performance and maneuverability of those vehicles depend so heavily on weight. Composite construction also leads to smooth surfaces, which reduce drag. Composite structural elements such as horizontal and vertical stabilizers, flaps, wing skins and various control surfaces have been used in fighter aircraft such as the F-14, F-15 and F-16 with typical weight savings of about 20 percent. The AV-8B has graphite/epoxy wing-box skins, forward fuselage, horizontal stabilizer, elevators, rudder and other control surfaces. One of the most demanding applications thus far is the use of graphite/epoxy composite wing structures on the experimental forward-swept wing X-29 fighter. Although concept of a forward-swept wing for improved maneuverability is not new, conventional aluminum structures could not withstand the aerodynamic forces acting on such a wing, so the implementation of the concept had to wait for the development of advanced composites.

1.2 Tapered Laminates

For most applications, thickness tapering is desirable. Except in pressure vessels where stress distributions are uniform, stresses tend to vary significantly within a structure. Tapering thus saves weight by removing the unnecessary material in low stress areas, it also conforms to geometric shape requirements such as those dictated by aerodynamics.

Tapering of metal structures is essentially done by removing material whereas tapering of composite structures is done by selectively building up material. Indeed, a metallic slab of uniform thickness is either machined or chemically milled, using masks, generating lots of scrap chips.

Laminated composite plates consist of thin plies having different fibre orientations. Many composite structures are made from laminated plies of different materials. One of the advantages of using composite materials is that laminated plies can be tailored to follow the load-bearing direction so that the strength of the composite structures can be optimized. One technique used to optimize structural design is to taper the thickness of a component to match the specific load-carrying and stiffness requirements along the component. This is accomplished in metallic structures by machining the component. Since composite laminates are composed of plies with a fixed thickness, the best way to vary the thickness, and thus the stiffness and strength, of a composite structure is to terminate or "drop off" plies inside the laminate. The method used to produce a change in thickness by cutting one or more plies short to produce a step change in thickness is called "ply drop-off" technique.

Introducing taper in composite structures may permit structural tailoring which is unattainable with flat laminates. Internal plies are terminated at various spanwise locations on a wing skin to tailor a reduction in stiffness from root to tip. A laminated aircraft wing skin is typically thicker at the wing

root and thinner near the tip. Ply drops in the horizontal stabilizer of General Dynamics F-16 A/B is shown in Figure 1.1. Also plies may be inserted in a laminate at joints to strengthen the joint, or inserted locally in a panel to act as a stiffener. A composite flexbeam of a helicopter rotor hub is another example of the application of taper to the design of a composite structure. A flexbeam must be stiff at the hub end, where large structural displacements are undesirable, yet flexible at the blade end, where large flapping motions of the blade must be managed. Another typical example is a helicopter rotor blade, where increased thickness is necessary near the root. Rotor blades are often made predominantly loading is mainly in the spanwise direction. Glass fiber/epoxy is a frequently used material because of its good strength and damage tolerance. A schematic of a typical tapered laminate with ply drops is given in Figure 1.2.

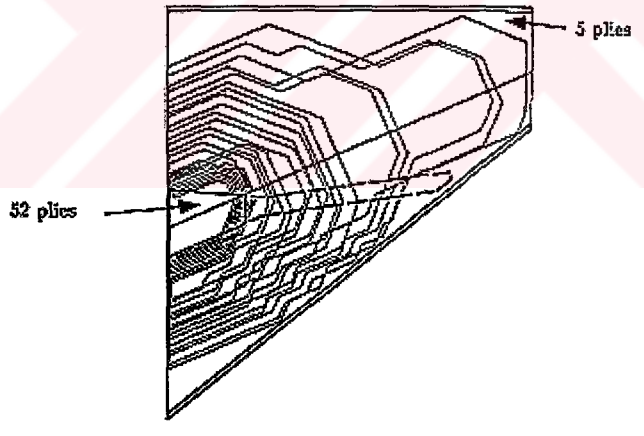

Figure 1.1: Ply Drops in The Horizontal Stabilizer of General Dynamics F-16

Tapering thickness of structural components poses specific problems in applications using laminated composite materials. Dropped plies result in an abrupt change in thickness and consequently, produce a concentration of stress. Potential benefits in tailoring the stiffness by dropping plies in a composite structure may be compromised by a premature failure due to stress concentrations at the dropped-ply location. The inherent weakness of this structural element is the lack of fiber reinforcement in the weak interlaminar direction. Interlaminar loads are induced in tapered laminates that may initiate delamination. Subsequent growth may directly affect structural performance of the component.

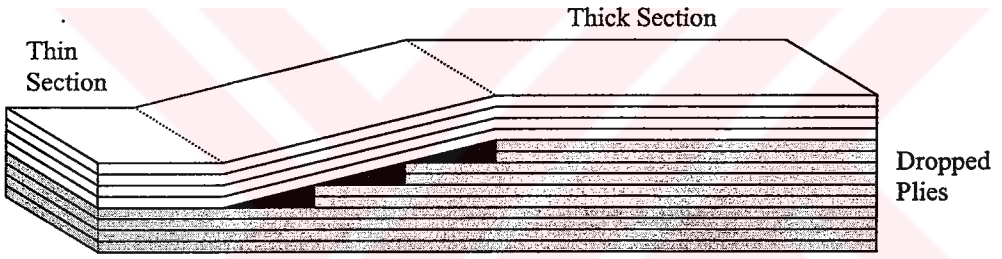

Figure 1.2: Typical Tapered Laminate With Ply Drops

1.3 Delamination

One of the main disadvantages of advanced composites is their low stiffness and strength in directions perpendicular to the fibers. This means failure can easily occur when there are interlaminar, or through the thickness stresses present. This type of failure is called delamination, when cracks propagate between plies causing them to debond. Interlaminar stresses can be present where there is curvature, out-of-plane loading or discontinuous plies. Another main source of interlaminar stresses is the mismatch in Poisson's ratio

at the interface of plies with different orientations. This leads to the "edge effect" and results in delamination spreading inwards from the free edge.

Failures in composite materials often begin as matrix microcracking and delamination. These modes of damage are essentially three-dimensional in nature, and interlaminar stresses are primarily responsible for them. Steep stress gradients are encountered in regions such as free edges, ply termination, zones of delamination, and voids and holes.

1.3.1 Out-of-Plane Delamination Failure

A major asset of composite laminates is the ability to orient fibers to achieve directional strength and stiffness properties that match the expected loading environment of the structural elements. Composite materials are uniquely suited to this objective because the principle material directions of each layer can be oriented according to need. However, interlaminar stresses develop in laminated composite because of the mismatch in engineering properties between individual lamina within the laminate. These stresses are instrumental in delamination initiation and propagation. [48]

Delamination by definition is matrix crack development the lamina interfaces. The causes of delamination can be attributed, in general terms, to the existence of out-of-plane (interlaminar normal and shear) stresses that develop at structural discontinuities.

More important in structural applications, out-of-plane stresses are also induced at a variety of common design features involving local discontinuities. Figure 1.3 depicts five of the most common design details incorporated in structures. Even under in-plane loading, interlaminar shear and normal stresses develop in the gradient stress fields that form at these locations because of local discontinuities. [48]

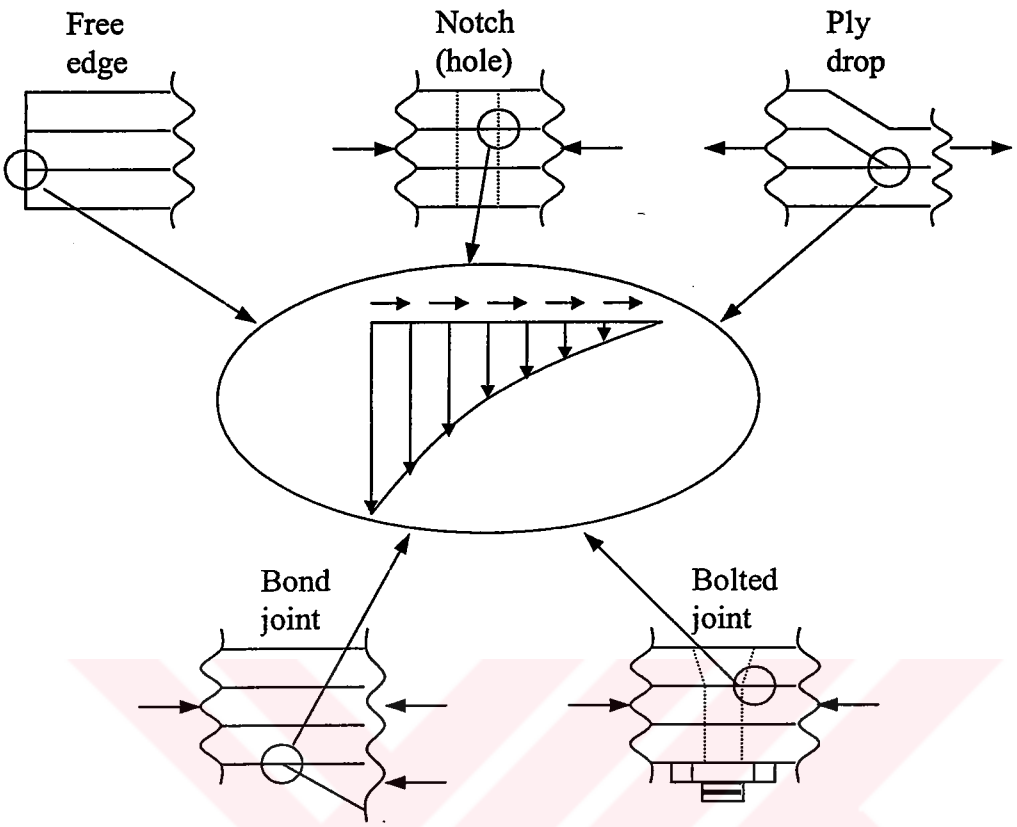

Figure 1.3: Sources of Out-of-Plane Loads in Typical Aircraft Design

1.4 Strength Analysis and Theories of Failure

For the determination of strength of any material it is the usual practice to estimate the stress at the time and location when failure occurs. In the case of conventional materials we need only to determine the maximum tensile, compressive, or shear stress and can then make some statement about the failure and failure mechanism. This procedure is relatively straightforward because isotropic materials have no preferential orientation and usually one strength constant will suffice.

For composite materials, however, the one-constant approach for stiffness or for strength is no longer adequate. We know that unidirectional composites have highly directionally dependent strengths. So for any state of applied stress, all three stress components must be examined before a judgement on the cause of failure can be made.

The determination of strength using failure criteria is based on the assumption that the material is homogeneous (properties do not vary from point to point) and its strength can be experimentally measured with simple tests. Failure criteria provide analytic relation for the strength under the applied stresses.

For composite materials, we need a failure criterion for the unidirectional plies. The strength of a laminated composite is based on the strength of individual plies within a laminate.

There are two popular approaches for failure criteria of unidirectional composites. They are all based on the on-axis stress or strain as the basic variable.

a) The Maximum Stress and Strain Criteria

In maximum stress criterion, failure results when any one of the stress components is equal to its corresponding strength property and the maximum strain criterion is totally analogous to the maximum stress criterion, that is, failure results when any one of the strain components is equal to its corresponding ultimate strain.

b) The Polynomial Failure Criteria

The most general polynomial failure criterion for composite materials is the tensor polynomial criterion by Tsai [50]. All other polynomial failure criteria are degenerate cases of this criterion. In index notation, the tensor polynomial failure criterion is expressed in Equation 1.1.

$$F_i\sigma_i + F_{ij}\sigma_i\sigma_j + F_{ijk}\sigma_i\sigma_j\sigma_k + \ldots \geq 1 \qquad (1.1)$$

The maximum stress and strain criterion can also be expressed as a tensor polynomial criterion. Without giving the expressions, some other types of failure criteria are Tsai-Hill's criterion, Hoffman's criterion, Tsai-Wu's criterion and Hashin's criterion.

1.5 Main Objectives and Scope of the Study

The main objective of this study is to investigate the effect of dropped plies on the strength of fiber-reinforced tapered composite laminates. Finite Element Package MARC© was used in the analysis of tapered laminates with ply drops. The numerical results were verified with experimental results.

A three-dimensional finite element model including a resin-rich interply region was constructed to analyze the interlaminar stress state at the ply drops. A fine mesh was employed at the stress critical locations. The boundary conditions were given to simulate the experimental test conditions. Equivalent von Mises Stress was used to predict the location of delamination initiation. Maximum stress criterion and the modified Tsai-Wu as delamination failure criterion with application of average stress concept were used to predict delamination initiation load in the resin interfaces surrounding ply drops.

Seven different configurations were investigated with the finite element analysis and five different configurations were investigated experimentally in the study. Configurations consisted of five different stacking sequences. Additionally two of the configurations investigated with the finite element method were resolved to simulate the migration of fibers in 90° plies into the resin pocket at the dropoff point. All of the laminates contain 14 plies in the thick section and 8 plies in the thin section dropping six plies in groups of two with one surface of the laminate flat as would be done in actual applications.

The material properties of the prepreg material are determined with several tests according to the ASTM standards. The material properties used in finite element analysis are the combination of the results of these tests and the material properties given by manufacturer.

A preliminary study is conducted for making a valid reliable 3-D finite element model by investigating the effect of aspect ratio and interply resin regions on the interlaminar stress distribution.

Manufacturing of tapered laminates with ply drops with a controlled geometry is also investigated by applying three different lay-up methods for autoclave molding. A new method was developed and used for the lay-up of tapered specimens.

The numerical and experimental analyses are restricted to the linear material and geometric cases.

CHAPTER 2

LITERATURE SURVEY AND REVIEW

There is a very extensive literature on "Advanced Materials" such as "composites" and their manufacturing and applications in various areas of engineering. Failure analysis in Laminated composite plates and delamination in composite laminates have been studied extensively in recent years but little work has been directed towards the understanding of the failure mechanisms of tapered composites. Few references exist in the open literature on the dropped-ply problem.

2.1 Analysis and Design of Tapered Laminates

Most studies expose the critical characteristics of the presence of internal ply drops in a tapered composite laminate. In most cases the location of the ply drop was identified as the site of critical interlaminar stress states and delamination onset both numerically and experimentally. Here, the available literature on the analysis and design of tapered laminates, the effect of dropped plies on the strength of fiber-reinforced composite laminates and onset of delamination in laminated composites will be reviewed in detail.

The effects of stacking sequence, adhesive-film interlayers, and altered near-edge fiber orientation on the delamination resistance of tapered glass/epoxy laminates were investigated analytically and experimentally by

Llanos, Lee and Vizzini [3]. Two different stacking sequences and three equidistant internal double-ply drops were investigated. Three-dimensional FEM (Finite Element Method) models were constructed for the analytical approach. A maximum stress failure criterion was applied and delamination was predicted to initiate in the resin interfaces surrounding the ply drops at the last ply drop location. Tapered specimens were tested under quasi-static uniaxial tension. The experimental results showed a dependence of delamination onset location and load on laminate stacking sequence. The addition of internal adhesive layers at the critical delamination location also showed a dependence on laminate stacking sequence. The alteration of a small section of the internal edge of the last ply drop lead to significant reductions in the magnitudes and gradients of interlaminar shear stresses. Also the orientations of dropped plies had an effect on delamination onset.

Poon and Ruiz [4] modelled a tapered laminated carbon-fiber/epoxy composite with a dropped ply subjected to in-plane bending in which the strain fields were predicted by a three-dimensional finite element method. The finite element results highlighted the effect of strain concentrations at the ply drop-off and the free edge problems. The validation of the finite element analysis was performed by strain measurements on a tapered composite specimen. The validity of the finite element analysis was enhanced by the broad agreement with the experimental results.

Daoust and Hoa [5] studied tapered laminates by internal ply dropoffs with a finite element program using displacement formulation. Parameters, which can influence the strength of the laminate, were studied. These parameters include the location of the ply dropoff in the thickness direction, the degree of resin filling inside the dropoff, the effect of width of the laminate and the orientation of the lamina where the dropoff was made. They used maximum stress criterion for failure. The results showed that internal ply drops were stronger than external ply drops and extending the length of the dropoff

while keeping the same dropoff height reduces interlaminar stress levels. They have also simulated crack growth by consecutive removal of failed elements.

The effects of ply dropoffs on the stress-strain behavior, fracture strength and fracture modes of graphite/epoxy laminates in tension were investigated by Lagace and Cannon [6]. The study was conducted only experimentally. Test variables include the number, order, angular orientation and effective ply thickness of the dropped plies. The stress-strain behavior of the ply-drop specimens was compared with the flat laminates with similar layups. The failure stresses and modes of the ply dropoff laminates were found to be similar to those of the flat laminates having the same layups as the dropped section of the ply dropoff laminate. The tests indicated that the presence of ply dropoffs has little effect on the tensile global stress-strain behavior of laminates. Only the order of the ply dropoffs appeared to have any affect as laminates with all plies dropped adjacent to each other tended to delaminate away from the rest of the laminate in the undropped section.

The tensile strength of tapered composite laminates with multiple internal ply drop steps was investigated by Fish and Lee [7]. Both experimental testing and finite element modeling of the tapered region were conducted. The average stress concept was applied to out-of-plane stresses from a three-dimensional finite element model. Delamination failure criteria were then used to predict strength based on ply failure and interply resin failure. It was found that delamination in the tapered laminates was due to interlaminar shear failure of the interply resin surrounding the last ply drop step. Strength predictions based on interply resin failure, using a stress averaging distance of one ply thickness, were found to correlate well with the experimental results.

In the study of Wisnom, Jones and Cui [8], rapidly tapered sections with dropped plies were designed, manufactured and tested with different materials. Under static loading, close to net section tensile strength was

achieved. They found that the most significant factor controlling strength was the number of plies dropped together.

Curry, Johnson and Starnes [11] studied the reduction in the compressive and tensile strength of graphite/epoxy laminates with thickness discontinuities due to dropped plies by experiment and analysis. In their study they found that the axial strength of a laminate with dropped plies was less than the strength of its thin section, and compressive strength of a laminate with dropped plies was less than its tensile strength. They used three-dimensional state of stress in the dropped ply region and examined the mechanism of failure with finite element method. They found the correct location of failure but they underestimated the failure load by using a tensile interlaminar criterion.

In the study of Cairns, Mandell, Scott and Maccagnano [12] various factors for design of composite structures with ply drops considered. These factors include thickness, ply stacking sequences, ply drop geometries and manufacturing considerations. In addition, fatigue loading was considered with respect to delamination initiation and growth. They used virtual crack closure method in finite element analysis and verified experimentally. From the results they found an optimum configuration of dropping plies.

Delamination suppression by altering the sequence of ply drops was evaluated for tapered glass/epoxy laminates by Botting, Vizzini and Lee [13]. A finite element model using three-dimensional solid elements was constructed to evaluate the state of interlaminar stress in and around the ply drops. The effect of the stress-free edge was considered by providing a mesh refinement near the free edge. They considered two different stacking sequences and employed two failure criteria, the Von Mises stress and maximum principal shear stress. Tapered specimens were manufactured and tested under quasistatic uniaxial tension. The measured delamination strengths came out to be insensitive to the ply-drop sequence, although the finite element model

indicates a stronger sensitivity but in general the finite element model correlated well with the experimental data.

An energy based damage tolerance methodology has been applied by Trethewey, Gillespie and Wilkins [14] to assess the influence of induced interlaminar loads on the structural performance of thickness-tapered laminates with discontinuous plies. Their analytic model was based on shear deformation plate theory with a through-width delamination embedded at the interface between continuous and discontinuous sublaminates. Also a parametric study was conducted to determine the influence of geometry and material properties on the structural performance of tapered laminate.

In the work of Ochoa and Chan [15] the effect of ply termination on laminates subjected to multiaxial loads (tension, bending and torsion) was investigated. Interlaminar stresses were evaluated with a special finite element developed for multiaxial response. The strain energy release rates were presented to guide the material and stacking sequence choices.

Cui, Wisnom and Jones [18] created a new model called the variable fracture energy model for predicting static strength of tapered laminates. The model was established based on comprehensive experimental and analytical study on constant thickness specimens with the central plies cut across the complete width. Experimental results on tapered specimens showed that the model could predict delamination of tapered laminates very well.

A study to analyze tapered composite laminates under tensile loading was conducted by Armanios and Parnas [19]. A tapered construction made of glass/epoxy laminate was used to achieve a thickness reduction using three consecutive dropped plies. The principle of minimum complementary potential energy was used to determine interlaminar stresses. The interlaminar peel stress distribution showed a higher tensile intensity at the taper/thin portion

juncture. The interlaminar stresses were determined on the basis of equilibrium conditions and local stiffness variations at the ply drop locations. The total strain energy release rate was determined using a simplified membrane model. Results were compared with a finite element simulation. The interlaminar stresses and the total strain energy release rate distributions were in agreement with the finite element solution.

Tapered (in steps) laminated plates under a uniform inplane load was analyzed by Wu and Weber [20] with a three-dimensional isoparametric finite element. Stress fields were obtained for a single-step dropoff problem for three basic layups. The analysis showed that very high peak stresses exist in the corner region of the step. The inclusion of a resin rich layer at the interface between the outer plies and inner plies, together with a triangular fillet of glue at the step had the effect of causing significant reductions in the peak stress levels.

Tapered laminates of unidirectional layers of glass/epoxy and graphite/epoxy were investigated by Hoa, Daoust and Du [23]. Thickness variation was accomplished by dropping off plies near the midlength of the laminate. Three-dimensional finite element models were used for stress strain variations. The analytical approach was verified by an experimental study. Calculated values using the finite element method compared well with experimental results for the point of first delamination. This agreement allowed the determination of a suitable finite element mesh for subsequent models of other tapered laminates with fiber orientations other than unidirectional. Also they pointed out that a reasonable finite element mesh must be established for the determination of interlaminar stresses in tapered laminates made of unidirectional layers.

Wisnom [24] discussed the mechanism of delamination in tapered unidirectional specimens with dropped plies. He presented results from static

tests with different numbers of dropped and continuous plies. In all cases failure occurred by delamination into the thick section both above and below the dropped plies. He compared the results with predictions from a simple formula based on the strain energy release rate associated with the terminating plies, with the fracture energy determined from tension tests. He found a good correlation between the results. He concluded that the critical parameter affecting delamination in tapered unidirectional composites with ply dropoffs was the strain energy release rate associated with the terminating plies.

Vizzini [26] developed a methodology to predict the strength of laminated composites with internal discontinuities parallel to a uniaxially applied load. He used a quasi-three-dimensional finite element analysis to determine the state of stress at and near the internal discontinuity. Two techniques were developed to predict the strength. In one technique, the state of stress in a small resin pocket at the discontinuity was used with an isotropic failure criterion. In the other technique he used the in-plane state of stress around the discontinuity with a failure criterion based on an analogy with an individual ply. He verified his predictions with experiments.

The effect of various factors on delamination has been studied by Cui, Wisnom and Jones [28]. They used specimens with cut central plies. A simple model was proposed to take account of fracture energy. The factors they investigated were the specimen thickness and the through thickness normal stress. They obtained an excellent correlation with experimental results.

Wisnom [29] also studied the delamination of tapered specimens of unidirectional E glass/epoxy with dropped plies by means of tensile tests and finite element analysis. In his study he also investigated the behavior of untapered specimens with discontinuous plies and specimens with the geometry of tapered sections but without the terminating plies. He found that the strain energy release rate associated with the terminating plies was the

critical parameter controlling delamination. Finite element predictions of delamination in tapered specimens with dropped plies were less satisfactory, with the results varying from -19% to +26% experimental values.

Fish and Lee [30] investigated the delamination of tapered composite laminates with multiple internal ply drop steps. Both experimental testing of glass/epoxy specimens and the finite element modeling of the tapered region were conducted. They applied the average stress concept to out-of-plane stresses from a three-dimensional finite element model. Delamination failure criterion was then used to predict strength based on ply failure and interply resin failure. The results showed that strength predictions based on interply resin failure using a stress averaging distance of one ply thickness were found to correlate well with the experimental results. They found that delamination in the tapered laminates was due to interlaminar shear failure of the interply resin surrounding the last ply drop step. Fish and Lee [30] concluded that if the stacking sequence was arranged such that the stiffest (extensionally) plies lie above the ply drop steps, more of the load carried by the plies can be transferred to the sublaminate above the dropped plies, reducing the peak interlaminar shear stress in the laminates.

The tensile strength of quasi-isotropic tapered composite laminates with multiple internal ply drop steps were investigated by Fish and Lee [43]. Both experimental testing of glass/epoxy specimens and finite element modeling of the tapered laminates were conducted. The interlaminar stress states created by the free-edge effect and the internal ply drops were determined using a quasi-three-dimensional finite element model of a laminate cross-section and a three-dimensional model of the tapered geometry, respectively. Both models incorporated an interply resin layer at the ply interface. The average stress concept was applied to the two interlaminar stress states, which were superimposed near the root of the taper, and a quadratic delamination failure criterion was used to predict delamination onset. Strength prediction based on

failure on the interply resin correlated well with the experimentally determined strengths.

Tapered carbon fiber/epoxy specimens were tested in tension to study delamination in asymmetrically tapered composites by Wisnom, Dixon and Hill [46]. Good predictions for delamination load were obtained with an equation developed for symmetric specimens based on the strain energy release rate associated with the discontinuous plies. As a result the asymmetry did not appear to be a critical factor for delamination.

The structural performance of thickness tapered laminates had been investigated using an energy-based damage tolerance methodology by Trethewey, Gillespie and Wilkins [53]. The geometry studied was a thin laminate with discontinuous internal plies and a through-width delamination embedded at the interface between continuous and discontinuous sublaminates. An analytic model based on shear deformation plate theory and linear-elastic fracture mechanics was employed. A two-dimensional plane strain finite element analysis was conducted to confirm the accuracy of the analytic predictions. Finally the studies were verified by experiments and reasonable agreement observed.

Vizzini and Lee [55] investigated the stress state and the resulting failure mechanisms of composite tapered components. Finite-element modeling and experimental evidence were used to determine the location of the damage initiation, the interaction between the free-edge and the taper discontinuities, the effect of realistic geometries, the extent and mode of damage growth, and the ability of simple physical models to explain the occurrence of the interlaminar stress state.

Rhim and Vizzini [56] formulated a high-order polynomial interpolation element to determine the interlaminar stresses in an internally

dropped ply region. The principle of virtual work was applied to determine the coefficients of the polynomial terms and thus determine the displacements within individual elements. Pure extension, pure bending and extension-bending coupling cases were studied. The interlaminar stresses determined by this approach agreed with the finite element model.

Vizzini [57] developed a finite element model of a tapered specimen that incorporates naturally occurring realistic geometries such as ill-formed resin pockets, unsymmetric and offset ply drop locations, varying ply thickness, and voids. Parametric studies were performed to determine the effects of these geometries, which occur naturally in manufactured specimen. The study showed that ill-formed resin pocket increase the effective taper angle at the ply drop and cause a corresponding increase in the interlaminar stresses. The effect of ply drops occurring unsymmetrically about the midplane was significant for offset values that occur as a result of the manufacturing process. And the location for damage onset was dependent on the amount of the offset of the resin pocket. Voids or fracture within the resin pocket significantly increased the interlaminar stresses at the drop and thus decreased the damage onset load.

Fish and Vizzini [58] investigated the delamination of ply drop configurations. In their study unidirectional glass/epoxy specimens were manufactured and tested under static tension and tension-tension fatigue. Four different ply drop configurations were studied with either grouped or dispersed plies and either staircased or overlapped dropped plies. The static tests indicated that the staircased-grouped and dispersed –overlapped specimens exhibited preferred structural performance by retaining their bending stiffness up to failure. The dispersed-overlapped specimen exhibited stable delamination growth.

2.2 Delamination in Laminated Composites

Delamination between layers in a laminate composite element plays an important role in the damage of many components. The beginning of delamination has often been related to the onset of multiaxial stress field near the free edges that occurs in laminates formed by many layers with different orientations.

Research projects are being carried out to understand and predict the occurrence of delamination caused by discontinuous plies, curvature and edge effects. A great amount of work has been reported on the free-edge problem in composite laminates, and indicated that free-edge delamination was mainly attributed to the existence of interlaminar stresses, which are highly localized in the neighborhood of free-edge under in-plane loading.

The onset of delamination was determined by Kim and Soni [10] on the basis of acoustic emission data. A two parameter failure criterion, average interlaminar normal stress failure criterion was used in conjunction with the stress analysis done by applying a global local model. The onset of edge delamination load was verified by experiments. Although the approach was based upon two parameters, the results agreed well with the experimental data for graphite/epoxy laminates under both in-plane tensile and compressive loading.

Interlaminar stresses in composite laminates under uniform axial extension were studied by Pipes and Pagano [34]. The response of a finite width composite laminate under uniform axial strain was treated through the application of classical elasticity theory. Finite difference solution techniques were employed to obtain solutions for stresses and displacements.

Methods for controlling free-edge delamination were considered in the study of Chan, Rogers, Cronkhite and Martin [54]. The study includes changing the ply-stacking sequence, minimizing Poisson's ratio mismatch, and adding an adhesive layer to the laminates. The finite element method was employed to evaluate the interlaminar stresses and strain energy release rate. From analytical and experimental results, it was concluded that with a reduction in the Poisson's ratio mismatch between plies, the interlaminar stress can be reduced and the delamination strength can be significantly increased and proper placement of an adhesive layer can significantly increase the delamination strength.

2.3 Delamination Due to Interlaminar Stresses and Theories of Failure

Tapered laminates have wide applications in engineering structures. However, the problem of predicting static strength accurately has not been satisfactorily resolved. Many models are available but all have limitations.

A number of authors have investigated static strength of tapered laminates. However there is no consensus on how to predict failure. Finite element modeling and stress based failure criteria were mostly used to predict the strength of tapered laminates of a variety of different materials and different internal ply drop configurations. Stress based failure criteria have been based on maximum stress, stress avaraged over a distance and stress evaluated at a characteristic distance. Another approach to study delamination in tapered laminates under axial loading is based on strain energy release rate.

Delamination due to interlaminar stresses can reduce the failure stress of the laminate below that predicted by the in-plane failure criteria. Failure by delamination is not necessarily the same as the initiation of delamination. However the initiation of delamination is generally fallowed by stable delamination growth, which leads to unstable growth and ultimate failure.

The average stress criterion of Kim and Soni [51] was one of the first mechanics of materials approaches to the prediction of the onset of delamination. This criterion was based on the premise that delamination will begin once the average value of interlaminar tensile normal stress, $\overline{\sigma}_z$, near the free edge reaches the interlaminar tensile strength, $S_Z^{(+)}$. In this criterion the averaging was done over a critical length b_0, as shown in Equation 2.1 and Figure 2.1.

$$\overline{\sigma}_z = \frac{1}{b_0}\int_{b-b_0}^{b} \sigma_z(y,x)dy = S_Z^{(+)} \tag{2.1}$$

where b is the half-width of the laminate and the critical length b_0 (averaging distance) was assumed to be equal to one ply thickness.

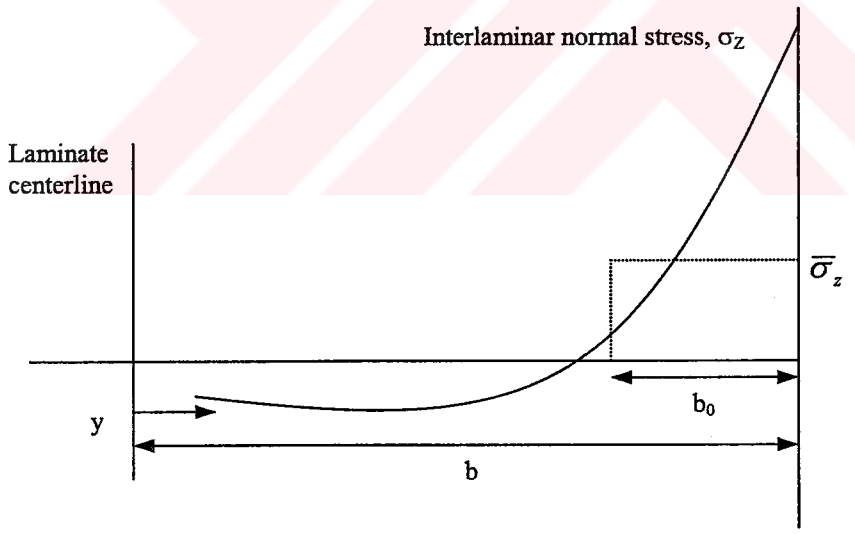

Figure 2.1: Graphical Interpretation of Average Interlaminar Normal Stress Near Free Edge According to the Kim-Soni Criterion.

Due to the difficulty of measuring $S_Z^{(+)}$, Kim and Soni assumed that $S_Z^{(+)}=S_T^{(+)}$.

Although this criterion provided reasonably accurate predictions of the onset of delamination in composites where the tensile normal stress, σ_Z, was the dominant interlaminate stress, the effect of interlaminar shear stresses were not considered.

Brewer and Lagace [52] proposed a quadratic delamination criterion for predicting onset of delamination. This criterion includes average interlaminar shear and normal stresses. They conducted some tests and after neglecting some terms, the quadratic delamination criterion took on the simplified form given in Equation 2.2.

$$\left(\frac{\overline{\sigma}_{xz}}{S_{xz}}\right)^2+\left(\frac{\overline{\sigma}^t{}_z}{S_z^{(+)}}\right)^2=1 \qquad (2.2)$$

where

$\overline{\sigma}_{xz}$ = Average interlaminar shear stress

$\overline{\sigma}^t{}_z$ = Average interlaminar tensile stress

S_{XZ}= Interlaminar shear strength

$S_Z^{(+)}$=Interlaminar tensile strength

$S_T^{(+)}$=Transverse tensile strength

Transverse isotropy was assumed, so that $S_Z^{(+)}=S_T^{(+)}$.

Fish and Lee [30] applied average stress concept to out-of-plane stresses from a three-dimensional finite element model of a tapered composite laminate. Delamination failure criteria were then used to predict strength based on ply failure and interply resin failure. They modified the Tsai-Wu failure criterion by uncoupling the inplane stresses from the out-of-plane stresses and considering strength to be independent of the sign of the shear stresses with an assumption of equal out-of plane shear strengths. The failure criterion is expressed in Equation 2.3.

$$F_3\sigma_{ZZ} + F_{33}\sigma_{ZZ}^2 + F_{44}(\sigma_{ZX}^2 + \sigma_{YZ}^2) = 1 \qquad (2.3)$$

Switching to the x, y, z coordinate system, the modified Tsai-Wu failure criterion for predicting delamination strength represented by Equation 2.4.

$$\frac{ZC - ZT}{ZC * ZT}\sigma_{ZZ} + \frac{1}{ZC * ZT}\sigma_{ZZ}^2 + \frac{1}{S^2}\left(\sigma_{YZ}^2 + \sigma_{XZ}^2\right) = 1 \qquad (2.4)$$

where ZT, ZC and S are the through-the-thickness tensile, compressive and shear strengths respectively.

In addition to this quadratic delamination failure criterion, the maximum stress failure criterion was considered to predict strength when the out-of-plane stress state was dominated by a single stress component.

For out-of-plane ply failure, the through-the-thickness tensile and compressive strengths were assumed to be equal to the transverse tensile and compressive strengths. In addition, the through-the-thickness shear strength was assumed to be equivalent to the inplane shear strength.

Failure was assumed to occur when the average stress over some distance, d_0, force the failure criterion above unity. Averaging concept was applied to out-of-plane stresses obtained from finite element model.

$$\overline{\sigma}_{ZZ} = \frac{1}{2d_0}\int_{-d_0}^{d_0} \sigma_{ZZ}(x)dx$$

$$\overline{\sigma}_{YZ} = \frac{1}{2d_0}\int_{-d_0}^{d_0} \sigma_{YZ}(x)dx \qquad (2.5)$$

$$\overline{\sigma}_{XZ} = \frac{1}{2d_0}\int_{-d_0}^{d_0} \sigma_{XZ}(x)dx$$

The smallest averaging distance considered was one half of a ply thickness (d_0=0.5H), which is the dimension, in the x-direction, of the smallest finite element. Stress averaging distance of up to 2H was investigated.

Vizzini [57] employed an isotropic failure criterion assuming that the delamination occur in the interply resin layer. Thus he used von Mises failure criterion to determine the point of failure in the finite element analysis of tapered composite beams and obtained good predictions compared with experiments. No attempt was made to predict delamination onset load but only relative level of different stress states were investigated.

All six stress components are used to determine the equivalent von Mises stress given in Equation 2.6.

$$\sigma_0 = \sqrt{\sigma_{XX}^2 + \sigma_{YY}^2 + \sigma_{ZZ}^2 - \sigma_{YY}\sigma_{ZZ} - \sigma_{XX}\sigma_{ZZ} - \sigma_{YY}\sigma_{XX} + 3\left(\sigma_{YZ}^2 + \sigma_{ZX}^2 + \sigma_{XY}^2\right)} \qquad (2.6)$$

In the study of Curry, Johnson and Starnes [11] interlaminar stresses computed with finite element analysis and delamination failure criterion was used to predict the delamination onset load of graphite/epoxy laminates with thickness discontinuities due to dropped plies. The delamination criterion, or the tensile interlaminar failure mode criterion used in the study is given Equation 2.7.

$$\left(\frac{\sigma_{zz}}{Y_t}\right)^2 + \frac{\left(\sigma_{xz}^2 + \sigma_{yz}^2\right)}{S_{yz}^2} = 1; \qquad \sigma_{zz} > 0 \tag{2.7}$$

This criterion is a modification of the interlaminar tensile matrix mode criterion given by Hashin [49]. The modification was accomplished by neglecting the noninterlaminar stress components.

CHAPTER 3

FINITE ELEMENT ANALYSIS (FEA) OF TAPERED LAMINATES

3.1 General Remarks About the Finite Element Method (FEM)

The finite element method is the most powerful numerical technique ever devised for solving solid and structural mechanics problems in geometrically complicated regions. The finite element analysis of a problem is so systematic that it can be divided into a set of logical steps that can be implemented on a digital computer and can be used to solve a wide range of problems by changing the data input defining the domain, its physical properties and initial and boundary conditions. It is this feature that gave the finite element method success in the modeling and simulation of practical engineering problems. [49]

The finite element technique is endowed with two distinct features that no other method shares:

1. The domain of the problem is viewed as a collection of nonintersecting simple subdomains, called finite elements. The word domain is used to denote the physical system, or material

region over which the governing equations are to be solved. The collection of the elements is called the finite element mesh of the domain.

2. Over each finite element, the solution of the governing equations is approximated by a linear combination of undetermined parameters and preselected approximation functions.

3.2 Finite Element Analysis with MARC©

The finite element package program, MARC© K7 with its pre and post processor MENTAT© 2.3.3 was used for the finite element analysis of tapered laminates. The Marc system is briefly described below.

3.2.1 The Marc System

The Marc system contains a series of integrated programs that facilitate analysis of engineering problems in the fields of structural mechanics, heat transfer and electromagnetics. The Marc system consists of Marc and Mentat programs. These programs work together to generate geometric information that defines the structure, to analyze the structure and to graphically depict the results. Figure 3.1 shows the interrelationships among these programs.

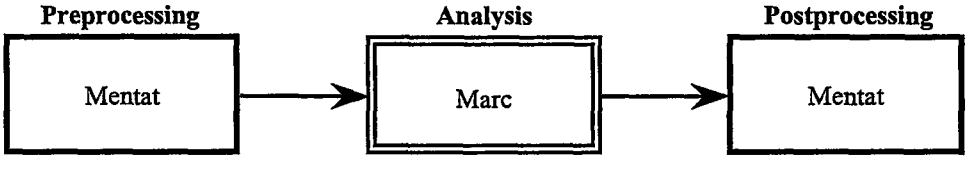

Figure 3.1: The Marc System

3.3 Modeling Considerations

Finite element analysis of a structural problem is a numerical analysis of the mathematical model used to present the behavior of the structure. Therefore, finite element modeling involves assumptions concerning the representation of the geometry of the structure and its behavior.

Mesh generation, load representation and imposition of boundary conditions, are the main considerations for the finite element modeling.

3.4 Stresses in Tapered Laminates and Modeling Approach

The modeling approach used for a particular problem is one of the most important points for finite element analysis. The accuracy of the solution mostly depends on how successively the problem is modeled. Thus, stress states of the problem must be predicted before constructing the model. Predicting stress states leads to the right choice of element types, element classes, mesh division and geometry.

Before constructing the finite element model for the analysis of tapered laminates, stress-states on tapered laminates were investigated from literature and from preliminary studies. Expected stress-states and some key points in modeling approach of tapered laminates are given below.

Whenever there is a discontinuity in a laminated composite structure, interlaminar stresses arise and initiate delamination. In a finite-width tapered laminate these interlaminar stresses are produced by both the free-edge effect and the internal ply drops. Two-dimensional modeling of the laminate cannot adequately include the effects of stress-free edges.

Besides the need for a three-dimensional analysis to capture the effects of stress-free edges, it is evident that a three-dimensional model with only one element in the width direction is not sufficient. Thus, multiple elements in the width direction are required for a good approximation of the effect of the stress-free edge.

As a result of the manufacture and cure-processes, resin-rich pockets form at the end of the dropped plies. In the tapered region, the load carried by the dropped plies is transferred to the continuous and discontinuous plies. This load transfer takes place roughly through the thin interply resin layers surrounding the ply drops and give rise to significant interlaminar stresses that promote delamination. The out-of-plane stresses peak at each of the ply drops and at the root of the taper. The interply resin layers are the weak link in the component and will fail first. Fracture of the resin layers will result in delamination in the taper region [55].

The interlaminar stresses lead to onset of delamination. Delamination depends on the strength of very thin interlaminar resin layers in structures. For a good approximation of delamination strength, these interply resin layers must be considered. Modeling thin interlaminar resin layers between the dropped plies and the covering plies increase the accuracy of the model and provide direct calculation of the interlaminar stresses. In most of the previous studies a three-dimensional finite element model of laminates, including a resin-rich interply region representing the interface of the ply drops with the adjacent plies are modeled.

Llanos, Lee and Vizzini [3] demonstrated the benefits of modeling a thin interply matrix region by setting the modulus of the assumed resin layer to a sufficiently large value so that the interply matrix layer was rigid relative to the composite laminate. They have concluded that the presence of interply

matrix region was essential in determining the proper stress distribution in and around the ply drop.

Fish and Lee [30] accurately predicted the strength of tapered composite structure by considering delamination based on the interply resin surrounding the internal ply drops.

In another study of Fish and Lee [43] the edge effects were investigated in quasi-isotropic tapered composite structures. They have predicted strength based on out-of-plane failure of the interply resin layer and the results correlated well with the experimentally determined strengths.

3.5 Preliminary Study for the Analysis of Tapered Laminates

Two preliminary studies were conducted to determine the effects of aspect ratio and interply resin layers. Considering the stresses in tapered laminates, a simple three-dimensional laminate was modeled with MARC. The influence of aspect ratio of elements and interply resin layers on the interlaminar stresses were investigated with the help of this simple model.

A finite element model using three-dimensional solid elements was constructed for the preliminary studies. A flat rectangular glass/epoxy (SP-250-S29) [3,13] laminate under tension was examined. The basic model was constructed with the same element types and classes with the tapered model. The plies were modeled in groups of two as in the tapered model. The information about the element types and classes are given in Section 3.6. The model is shown in Figure 3.2.

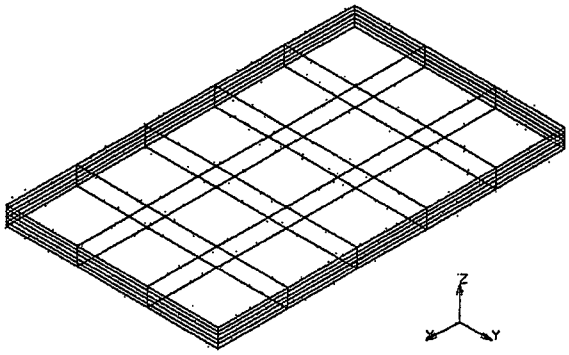

Figure 3.2: Basic Model

The model was composed of 10 plies with the stacking sequence [0_2 / ±45 / 90_2 / ±45 / 0_2]. The model was 62.2mm in length, 38.1mm in width and 3.32mm in thickness (+ 0.064 mm for interply resin layers). The boundary conditions are shown in Figure 3.3. The material properties are given in Table 3.1.

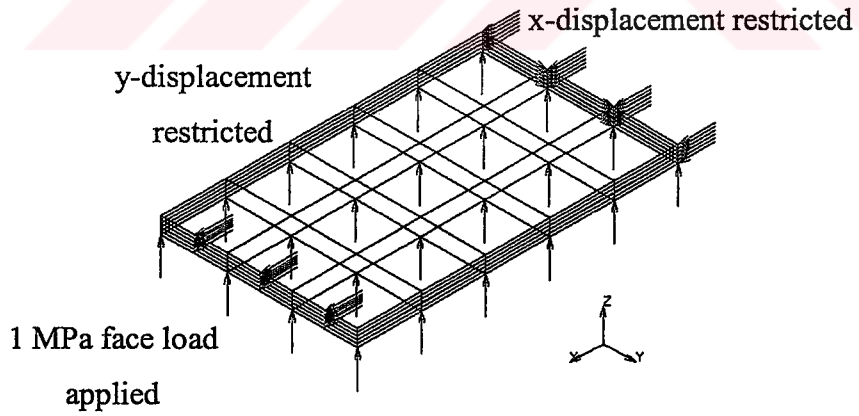

Figure 3.3: Boundary Conditions Applied to the Basic Model

Table 3.1: Material Properties Used for Glass/Epoxy (SP-250-S29)

E_x, (GPa)	48.3
E_y, (GPa)	14.5
E_z, (GPa)	14.5
G_{xy}, (GPa)	5.5
G_{yz}, (GPa)	4.8
G_{zx}, (GPa)	5.5
ν_{xy}	0.26
ν_{xz}	0.26
ν_{yz}	0.50
Ply thickness, (mm)	0.32
E_{resin}, (GPa)	3.9
G_{resin}, (GPa)	1
ν	0.37
Interply resin thickness, (mm)	0.032

The basic model was created in the same way as the tapered model, the detailed information about the model is not given in the preliminary study. But the tapered model is explained in detail in Section 3.6.

The study "Analysis of Interlaminar stresses in Composite Laminates With and Without Edge Delamination" of Whitcomb and Raju [59] was taken as reference to investigate the effects of the parameters described. The orientation of the reference model and the basic model here were the same and reference study used FEM also. But material properties in reference study were different from the material properties used for preliminary studies. Thus, only the behavior of the stresses were considered for comparison.

3.5.1 Effect of Aspect Ratio

As discussed in the previous section three-dimensional elements are essential because of the three-dimensional nature of the stresses. However since it is known that finite element results for interlaminar stresses depend on the finite element mesh size, it is necessary to determine the proper finite element mesh size first.

The element aspect ratio is the quotient between the longest and the shortest element dimensions. The ratio is by definition greater then or equal to one. If the aspect ratio is 1, the element is considered to be ideal with respect to this measure. Acceptable ranges for the aspect ratio are element and problem dependent.

The basic model with two interply resin layers was solved for interlaminar stresses. Interply resin layers were placed on both above and below two 90° plies. The cross-section (x-z plane) of the basic model and interply resin layers is shown in Figure 3.4.

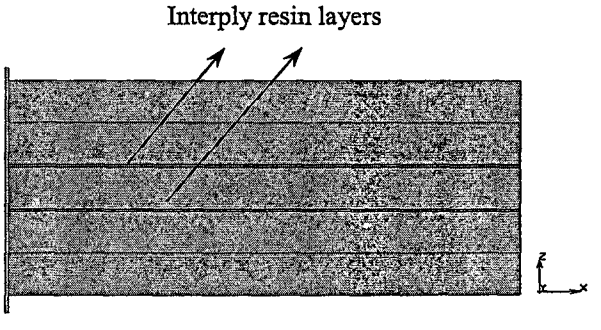

Figure 3.4: Interply Resin Layers in the Basic Model

Interlaminar stresses were investigated for four values of the aspect ratio. In thickness direction (z-axis) the division of the elements was fixed.

Aspect ratio depends on the division along the x and y axes. The aspect ratios and corresponding element divisions are given in Table 3.2.

Table 3.2: Aspect Ratios (AR) and Corresponding Element Divisions

AR	Division along x	Division along y
20	5	3
10	10	6
5	20	12
2.5	40	24

The solutions were plotted for different aspect ratios, along the thickness direction at the mid-span of the plate on the free edge and center.

a) Longitudinal stress distribution at the free edge is given in Figure 3.5. The plot shows that longitudinal stress (σ_{xx}) did not change with a decreasing aspect ratio.

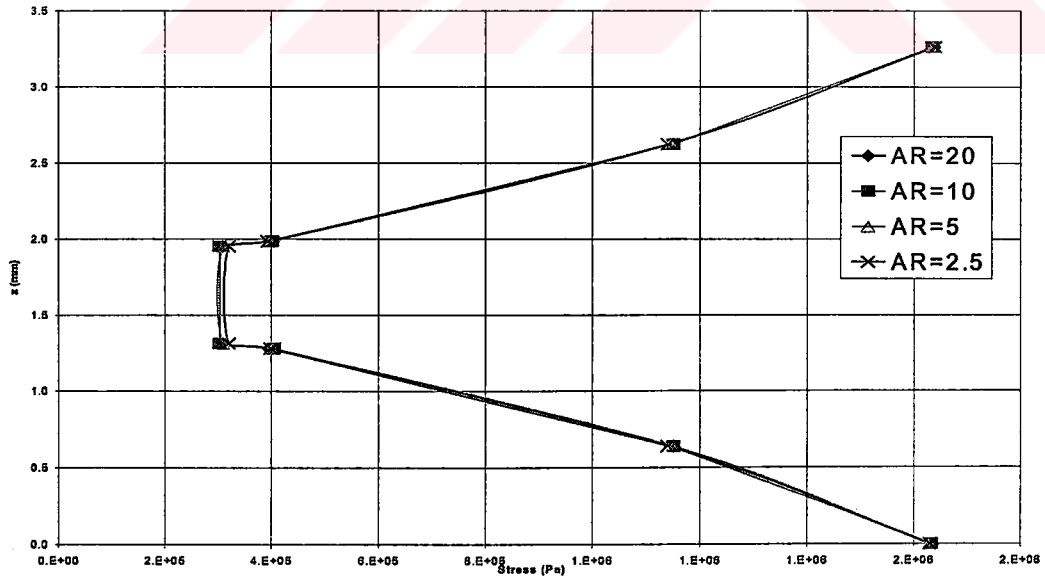

Figure 3.5: σ_{xx} at the Free Edge

b) Interlaminar normal stress distribution at the free edge is given in Figure 3.6. The interlaminar normal stress (σ_{zz}) tended to increase with a decreasing aspect ratio. This was expected because of the free-edge effect. Decreasing aspect ratio furthermore would increase σ_{zz} to higher values. In the reference study maximum interlaminar normal stresses appeared around 90^{o} plies which corresponds to z=1.312 mm and z=1.952 mm in the basic laminate. Thus, the interlaminar normal stress results with AR=10, 5, 2.5 showed the same behavior as the reference. To understand the effect of aspect ratio on the accuracy of the solution better, interlaminar normal stress distribution at the center (i.e., center in the width direction) was investigated additionally. This plot is given in Figure 3.7.

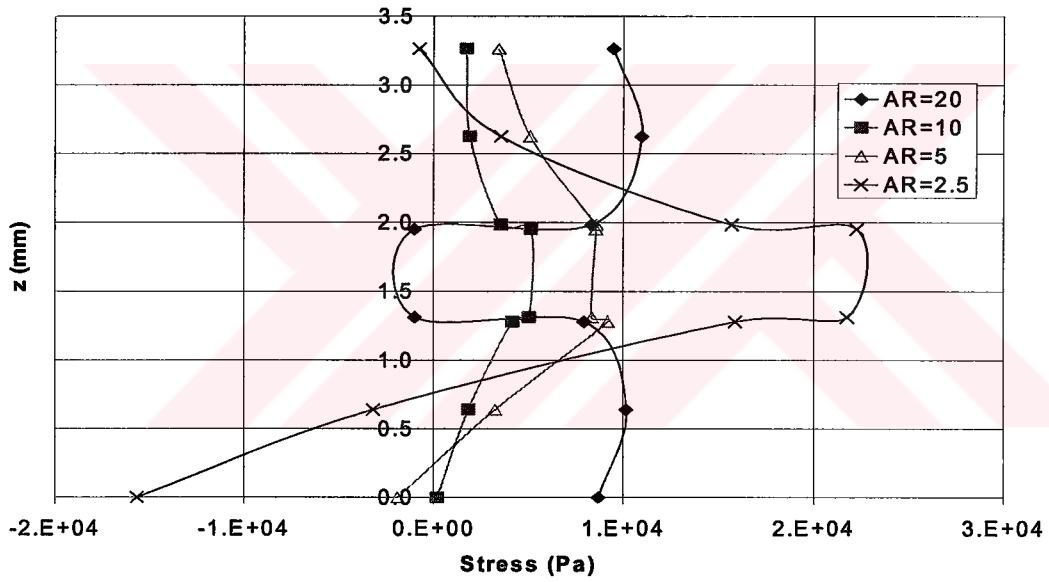

Figure 3.6: σ_{zz} at the Free Edge

Interlaminar normal stress was expected to be small at the center compared to the free edge. As shown in Figure 3.7 interlaminar normal stresses at the center decreased with a decreasing aspect ratio. Comparing the stresses at the free edge and at the center, the stress difference was less than expected for AR=10. Thus, it was concluded that the suitable aspect ratios are 2.5 and 5 for the interlaminar normal stress distribution.

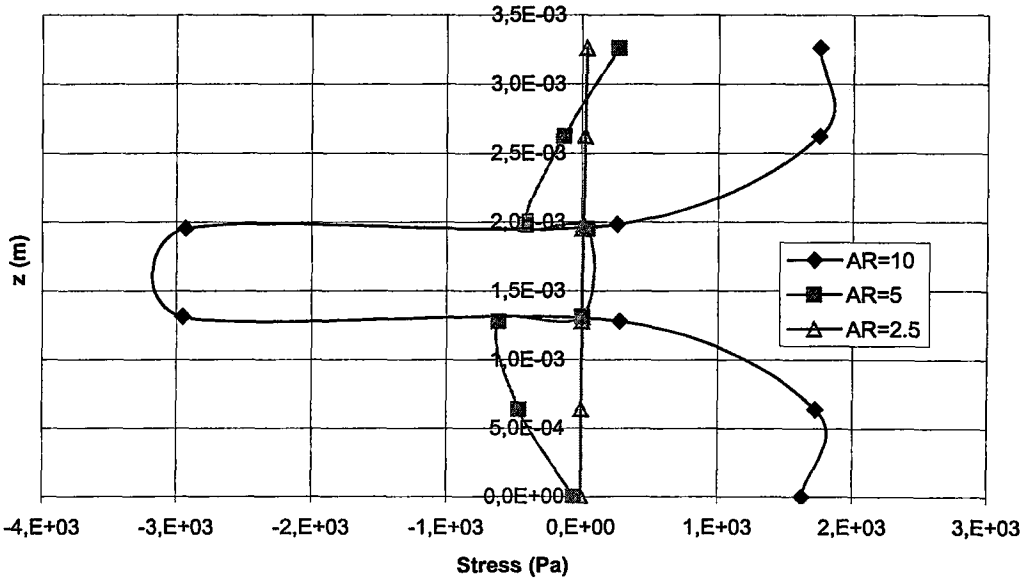

Figure 3.7: σ_{zz} at the Center

c) Interlaminar shear stress distribution at the free edge and at the center are given in Figure 3.8 and 3.9 respectively. Interlaminar shear stress (σ_{zx}) at the free edge tended to increase with a decreasing aspect ratio as expected due to the free-edge effect. In the reference study maximum interlaminar shear stresses were appeared between 45° and 0° plies which corresponds to z=2.624 mm and z=0.640 mm in the basic laminate. From the Figure 3.8 the plots of AR= 10, 5, 2.5 showed the same behavior. Also at the center of the laminate the interlaminar shear stress was expected to be very small. Thus, for the best approximation of interlaminar shear stress distribution, the suitable aspect ratios were determined to be 5 and 2.5. This behavior is evident in Figures 3.8 and 3.9.

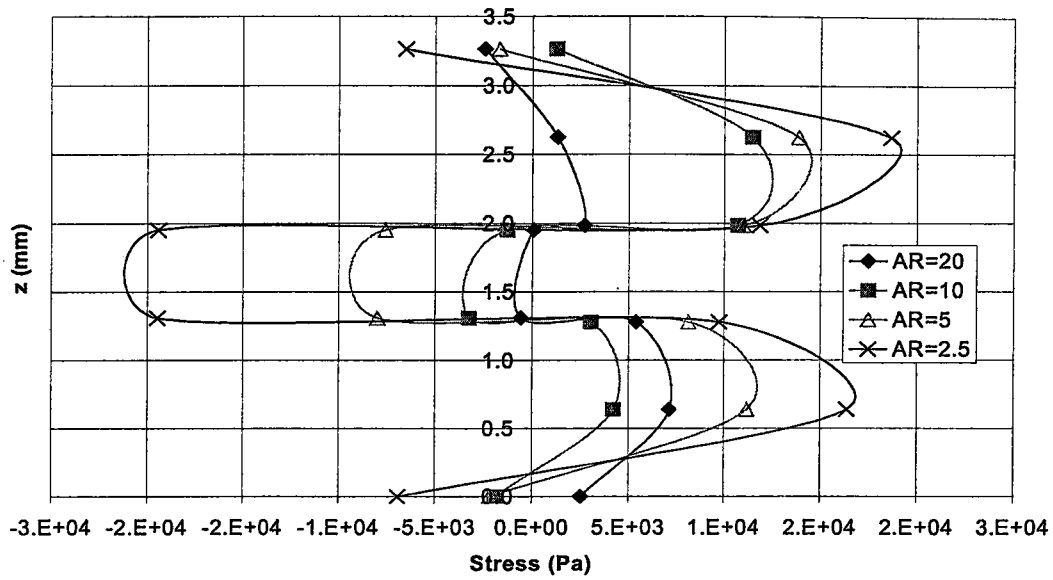

Figure 3.8: σ_{zx} at the Free Edge

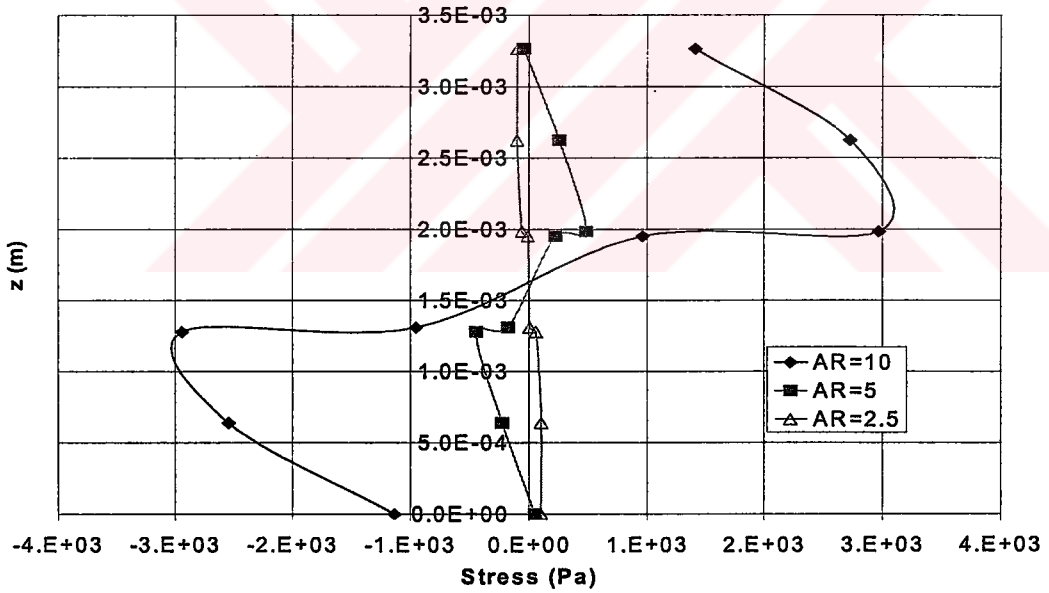

Figure 3.9: σ_{zx} at the Center

The study to determine the suitable aspect ratio to be used in the tapered model showed that decreasing the aspect ratio gives better results for interlaminar stresses. Although out-of-plane stresses were better approximated by decreasing the aspect ratio, in-plane stresses were not affected significantly.

The tapered model was more complicated than the basic model and the number of elements in the tapered model was twice (AR=2.5 configuration) of the basic model. So, considering the hardware capability of the MARC server (SGI, Octane, 250 MHz CPU R10000 Processor, 512 MB RAM) the suitable aspect ratio was chosen to be 5. Thus, the divisions along the x and y axes corresponding to this aspect ratio was applied on the tapered model.

3.5.2 Effect of Interply Resin Layers

In this part of the preliminary study for modeling, the effect of interply resin layers were investigated. The basic flat laminate model was solved for three different cases. Element types, element classes, boundary conditions and the dimensions were kept the same with the basic model. The element aspect ratio was taken to be 5.

In the model with no interply resin layers the interlaminar stresses were small. The model could not capture the effect of the resin layer between the plies. But, in real case, there exist a very thin resin layer between the plies. This thickness is usually assumed to be 1/10 of a ply thickness. Using two row of elements at this interface enables us calculation of the stresses in the middle of the resin layer. In Figure 3.10 the plots of interlaminar shear stresses are given for a model without interply resin layer, with an interply resin layer with one row of elements and with an interply resin layer with two row of elements.

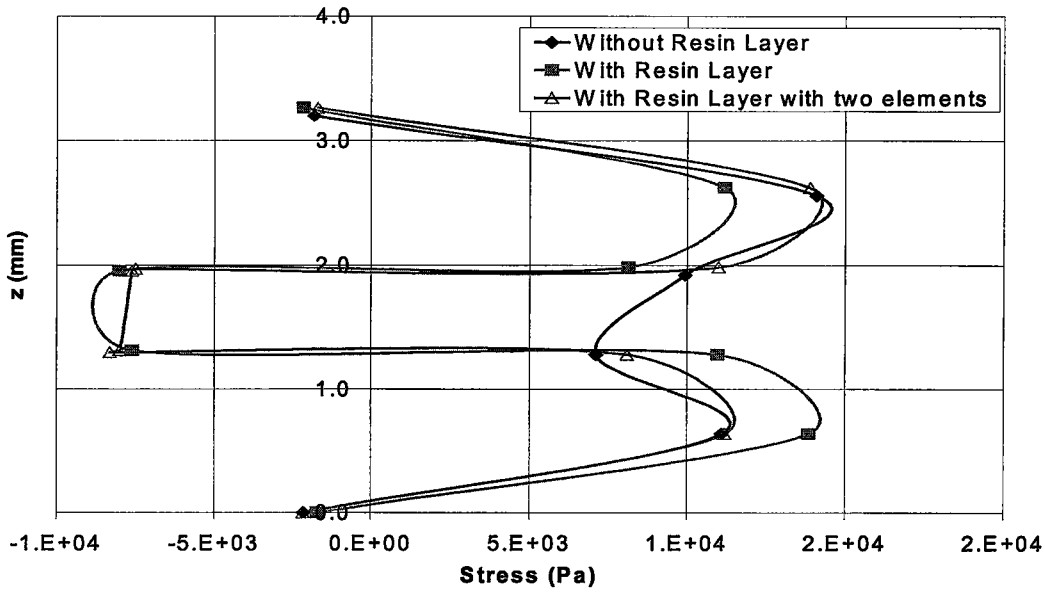

Figure 3.10: Interlaminar Shear Stress

This study showed that there was a considerable difference between the results of the model with and without interply resin layers. The behavior of the interlaminar shear stresses calculated with resin layers was similar to the reference study. Considering also the issues discussed before, it was decided that the interply resin region would be modeled with two rows of elements. This approach was more realistic and the stress values in the middle of the resin layers could be calculated.

3.6 Finite Element Analysis of Tapered Laminates

A three-dimensional finite element model was constructed for the analysis of tapered laminates with internal ply drops. The model end in the thick and thin sections of the laminates at a location away from the ply drops where it was safe to assume that the effect of the taper is negligible and that the laminate behaves as a flat plate. This condition was verified by matching the in-plane stresses at the thin and thick parts of the laminate with uniform-

thickness laminates representing thin and thick parts under the same uniaxial tensile load.

Each two of the plies were modeled with one element through the thickness. The interply resin layers were modeled with two elements through the thickness. Mesh became very fine at the last ply drop step and at the root of the taper where the maximum interlaminar stresses were located.

A tapered configuration was chosen to consist of 14 plies in thick part and 8 plies in thin part. Six plies were terminated in groups of two at three equally spaced locations. The taper angle was nominally 5.71°, corresponding to 10-to-1 taper ratio.

The model dimensions were the same with the gage length of test specimens. The model was 127 mm in length and 25.4 mm in width. The distance between the dropped plies were 2.8 mm.

Two different types of the elements were used in the model. Eight node solid brick elements based on assumed strain formulation were used as the majority of the elements. Six-node pentahedral elements were used to model the tips of the resin-rich pockets. The element sizes, in length, ranged from 0.5 of the ply thickness at the fine mesh location, to 40 times the ply thickness at the ends. The ply thickness was assumed to be constant and measured ply thickness found as 0.14mm experimentally. A thin resin layer was included in the model representing the interface between the ply drops and the top and bottom plies adjacent to them. The thickness of the resin layers was assumed to be 1/10 of a ply thickness. Each two of the plies, 7 in thick section and 4 in the thin section, were modeled with a row of elements in the longitudinal direction (x-direction), equally spaced 12 elements in the transverse direction (y-direction) and one element in the normal direction (z-direction). Different from

orthotropic plies, isotropic interply resin layers were modeled with two elements in normal direction.

The finite element model was modified to analyze the different configurations by changing the stacking sequence or orientation of plies. Also configurations TL1 (tapered laminate, first configuration) and TL2 (tapered laminate, second configuration) were reanalyzed by replacing the isotropic resin pockets with 90^{o} plies to take into account of migrated plies. This was done due to high probability of migration of plies in actual case during cure process because of high pressure. These configurations were designated as TL1-M and TL2-M.

The analysis was conducted, for each configuration, by fixing the thick end of the model (clamped) and by applying a uniaxial stress of 1 MPa over the face of the thin end of the model.

The material was assumed to be homogeneous, linear elastic and orthotropic.

The elements used were class 8, isoparametric, three-dimensional brick elements with three direct and three shear stress components, giving a total of six stress components.

The model was consisted of 8544 eight-node hexahedral elements and 36 six-node pentahedral elements, totally 8580 elements and 10387 nodes. All the elements had three (u, v, w) degrees of freedom per node.

The three-dimensional outline of the model is shown in Figure 3.11 captured from a MENTAT screen. Top view and side view of the model is given in Figure 3.12. (The figures are not to scale.)

The boundary conditions applied to the model reflected the condition of a test specimen under static loading. Basically the model was clamped at the thick end and uniaxial tension was applied to the thin end of the model.

At the thick end of the model, all of the nodes were restricted to move along the x-direction, the nodes at the bottom edge were restricted to move along z-direction and the nodes along the z-direction in the middle of the width were restricted to move in the y-direction.

At the thin end of the model, a face load of 1 MPa was applied, the nodes at the bottom edge were restricted to move along the z-direction and the nodes along the z-direction in the middle of the width were restricted to move along the y-direction.

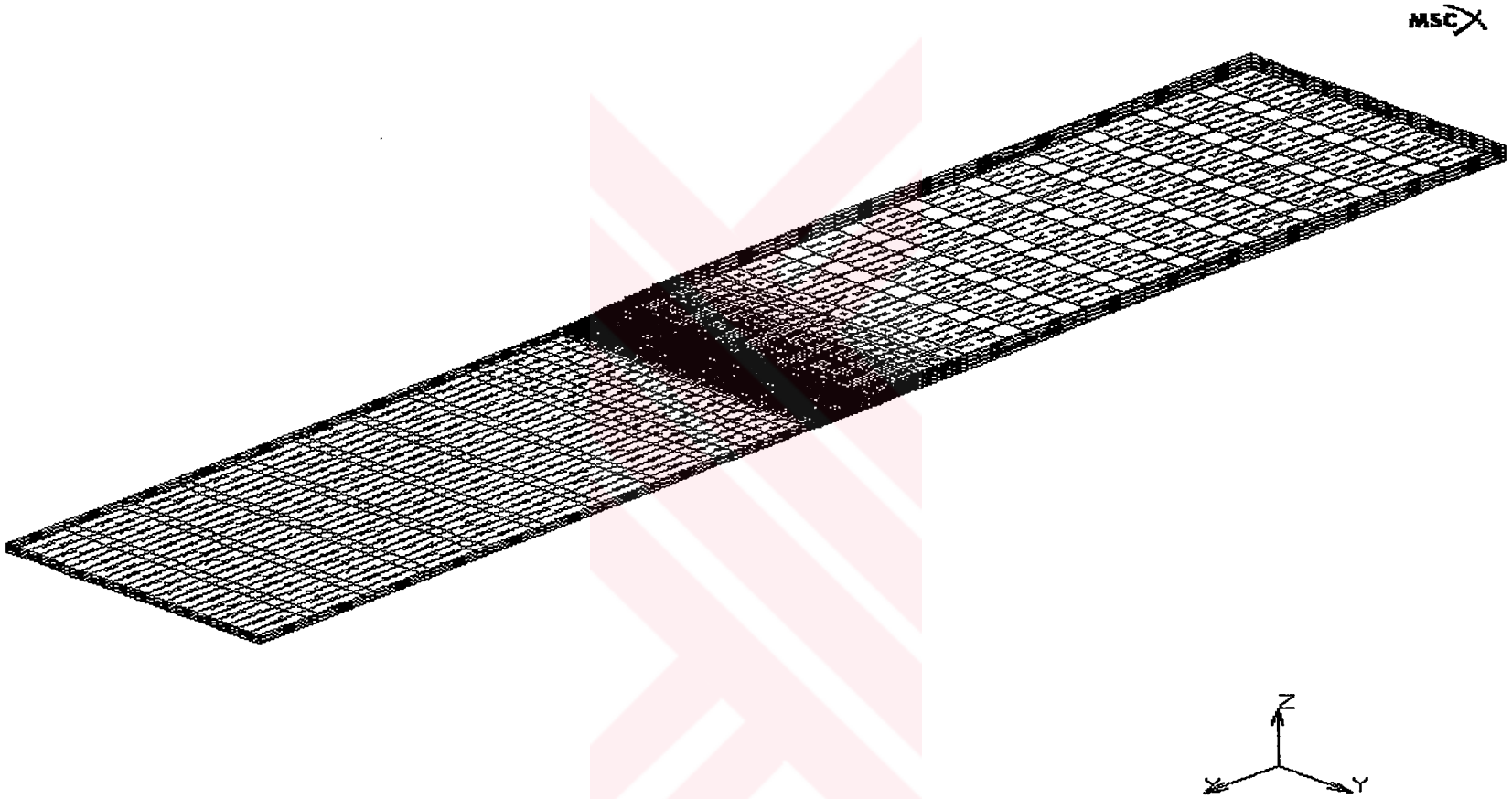

Figure 3.11: 3-D View of the Tapered Model

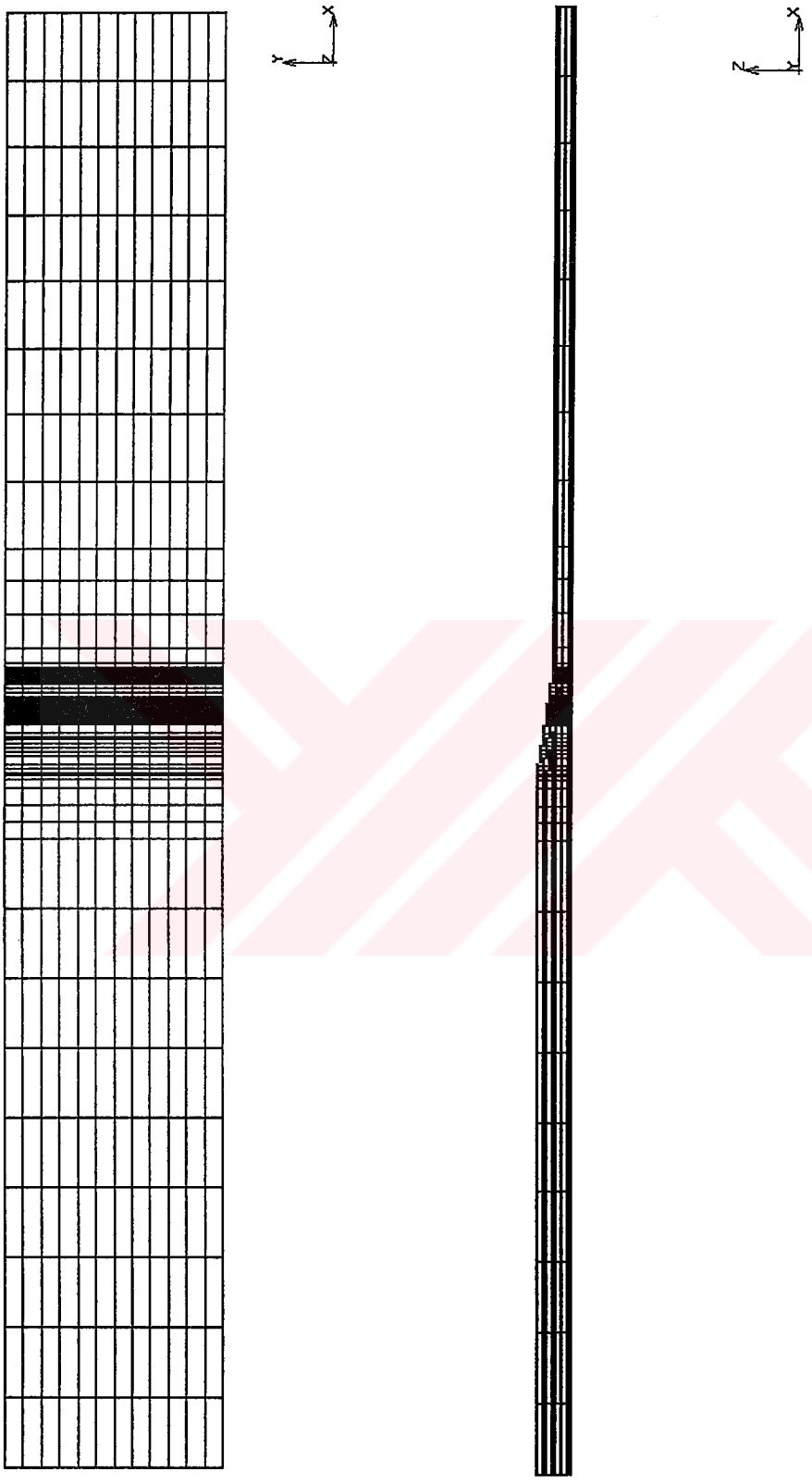

Figure 3.12: Top View and Side View of the Tapered Model

The elements of the model were equally spaced at the constant thickness regions. Finite element mesh size was decreased at stress-critical regions. These fine mesh regions were located around the last ply drop and the root of the taper. The aspect ratios of the elements far away from the fine mesh region were relatively large. Those elements were essentially under an in-plane stress state, thus, the effect of large aspect ratios on the stress state in the untapered region was negligible. Finite element mesh at the tapered region and fine mesh regions are shown in Figure 3.13.

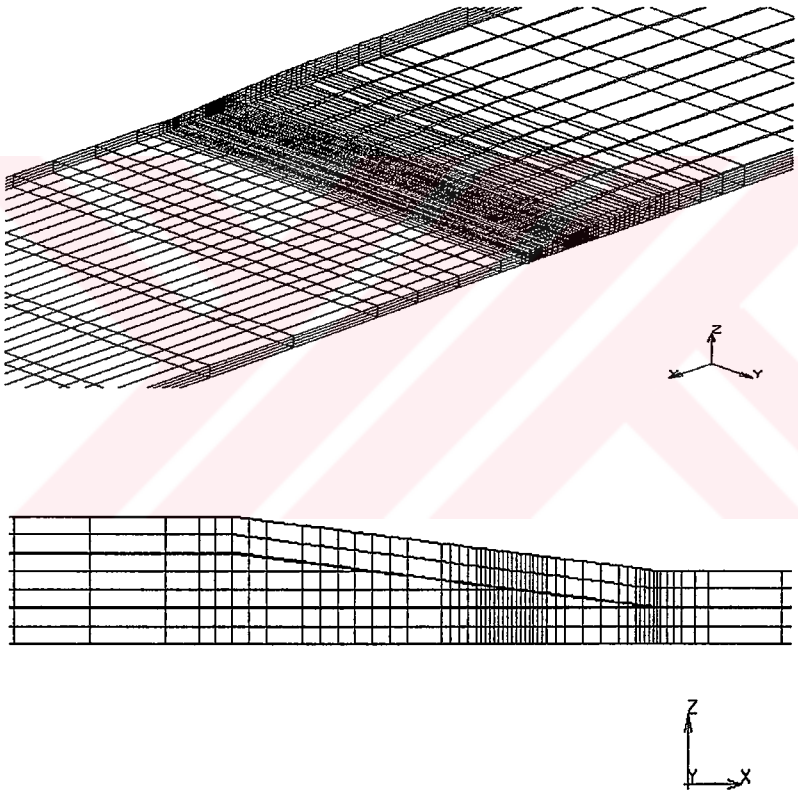

Figure 3.13: Finite Element Mesh at the Tapered Region

Interply resin layers were modeled on the top and bottom of the dropped plies and continues to the whole length. The resin rich pockets were modeled in front of the dropped plies giving the prescribed taper angle. All of the elements except the elements at the tip of resin pockets were 8 noded hexagonal brick elements and the tips of the resin pockets were modeled with 6 noded pentahedral elements. Element type 149 was used for composite elements and element type 7 was used for isotropic elements (interply resin regions and resin rich pockets). Interply resin layers and resin rich pockets at the last ply drop location are shown in Figure 3.14. In the figure the orange coloured regions represent isotropic resin properties and the purple coloured regions represent composite material properties.

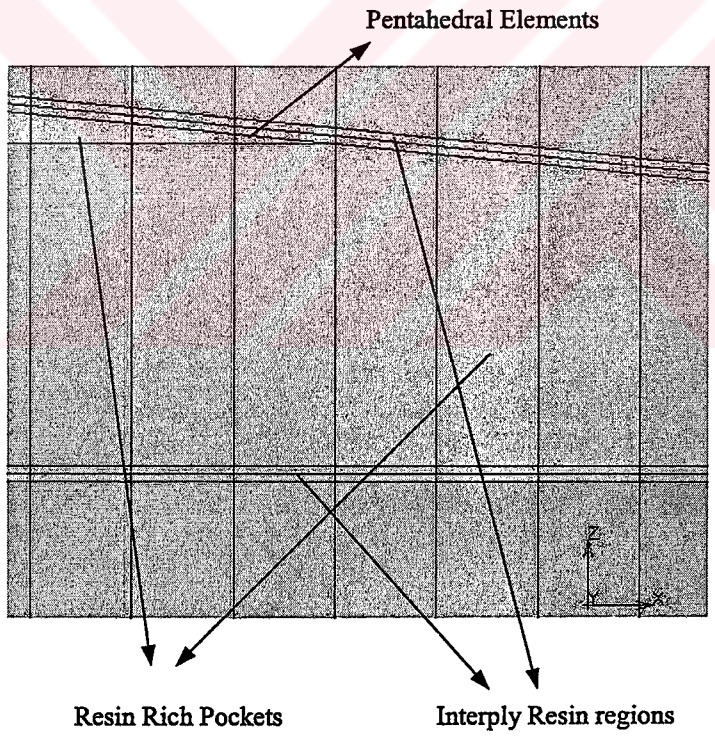

Figure 3.14: Resin Rich Pockets and Interply Resin Regions

3.7 Numerical Results

The finite element models of the tapered laminates were solved for different layup configurations with the described boundary conditions and loading. The model was the same for configurations TL1, TL2, TL3, TL4 and TL5. The orientations of plies were changed within the model to examine the stress states. For configurations TL1-M and TL2-M the model was modified to take into account the migrated 90° plies. Six stress resultants (σ_{xx}, σ_{yy}, σ_{zz}, σ_{xy}, σ_{yz}, σ_{zx}) and equivalent von Mises stresses were taken from the output file of MARC and plotted with MS EXCEL program.

Even though the thick and thin sections were laminated nearly symmetrically, there existed bending due to the geometric eccentricity of the middle planes of the thick and thin sections. The deformed and undeformed shape of the model with a deformation scale factor 1300 is given in Figure 3.15. This type of deformation was seen in all of the configurations.

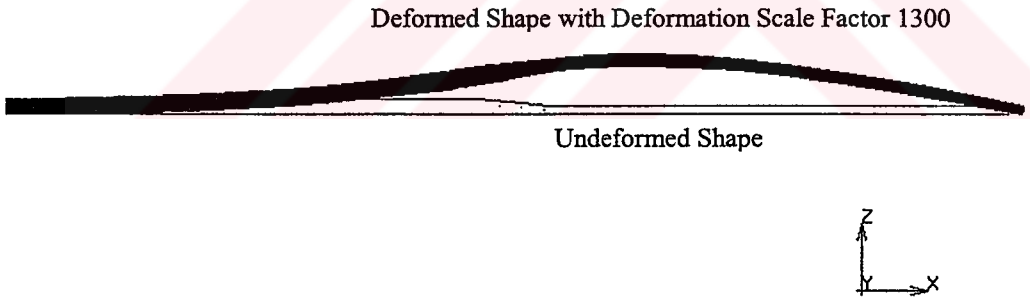

Figure 3.15: Deformed and Undeformed Shape of the Model

It was assumed that critical stresses occur at the tapered region and at the interply resin regions. Also delamination was assumed to be the primary failure mode and to occur in the interply resin layer. As delamination is an out-of-plane failure, out-of-plane stresses and equivalent von Mises stress were investigated throughout the study.

In the elements that are at an angle with respect to longitudinal axis of the specimen, the stresses were rotated so that they are in terms of the local (element) coordinate system. The expression used in this transformation is given in Appendix A.

The results are displayed by location versus stress graphs in the upper and lower interply resin layers at the free edge. The paths used for graphs are shown in Figure 3.16.

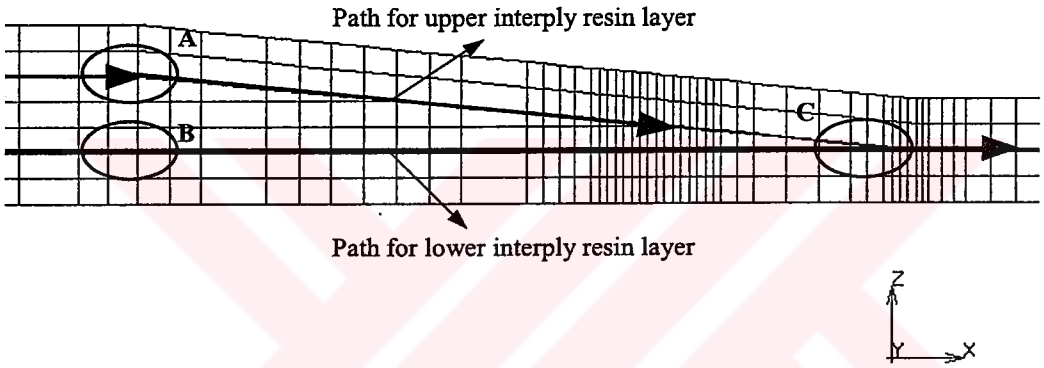

Figure 3.16: The Paths Used for Graphical Representation of Stresses

For graphical representation of stresses, the paths shown in Figure 3.16 was used. In MENTAT post processing, the nodes in the middle of the interply resin layers were used as the node path. Detailed view of the node paths at three different locations A, B, C is given in Figure 3.17.

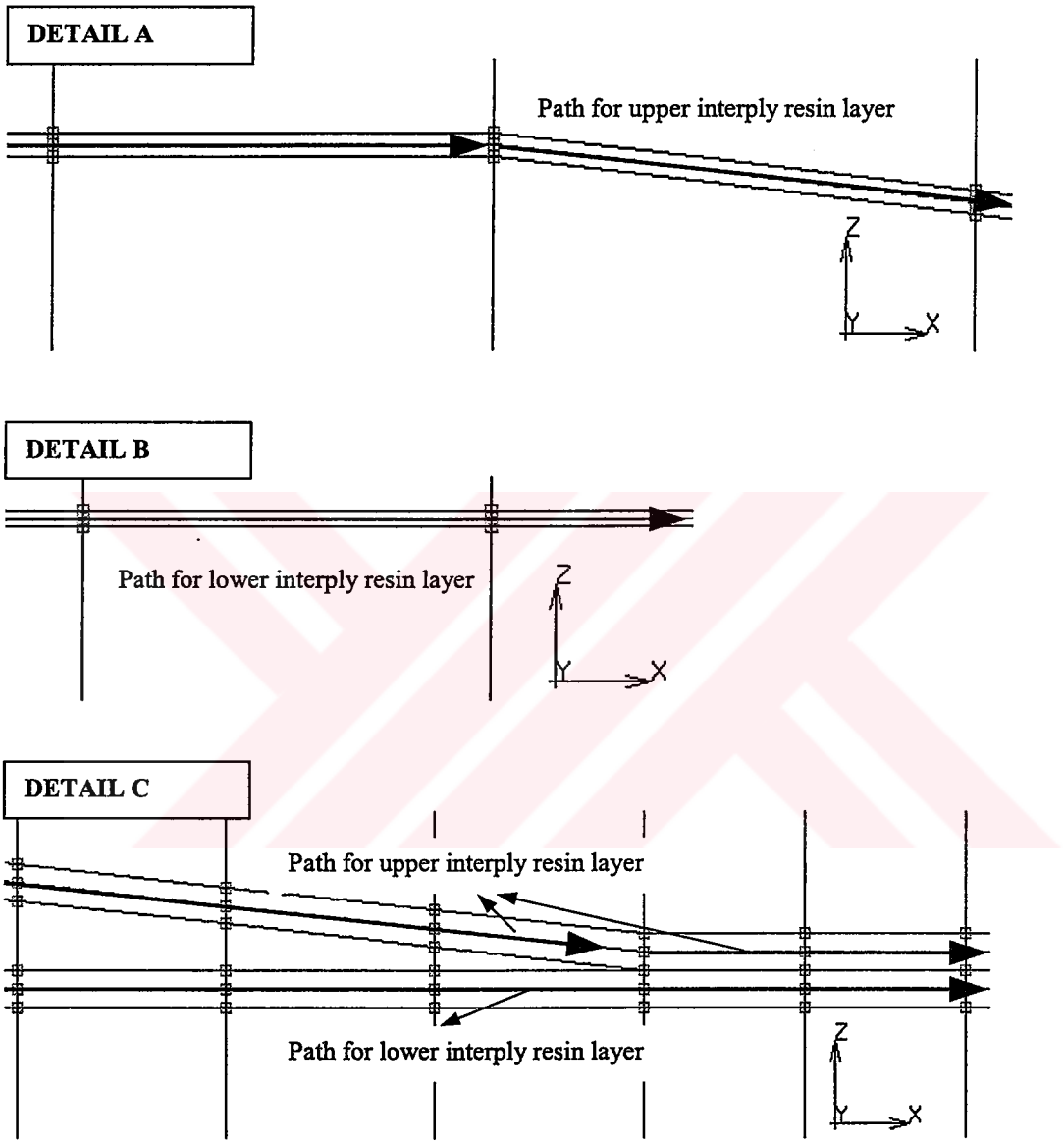

Figure 3.17: Detailed View of the Node Paths

3.7.1 Location of Delamination Onset Site

A failure criterion may be employed to determine the point of failure. Because the primary failure was assumed to be the delamination and occur in the interply resin layer, an isotropic failure criterion would be employed.

In most of the previous studies equivalent von Mises stress was used to locate the delamination onset site and to investigate the stress state of the interply resin layers. [13, 26, 57]

Equivalent von Mises stress considers equally both tensile and compressive values of interlaminar normal stress and in-plane stresses are included as well. Thus, the von Mises stress is a measure of overall stress state for a given configuration and was used to predict the location of the delamination onset site throughout this study.

Equivalent von Mises stress in the upper and lower interply resin layers are plotted and compared. The location of maximum stress was assumed to be the delamination onset site.

3.7.2 Calculation of Delamination Onset Load

There are many approaches to predict delamination onset load for tapered and flat composite structures in literature. In most of the studies average stress concept was used with a polynomial failure criterion. [7, 10, 11, 13, 19, 30, 31, 35, 43, 44]. Polynomial failure criteria such as Tsai-Wu, Hashin were modified and adapted to predict delamination strength of composite laminates.

Analytically weak stress singularities may exist at the free edge of composite laminates due to free edge effect and also in case of tapered

composite laminates with ply drops these singularities are more probable to occur because of material and geometrical discontinuity. These singularities may result as very high values of out-of-plane stresses. Any point stress criterion may be meaningless because of this reason. It is therefore likely that more appropriate approach is an average stress approach.

In average stress concept, failure is assumed to occur when the average stress over some distance, d_0, force the failure criterion above unity. Averaging concept was applied to out-of-plane stresses obtained from finite element model. The average out-of-plane stresses are expressed as

$$\overline{\sigma}_{zz} = \frac{1}{2d_0}\int_{d_0}^{d_0} \sigma_{zz}(x)dx$$

$$\overline{\sigma}_{yz} = \frac{1}{2d_0}\int_{d_0}^{d_0} \sigma_{yz}(x)dx \qquad (3.1)$$

$$\overline{\sigma}_{xz} = \frac{1}{2d_0}\int_{d_0}^{d_0} \sigma_{xz}(x)dx$$

where d_0= Stress Averaging Distance

In previous studies [10, 11, 13, 19, 30, 31, 35, 43, 44] good correlation between experimental and numerical results were obtained by basing strength on interply resin failure and using an interlaminar stress averaging distance of half of a ply thickness. Further increasing the averaging distance may lead to small average stresses and overestimated delamination onset loads. Thus, the smallest possible averaging distance, 0.5 of a ply thickness, which is the dimension, in the x-direction, of the smallest finite element, at the fine mesh region was taken as the averaging distance throughout this study.

Delamination is an out-of-plane failure mode and out-of-plane stresses should be the primary contributors to any delamination strength criteria. Most of the delamination failure criteria investigated in previous studies considers out-of-plane stresses. The most common used delamination failure criteria is the modified Tsai-Wu.

A delamination failure criterion was developed by modifying Tsai-Wu criterion to predict the delamination onset load by Fish and Lee [43]. This criterion was chosen as the delamination failure criterion. The modification of the Tsai-Wu criterion is given in Appendix B. The modified Tsai-Wu criterion is given Equation 3.2.

$$\frac{ZC-ZT}{ZC*ZT}\sigma_{zz}+\frac{1}{ZC*ZT}\sigma_{zz}^2+\frac{1}{S^2}\left[\sigma_{yz}^2+\sigma_{zx}^2\right]=1 \qquad (3.2)$$

where ZT, ZC and S are the through the thickness tensile, compressive and shear strengths, respectively.

Moreover, as σ_{ZZ} terms were negligibly small compared with σ_{YZ} and σ_{ZX} terms, they were removed from the expression. The final form of the delamination criterion became

$$\frac{1}{S^2}\left[\sigma_{yz}^2+\sigma_{zx}^2\right]=1 \qquad (3.3)$$

The average stress concept was applied to out-of-plane stresses with an averaging distance of 0.5 t_{ply}. Delamination failure criterion was then used with average stresses to predict strength based on interply resin failure.

T.C. YÜKSEKÖĞRETİM KURULU
DOKÜMANTASYON

In addition to this quadratic delamination failure criterion, the maximum stress failure criterion was used to predict strength when the out-of-plane stress state is dominated by a single stress component.

As the finite element is linear, the analytical results were easily scaled. The model was loaded with 1 MPa over the end face of thin section. Thus, applying 1 MPa face load over the thin end of the model with an area of 29.16 mm^2 corresponds to 29.160 N load. Failure indexes calculated for this loading condition and a multiplication factor was found to make the failure index 1. This factor is multiplied by 29.16 N and delamination onset load was found. Then stress on the thin section of the laminate is found by dividing the delamination onset load by the area of the thin section. This stress was compared with the experimentally determined stresses.

Through the reminder of this section the configurations TL1, TL2, TL1-M, TL2-M, TL3, TL4 and TL5 were investigated separately. The studied stacking sequences are given in Table 3.3, subscript D indicates the dropped (discontinuous) plies and configurations that considers the migration of fibers in 90^o plies designated with "M".

Table 3.3: Stacking Sequences of Configurations

Configurations	Stacking Sequences
TL1/ TL1-M	$[0_2/90_2/+-45_D/0_{2D}/-+45_D/90_2/0_2]$
TL2/ TL2-M	$[0_2/90_2/+-45_D/+-45_D/-+45_D/90_2/0_2]$
TL3	$[0_2/90/0/+-45_D/0_{2D}/-+45_D/0/90/0_2]$
TL4	$[0_2/90/0/+-45_D/+-45_D/-+45_D/0/90/0_2]$
TL5	$[0_2/90/0/+-45_D/+-45_D/0_{2D}/0/90/0_2]$

3.7.3 FEA of Configuration TL1

FEA results for configuration TL1 were studied to determine delamination onset site and delamination onset load. Equivalent von Mises stress and out-of-plane stresses are plotted in upper and lower interply resin layers in Figure 3.18 and 3.19. Through the rest of this section equivalent von Mises stresses are displayed with the initial capitals (EVMS).

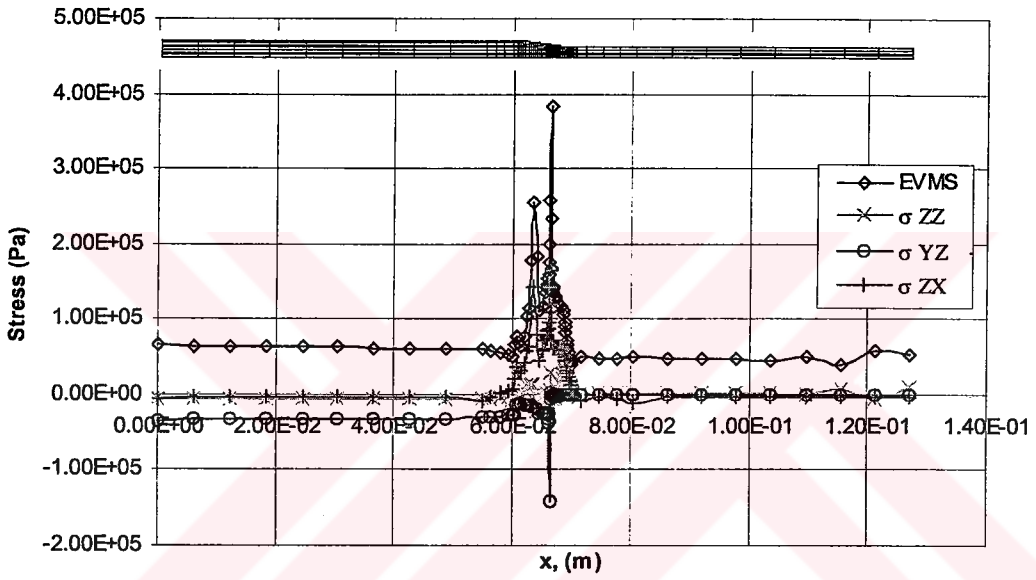

Figure 3.18: Equivalent von Mises Stress and Interlaminar Stresses in Upper Interply Resin Layer Over the Entire Model

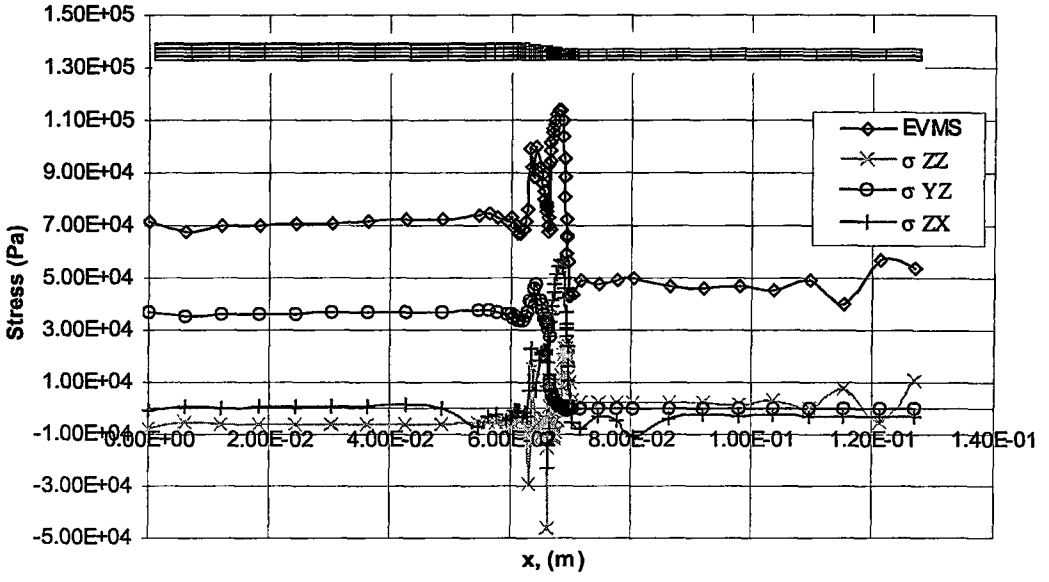

Figure 3.19: Equivalent von Mises Stress and Interlaminar Stresses in Lower Interply Resin Layer Over the Entire Model

It was seen that the stresses away from the tapered regions were approximately constant and small compared with the stresses at the tapered region. Figures 3.18 and 3.19 shows that critical stresses occurred at the tapered region. There was no need to investigate flat regions of the model. Thus, stresses are replotted at the tapered region between locations x=0.059 m and x=0.072 m.

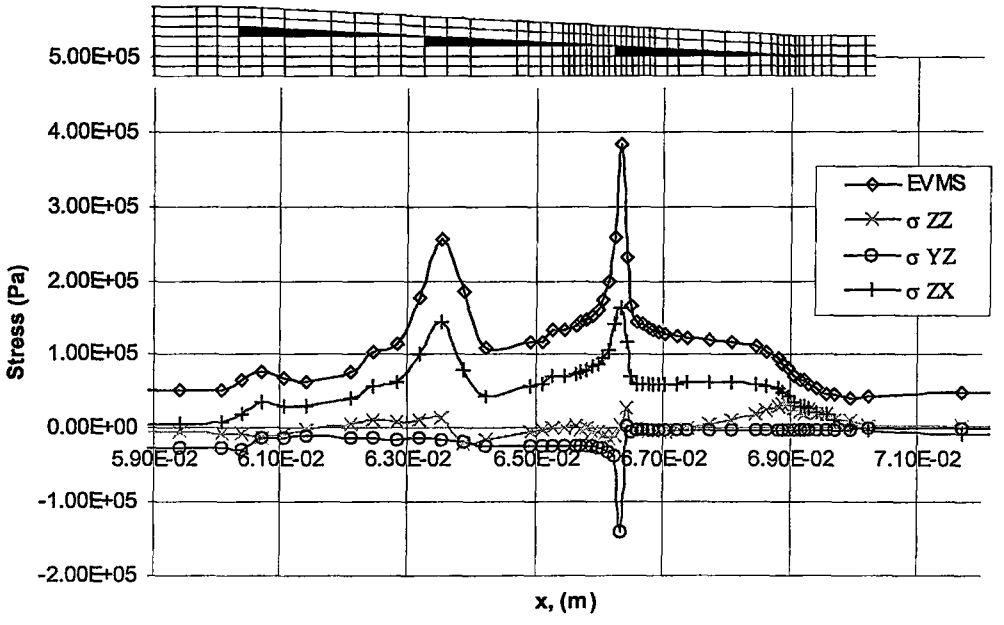

Figure 3.20: Equivalent von Mises Stress and Interlaminar Stresses in Upper Interply Resin Layer Over the Tapered Region

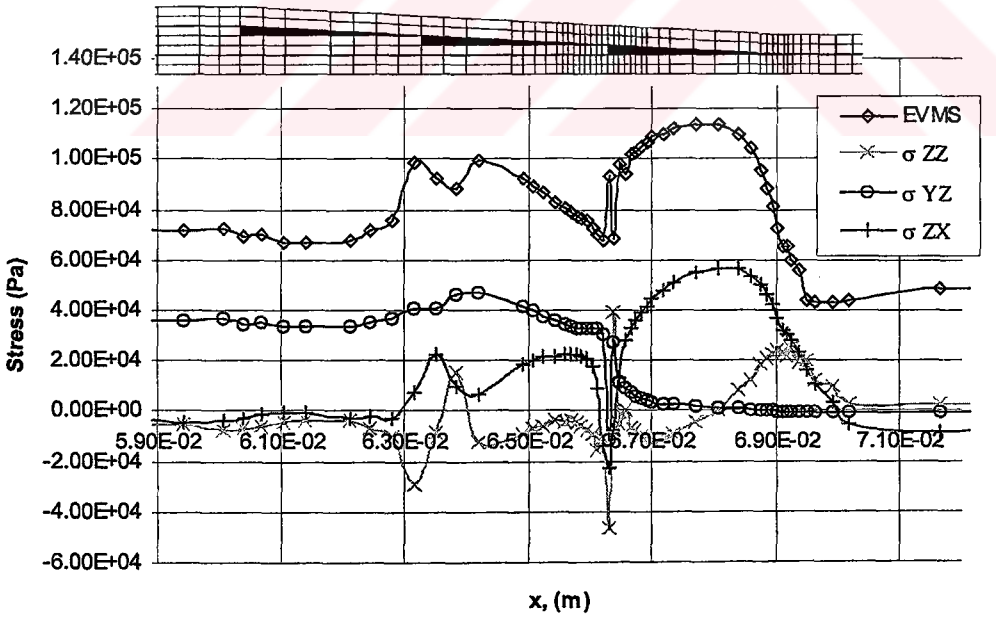

Figure 3.21: Equivalent von Mises Stress and Interlaminar Stresses in Lower Interply Resin Layer Over the Tapered Region

From Figure 3.20 it was observed that the stress state in the upper interply resin layer was dominated by the interlaminar shear stress σ_{ZX}. Interlaminar shear stress started to increase from the beginning of the taper from 0.00835 MPa and made two peaks at the tips of the dropped plies. The first peak was observed at the tip of the middle dropped plies with a value of 0.144 MPa. The second peak was observed at the tip of the last dropped ply with a value of 0.164 MPa. Interlaminar shear stress decreased to very small values just after the root of the taper.

The magnitudes of stresses, σ_{ZZ} and σ_{YZ} in the upper interply resin layer, were small compared with σ_{ZX}. Interlaminar normal stress σ_{ZZ} changed its attitude from compressive to tensile at the beginning of the taper and at the tips of the dropped plies. The maximum value of σ_{ZZ} was observed with a value of 0.0333 MPa at the root of the taper. σ_{YZ} made a peak at the tip of the last dropped ply with a value of –0.142 MPa and remained approximately constant for the rest of the interply resin layer.

From Figure 3.21 it was observed that the magnitudes of the stresses in the lower interply resin layer were considerably less than the stresses in the upper interply resin layer. At the tip of the middle dropped ply it was observed that σ_{ZZ} changed its attitude from compressive to tensile and σ_{ZX} made a small peak while σ_{YZ} remained constant. At the tip of the last dropped ply, σ_{YZ} and σ_{ZX} made a peak from a positive value to a negative value and became positive again. σ_{ZZ} made a sharp fluctuation from compressive to tensile and became compressive again then increased gradually making a peak at the root of the taper. The maximum stress was observed in σ_{ZX} between the last dropped ply and root of the taper with a value of 0.0569 MPa.

To predict the location of the delamination onset site equivalent von Mises stress was plotted for upper and lower interply resin at the tapered region layers in Figure 3.22.

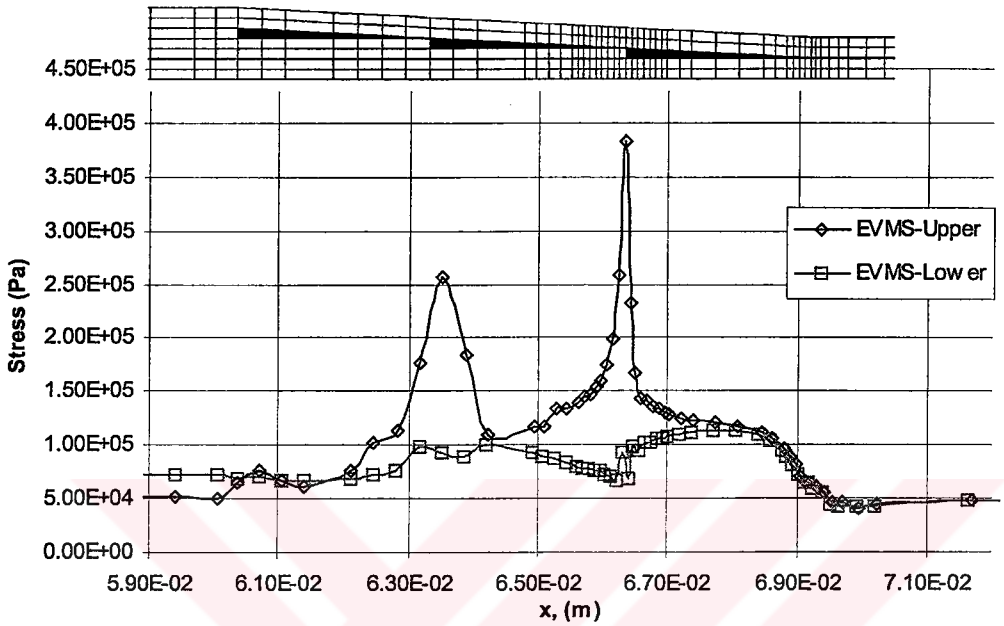

Figure 3.22: Equivalent von Mises Stresses in Upper and Lower Interply Resin Layers Over the Tapered Region

Maximum Equivalent Von Mises stress obtained as 0.383 MPa in the upper interply resin layer at x=0.0663 m. Thus, the location of delamination site for configuration TL1 was predicted at x=0.0663 m, in the upper interply resin layer, at the tip of the last dropped ply. The location is shown in Figure 3.23.

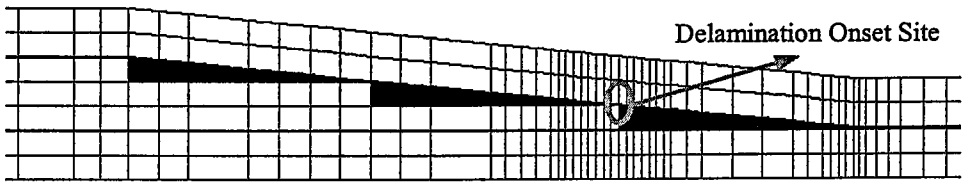

Figure 3.23: Predicted Delamination Onset Site for Configuration TL1

To calculate delamination onset load, interlaminar stresses were investigated at the predicted delamination onset site. Stress versus location plots are rescaled and marked for nodal values in Figure 3.24. Average stress concept was applied with an averaging distance of 0.5 t_{ply} by taking arithmetic mean of stresses at three data points.

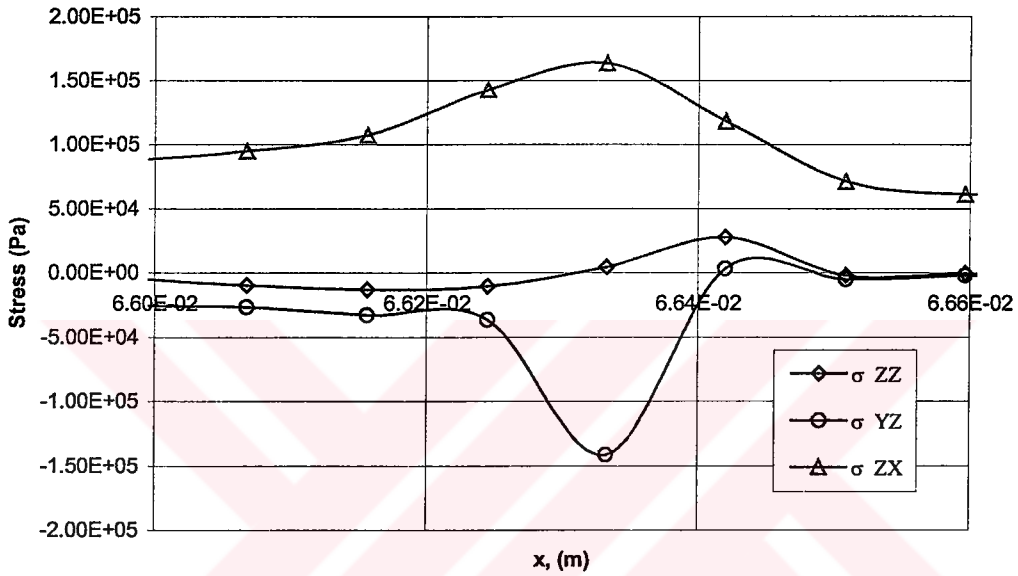

Figure 3.24: Interlaminar Stresses at the Predicted Delamination Onset Site

It was observed that σ_{ZZ} was negligibly small compared with σ_{YZ} and σ_{ZX}. The terms containing σ_{ZZ} terms had already been removed from the proposed delamination failure criterion. By applying the average stress concept and using the modified Tsai-Wu as delamination criterion, the predicted delamination onset load for configuration TL1 calculated as 17.890 kN which corresponds to 613 MPa stress on the thin section of the model.

Additionally maximum stress criterion was applied to interlaminar shear stress, σ_{ZX} without using an averaging concept. The predicted

delamination onset load for configuration TL1 was calculated as 16.713 kN which corresponds to a stress of 573 MPa on the thin section of the model.

The analysis of the configuration TL1 summarized in Table 3.4.

Table 3.4: Results of FEA of Configuration TL1

Delamination Onset Location	In the upper interply resin layer At the end of last dropped ply (±45°)	
Calculated Values	**Delamination Onset Load (kN)**	**Delamination Onset Stress based on thin section of the model (MPa)**
Delamination Failure Criterion	17.890	613
Maximum Stress Criterion	16.713	573

3.7.4 FEA of Configuration TL2

FEA results for configuration TL2 were studied to determine delamination onset site and delamination onset load. Equivalent Von Mises stress and out-of-plane stresses are plotted in upper and lower interply resin layers in Figure 3.25 and 3.26.

As in configuration TL1 the stresses away from the tapered regions were approximately constant and critical stresses were attained at the tapered region. Thus, stresses are replotted at the tapered region between locations x=0.059 m and x=0.072 m in Figures 3.27 and 3.28.

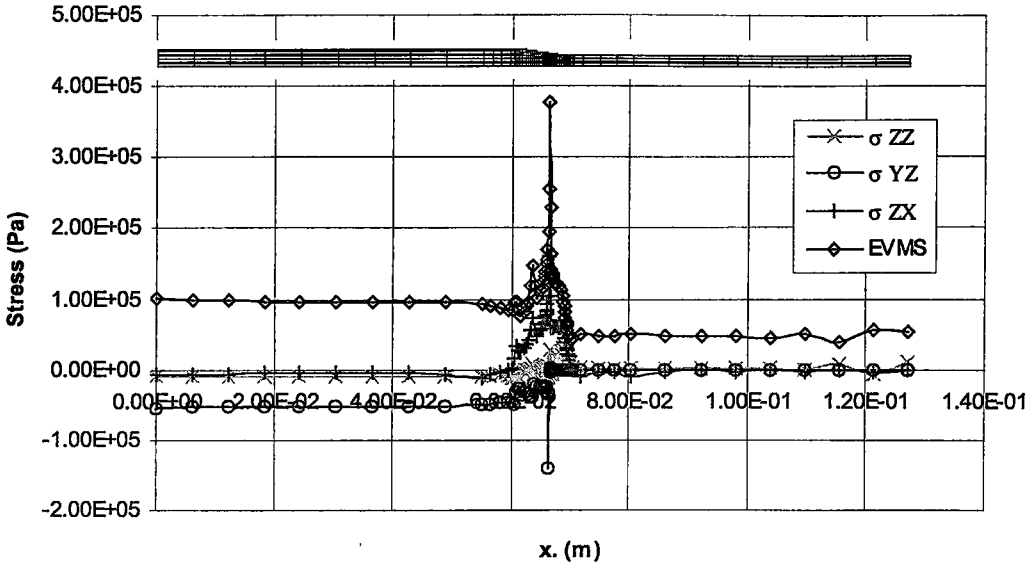

Figure 3.25: Equivalent von Mises Stress and Interlaminar Stresses in Upper Interply Resin Layer Over the Entire Model

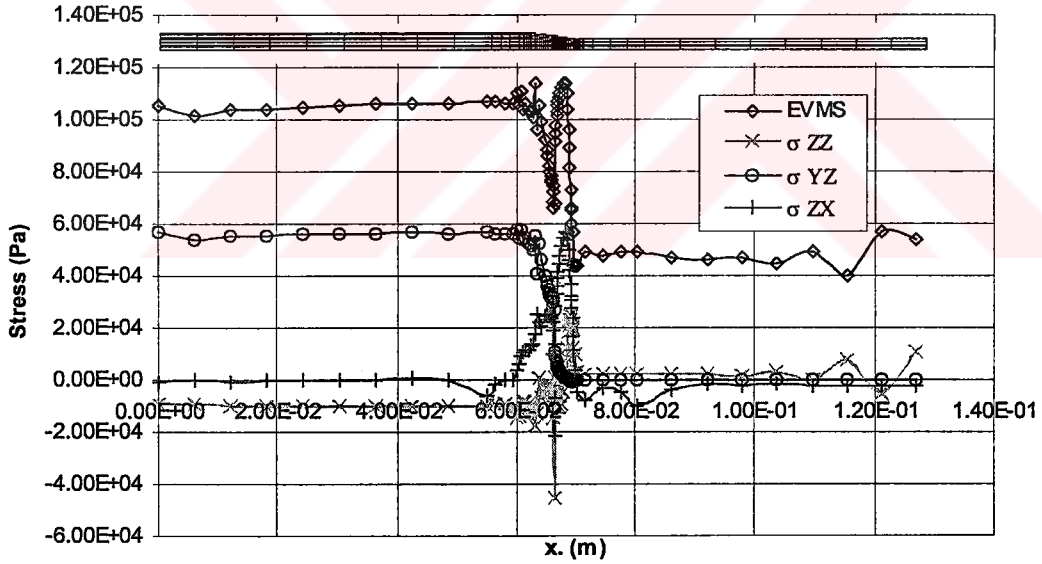

Figure 3.26: Equivalent von Mises Stress and Interlaminar Stresses in Lower Interply Resin Layer Over the Entire Model

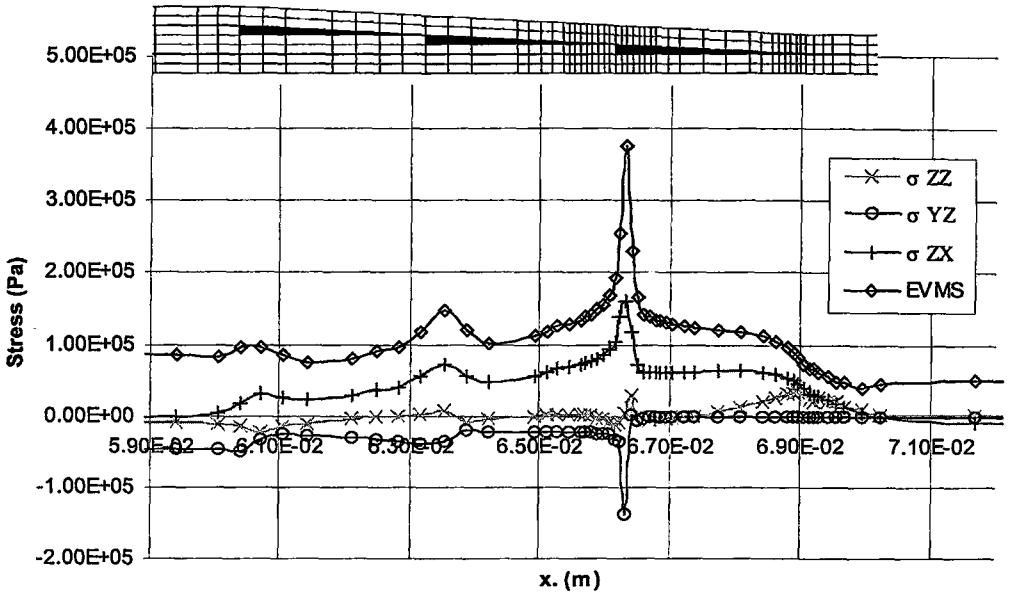

Figure 3.27: Equivalent von Mises Stress and Interlaminar Stresses in Upper Interply Resin Layer Over the Tapered Region

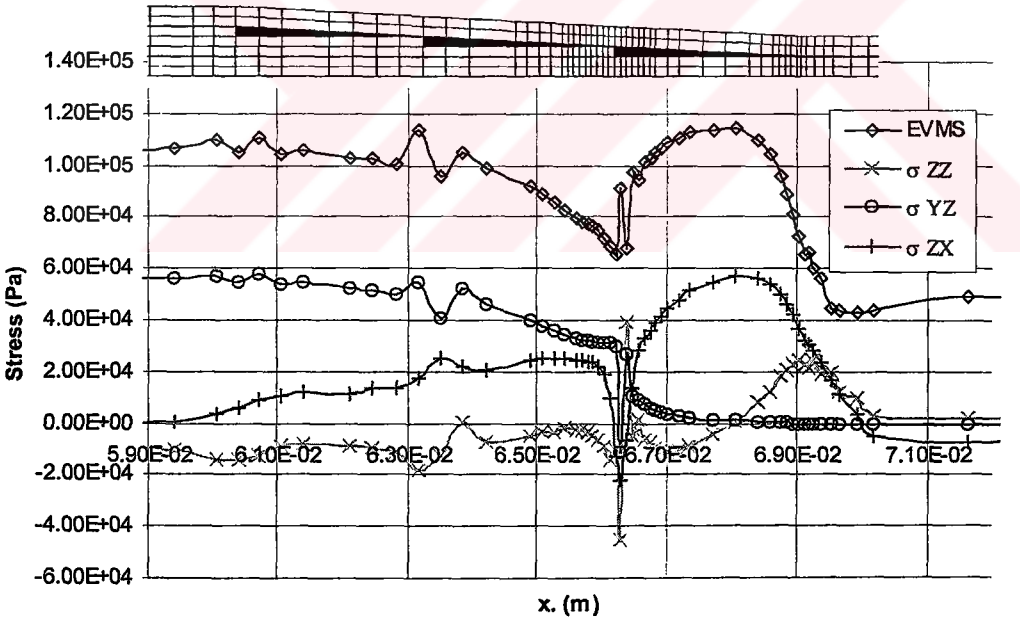

Figure 3.28: Equivalent von Mises Stress and Interlaminar Stresses in Lower Interply Resin Layer Over the Tapered Region

From Figure 3.27 it was observed that the stress state in the upper interply resin layer was dominated by the interlaminar shear stress σ_{ZX} as in configuration TL1. Interlaminar shear stress started to increase from the beginning of the taper from 0.00344 MPa and showed a similar behaviour as in TL1 with a peak value of 0.0723 MPa at the tip of the middle dropped plies and 0.161 MPa at the tip of the last dropped plies.

The magnitudes of stresses σ_{ZZ} and σ_{YZ} in the upper interply resin layer were small compared with σ_{ZX} as in configuration TL1. Interlaminar normal stress σ_{ZZ} changed its attitude from compressive to tensile at the beginning of the taper and at the tips of the dropped plies. The maximum value of σ_{ZZ} was observed with a value of 0.0395 MPa at the root of the taper. σ_{YZ} made a peak at the tip of the last dropped ply with a value of –0.139 MPa and remained approximately constant for the rest of the interply resin layer.

From Figure 3.28 it was observed that the magnitudes of the stresses in the lower interply resin layer were considerably less than the stresses in the upper interply resin layer as in configuration TL1. At the tip of the middle dropped ply it was observed that σ_{ZZ} changed its attitude from compressive to tensile and σ_{ZX} and σ_{YZ} made a small peak. At the tip of the last dropped ply, σ_{YZ} and σ_{ZX} made a peak from positive to negative value instantaneously and became positive again. σ_{ZZ} made a sharp fluctuation from compressive to tensile and became compressive again then increased gradually making a peak at the root of the taper. The maximum stress was observed in σ_{ZX} between the last dropped ply and root of the taper with a value of 0.0568 MPa.

Equivalent von Mises stress was plotted for upper and lower interply resin at the tapered region layers in Figure 3.29.

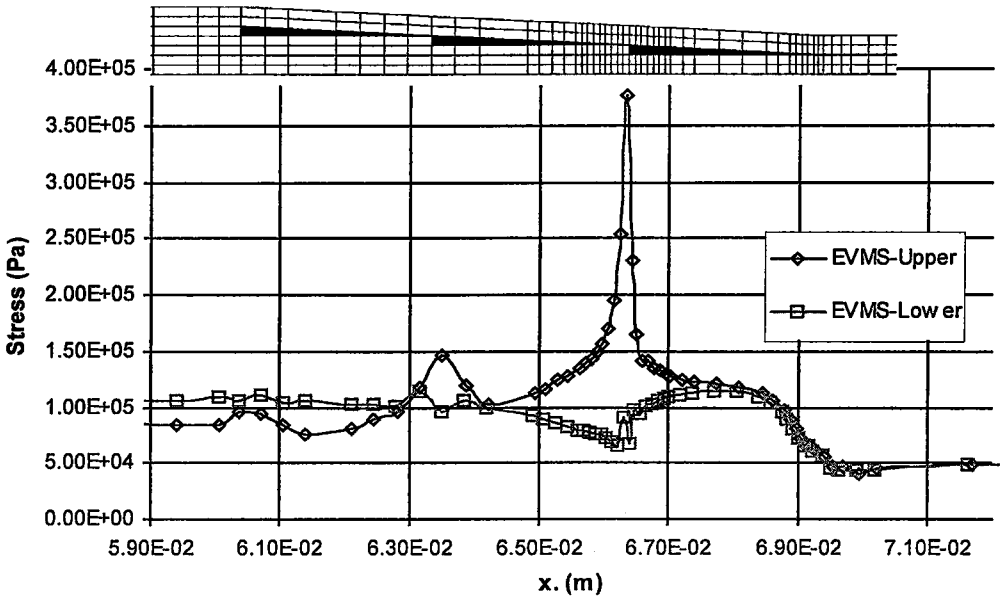

Figure 3.29: Equivalent von Mises Stresses in Upper and Lower Interply Resin Layers Over the Tapered Region

Maximum equivalent von Mises stress reached a value of 0.377 MPa in the upper interply resin layer at x=0.0663 m. Thus, the location of delamination site for configuration TL2 was predicted at x=0.0663 m, in the upper interply resin layer, at the tip of the last dropped ply. The location is shown in Figure 3.30.

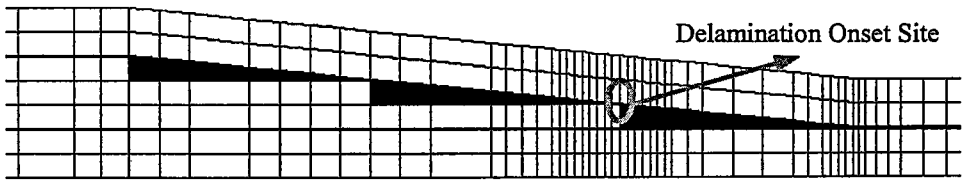

Figure 3.30: Predicted Delamination Onset Site for Configuration TL2

To calculate delamination onset load, interlaminar stresses were investigated at the predicted delamination onset site. Stress versus location plots are rescaled and marked for nodal values in Figure 3.31.

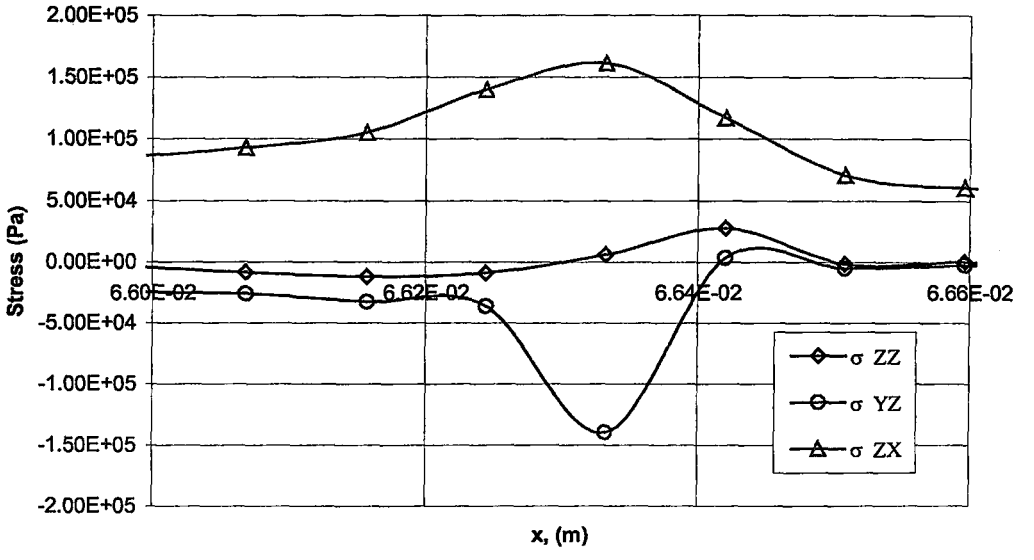

Figure 3.31: Interlaminar Stresses at the Predicted Delamination Onset Site

Applying the average stress concept and using the modified Tsai-Wu as delamination criterion, the predicted delamination onset load for configuration TL2 calculated as 18.197 kN which corresponds to 624 MPa stress on the thin section of the model.

Maximum stress criterion was applied to interlaminar shear stress, σ_{ZX} without using an averaging concept. The predicted delamination onset load for configuration TL2 was calculated as 17.025 kN which corresponds to a stress of 584 MPa on the thin section of the model.

The analysis of the configuration TL2 summarized in Table 3.5.

Table 3.5: Results of FEA of Configuration TL2

Delamination Onset Location	In the upper interply resin layer At the end of last dropped ply	
Calculated Values	**Delamination Onset Load (kN)**	**Delamination Onset Stress based on thin section of the model (MPa)**
Delamination Failure Criterion	18.197	624
Maximum Stress Criterion	17.025	584

3.7.5 FEA of Configurations TL1-M and TL2-M

FEA results for configuration TL1-M and TL2-M were studied to determine delamination onset site and delamination onset load. TL1-M and TL2-M configurations have the same layup as TL1 and TL2 respectively. In the analysis of TL1-M and TL2-M configurations it was assumed that the resin pockets in front of the dropped plies were filled with the migrated fibers of 90° plies. Thus the tapered model was modified by replacing the isotropic resin pockets with 90° plies.

For TL1-M and TL2-M configurations, the behavior of interlaminar stresses and the delamination onset location were the same as configurations TL1 and TL2 respectively. Very small reductions in magnitudes of stresses and delamination onset loads due to fiber migration were observed. Because of this reason, only plots of interlaminar stresses at the predicted delamination onset site are given in Figure 3.32 and 3.33 for configurations TL1-M and TL2-M.

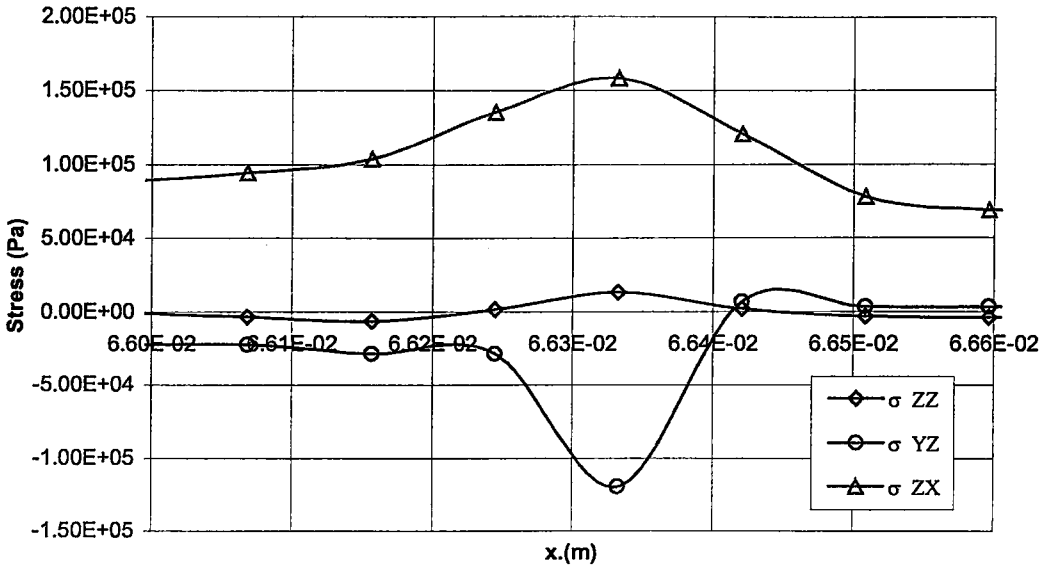

Figure 3.32: Interlaminar Stresses at the Predicted Delamination Onset Site for Configuration TL1-M

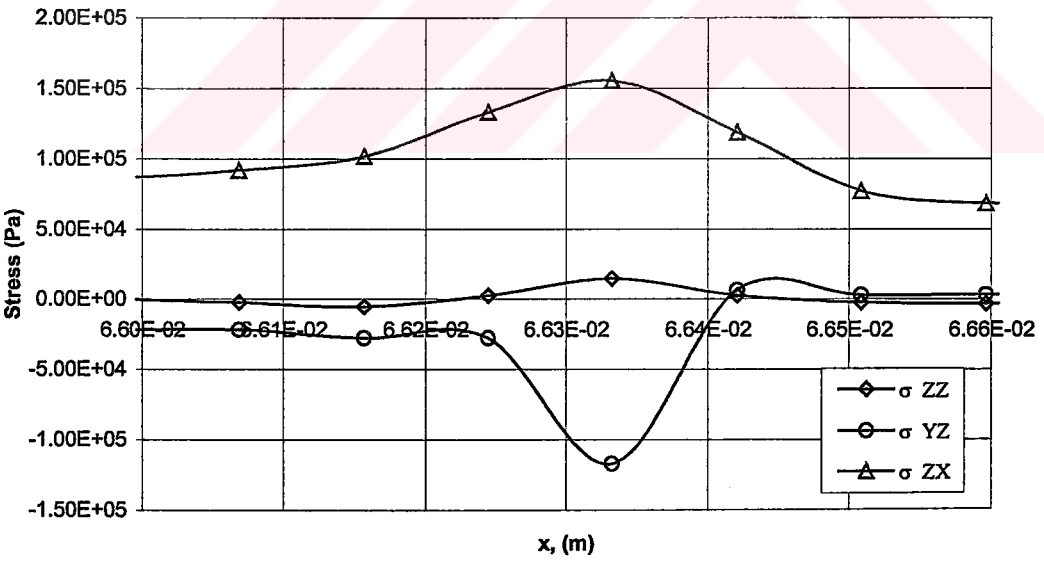

Figure 3.33: Interlaminar Stresses at the Predicted Delamination Onset Site for Configuration TL2-M

Interlaminar stresses were investigated at the predicted delamination onset site to calculate delamination onset loads and stresses. Values calculated by using the delamination failure criterion and maximum stress criterion, for configurations TL1-M and TL2-M are given in Table 3.6.

Table 3.6: Results of FEA of Configuration TL1-M and TL2-M

Delamination Onset Location	In the upper interply resin layer At the end of last dropped ply			
Calculated Values	**Delamination Onset Load (kN)**		**Delamination Onset Stress based on thin section of the model (MPa)**	
	TL1-M	**TL2-M**	**TL1-M**	**TL2-M**
Delamination Failure Criterion	18.728	19.093	642	655
Maximum Stress Criterion	17.239	17.571	591	602

3.7.6 FEA of Configuration TL3

FEA results for configuration TL3 were studied to determine delamination onset site and delamination onset load. Equivalent Von Mises stress and out-of-plane stresses are plotted in upper and lower interply resin layers in Figure 3.34 and 3.35.

Figures 3.34 and 3.35 show that critical stresses were attained at the tapered region. To observe the stress state at the tapered region, stresses are replotted between locations x=0.059 m and x=0.072 m.

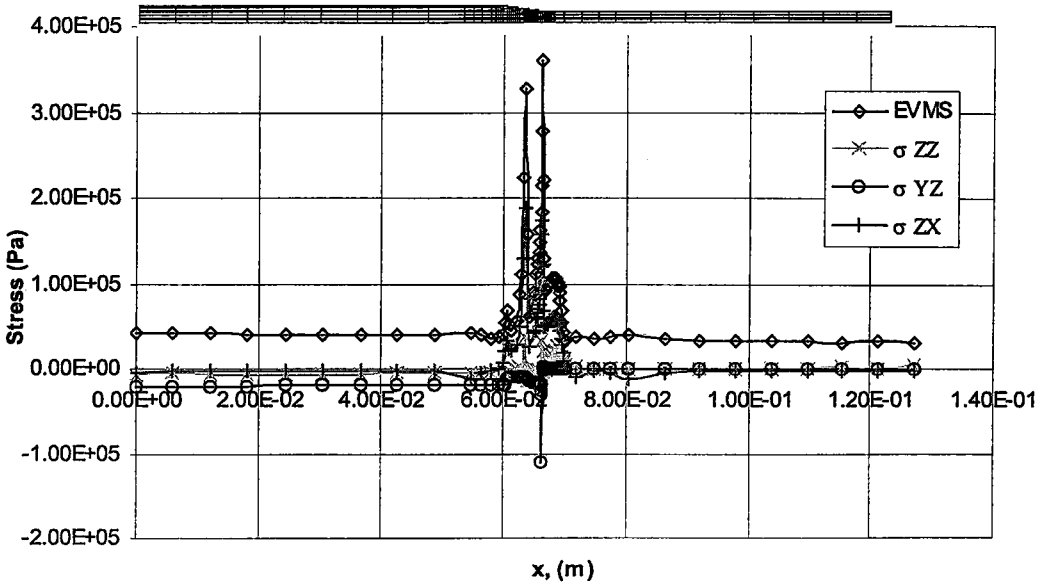

Figure 3.34: Equivalent von Mises Stress and Interlaminar Stresses in Upper Interply Resin Layer Over the Entire Model

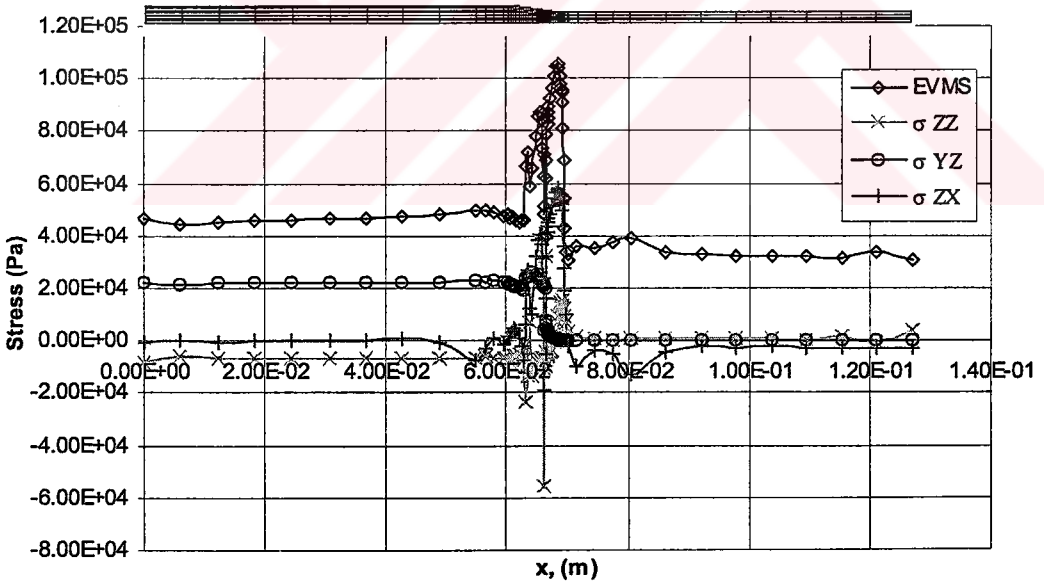

Figure 3.35: Equivalent von Mises Stress and Interlaminar Stresses in Lower Interply Resin Layer Over the Entire Model

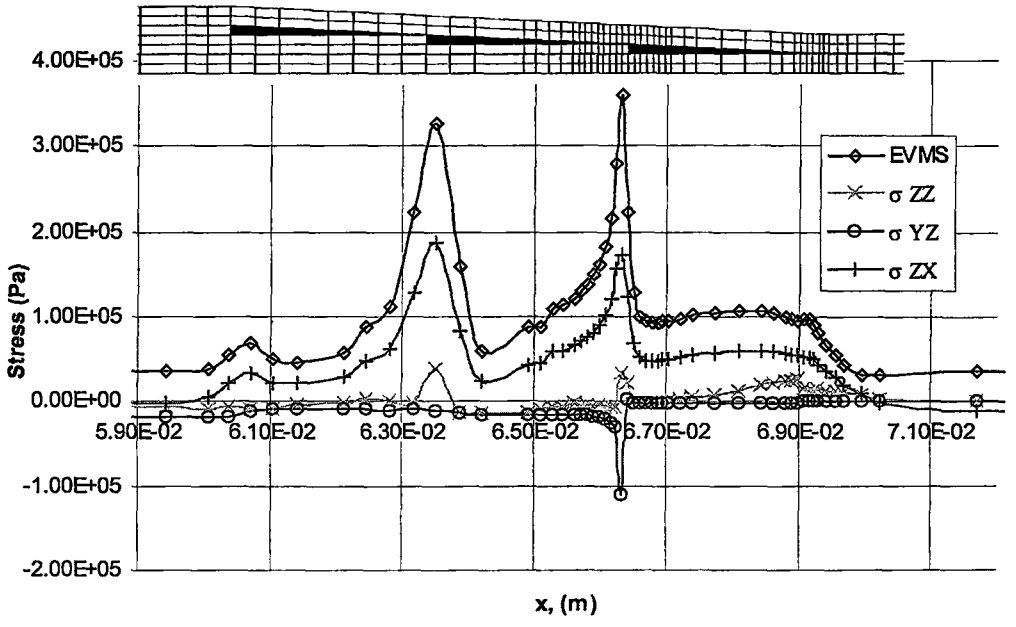

Figure 3.36: Equivalent von Mises Stress and Interlaminar Stresses in Upper Interply Resin Layer Over the Tapered Region

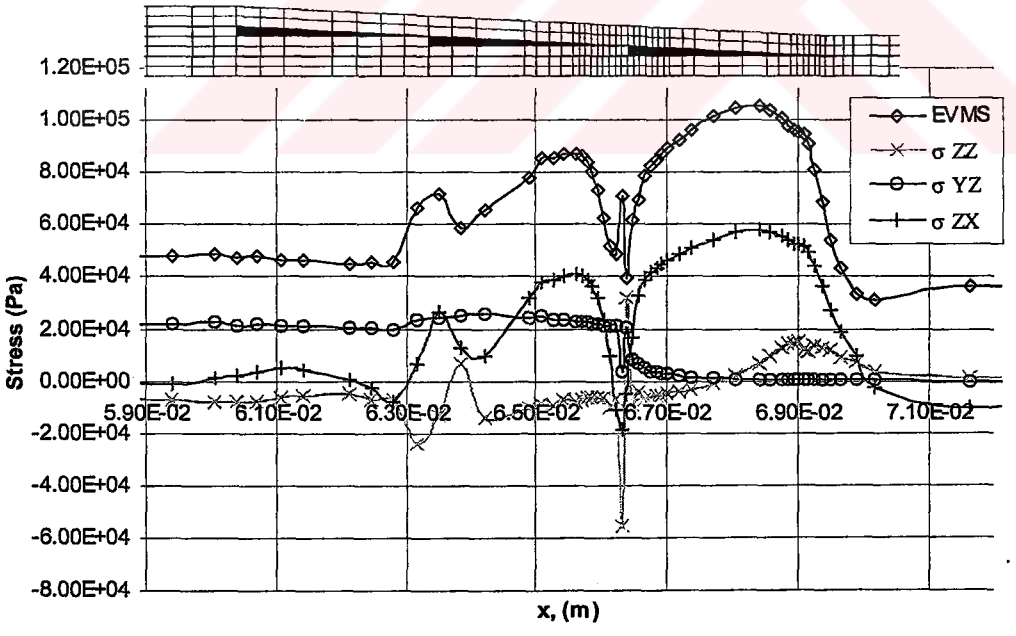

Figure 3.37: Equivalent von Mises Stress and Interlaminar Stresses in Lower Interply Resin Layer Over the Tapered Region

The stress state in the upper interply resin layer was dominated by the interlaminar shear stress, σ_{ZX}. Interlaminar shear stress started to increase from the beginning of the taper from 0.00620 MPa and made two peaks at the tips of the dropped plies. The first peak was observed at the tip of the middle dropped plies with a value of 0.188 MPa. The second peak was observed at the tip of the last dropped ply with a value of 0.174 MPa. Different from the configurations TL1 and TL2, the maximum value of σ_{ZX} was observed at the tip of the middle dropped ply. Interlaminar shear stress decreased to very small values just after the root of the taper.

The magnitudes of stresses σ_{ZZ} and σ_{YZ} in the upper interply resin layer were small compared to σ_{ZX}. Interlaminar normal stress σ_{ZZ} showed little variation through the tip of middle dropped ply. At this location, σ_{ZZ} made an instantaneous peak from compressive to tensile with a peak value of 0.0374 MPa. The same behavior was seen at the tip of the last ply drop with a peak value of 0.0333 MPa. It then increased gradually making another peak at the root of the taper with a value of 0.0258 MPa. The maximum value of σ_{ZZ} was observed at the tip of the middle dropped ply whereas the location for maximum σ_{ZZ} was the root of the taper for configurations TL1 and TL2. σ_{YZ} showed a similar behavior as in configurations TL1 and TL2 making a peak at the tip of the last dropped ply with a value of –0.111 MPa and remained approximately constant for the rest of the interply resin layer.

For TL1 configuration magnitudes of the stresses in the lower interply resin layer were considerably less than the stresses in the upper interply resin layer as in configurations TL1 and TL2. At the tip of the middle dropped ply it was observed that σ_{ZZ} and σ_{ZX} changed attitude from compressive to tensile and σ_{YZ} slightly increased. At the tip of the last dropped ply, σ_{ZX} made a peak from positive to negative value instantaneously and became positive again. σ_{ZZ}

made a sharp fluctuation from compressive to tensile and became compressive again then increased gradually making a peak at the root of the taper. σ_{YZ} remained positive through the lower interply layer. At the tip of the last dropped ply σ_{YZ} dropped suddenly from 0.0211 MPa to 0.00359 then returned back to 0.0204 MPa. σ_{YZ} decreased gradually to a very small value just in front of the last dropped ply. The maximum stress was observed in σ_{ZX} between the last dropped ply and root of the taper with a value of 0.0579 MPa.

To predict the location of the delamination onset site equivalent von Mises stress is plotted for upper and lower interply resin at the tapered region layers in Figure 3.38.

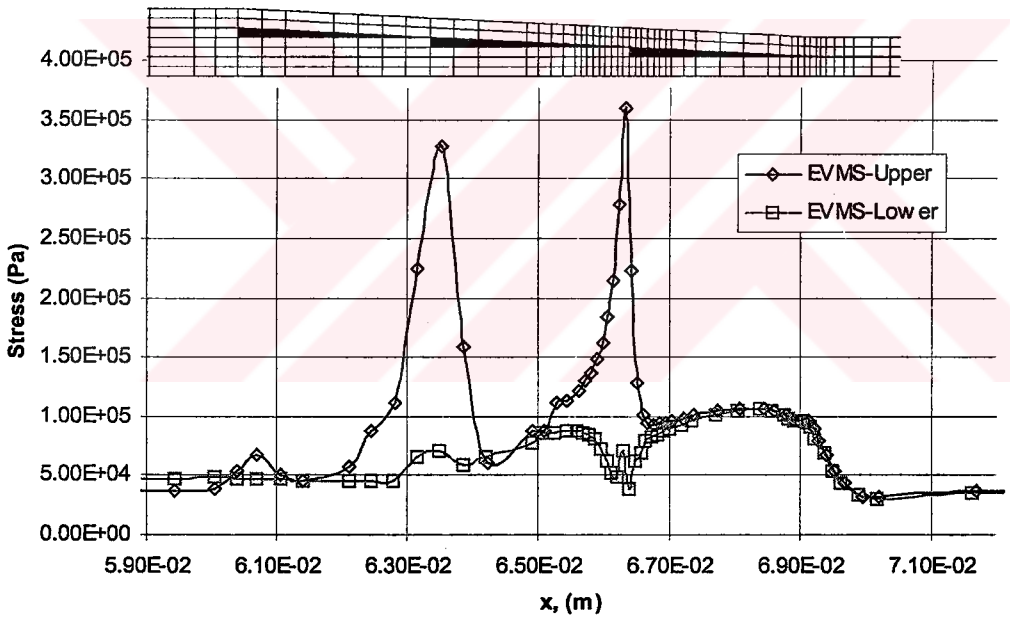

Figure 3.38: Equivalent von Mises Stresses in Upper and Lower Interply Resin Layers Over the Tapered Region

Maximum equivalent von Mises stress value attained was 0.360 MPa in the upper interply resin layer at x=0.0663 m. Also at x =0.0635 a value of 0.327 MPa was observed and at this location the dominant stress state, σ_{ZX},

was maximum. Although the magnitudes of the stresses were close to each other, sticking with the proposed criterion, the location of delamination site for configuration TL3 was predicted at x=0.0663 m, in the upper interply resin layer, at the tip of the last dropped ply. The location is shown in Figure 3.39.

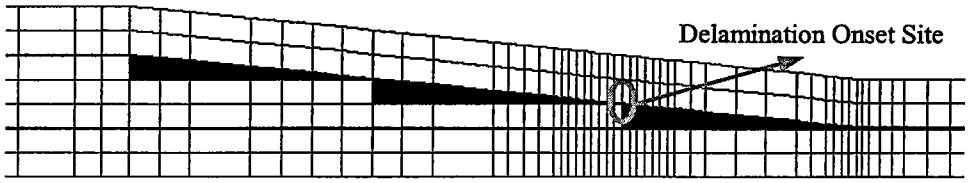

Figure 3.39: Predicted Delamination Onset Site for Configuration TL3

Delamination onset load was calculated using the interlaminar stresses at the predicted delamination onset site. Rescaled stress versus location plot is given in Figure 3.40.

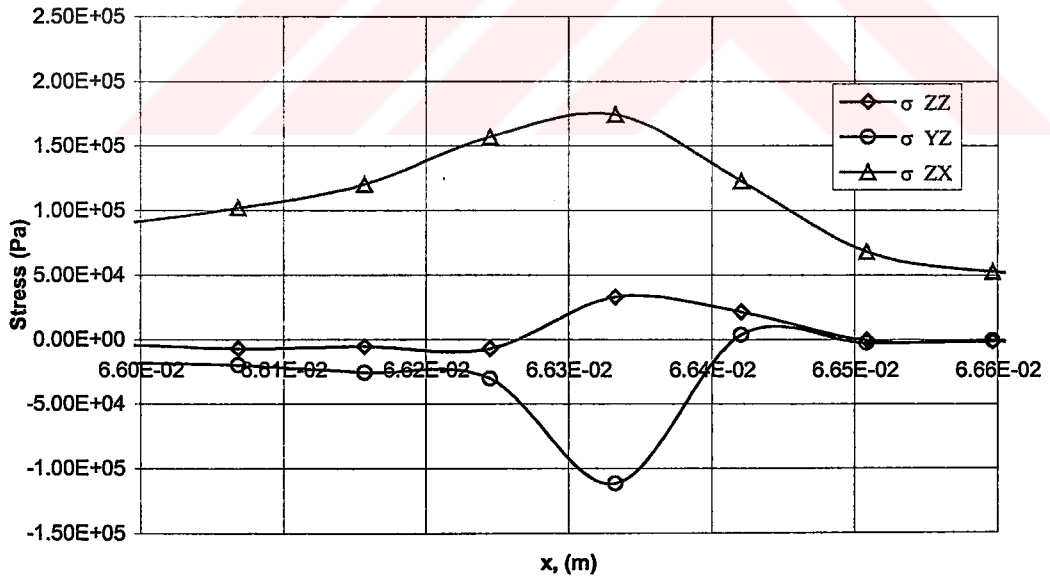

Figure 3.40: Interlaminar Stresses at the Predicted Delamination Onset Site

Average stress concept used with the modified Tsai-Wu delamination criterion and maximum stress criterion was applied to σ_{ZX}. The predicted delamination onset loads and stresses for configuration TL3 are given in Table 3.7.

Table 3.7: Results of FEA of Configuration TL3

Delamination Onset Location	In the upper interply resin layer At the end of last dropped ply	
Calculated Values	**Delamination Onset Load (kN)**	**Delamination Onset Stress based on thin section of the model (MPa)**
Delamination Failure Criterion	17.333	594
Maximum Stress Criterion	15.746	540

3.7.7 FEA of Configuration TL4

FEA results for configuration TL4 were studied to determine delamination onset site and delamination onset load. Equivalent von Mises stress and out-of-plane stresses are plotted in upper and lower interply resin layers in Figure 3.41 and 3.42.

Critical stresses appeared at the tapered region for configuration TL4 like other configurations. Figures 3.43 and 3.44 were plotted to investigate the stress state at the tapered region, between locations x=0.059 m and x=0.072 m.

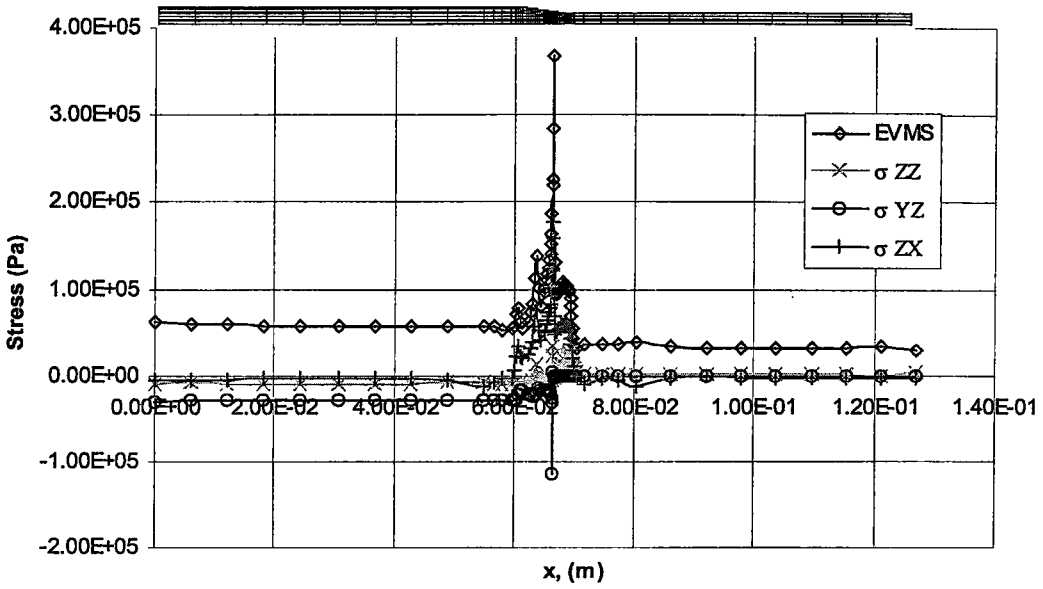

Figure 3.41: Equivalent Von Mises Stress and Interlaminar Stresses in Upper Interply Resin Layer Over the Entire Model

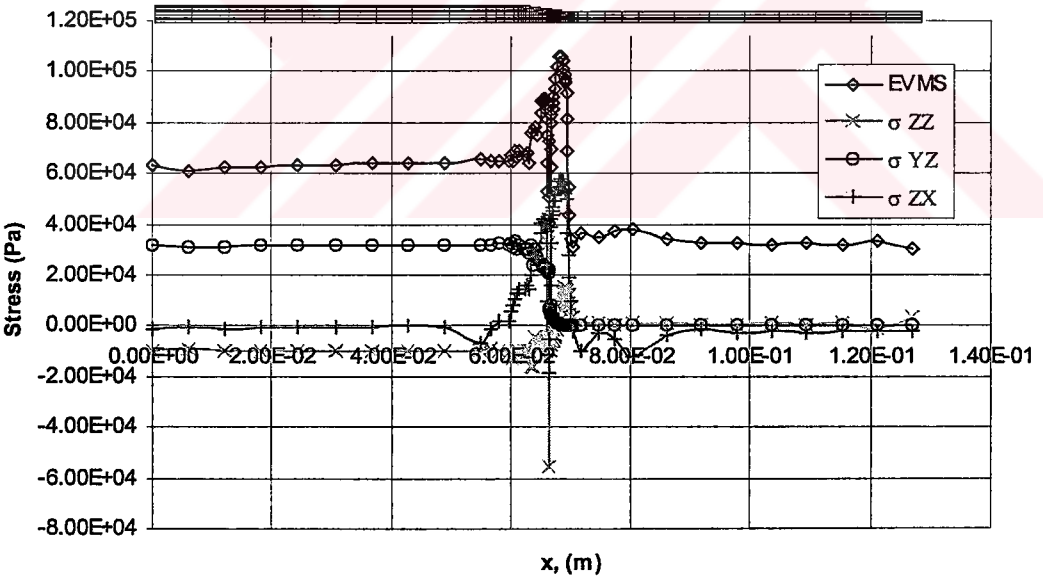

Figure 3.42: Equivalent Von Mises Stress and Interlaminar Stresses in Lower Interply Resin Layer Over the Entire Model

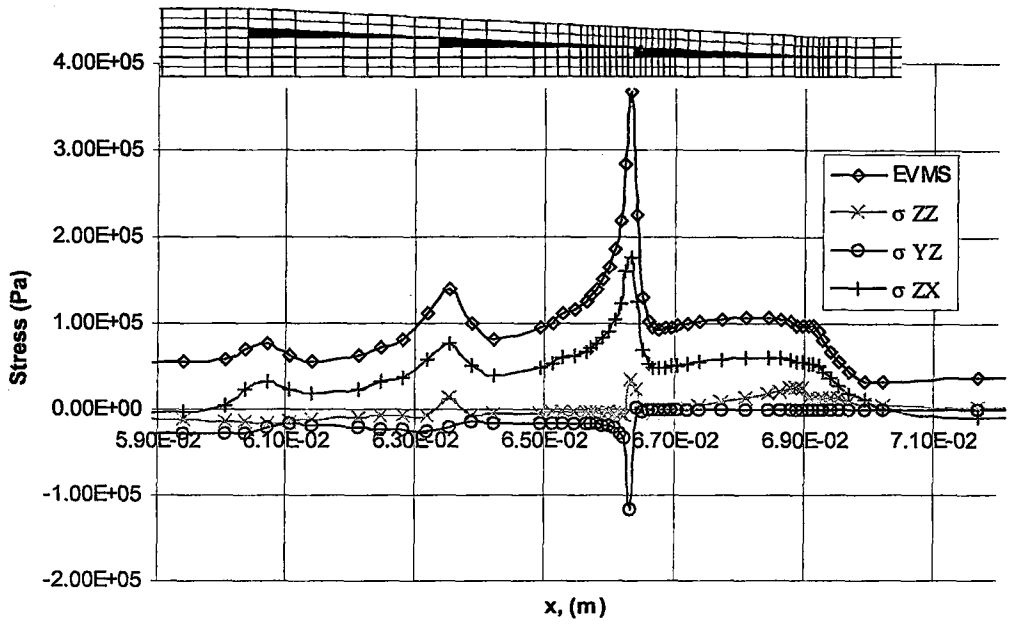

Figure 3.43: Equivalent Von Mises Stress and Interlaminar Stresses in Upper Interply Resin Layer Over the Tapered Region

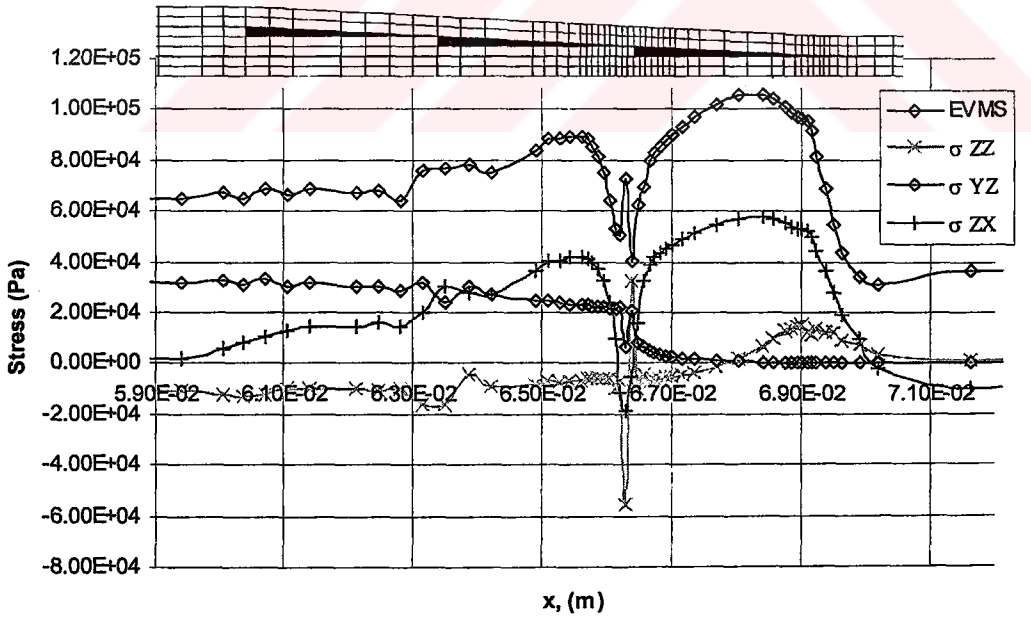

Figure 3.44: Equivalent von Mises Stress and Interlaminar Stresses in Lower Interply Resin Layer Over the Tapered Region

For the configuration TL4 the stress state in the upper interply resin layer was dominated by the interlaminar shear stress σ_{ZX} like other configurations. Interlaminar shear stress started to increase from the beginning of the taper from 0.00510 MPa and made two peaks at the tips of the dropped plies. The first peak was observed at the tip of the middle dropped plies with a value of 0.0758 MPa. The second peak was observed at the tip of the last dropped ply with a value of 0.177 MPa. The first peak was small compared with the second one whereas in configuration TL3 it was the opposite. The maximum value of σ_{ZX} was observed at the tip of last dropped ply. Interlaminar shear stress decreased to very small values just after the root of the taper.

The magnitudes of stresses σ_{ZZ} and σ_{YZ} in the upper interply resin layer were small again as in configuration TL3 compared with σ_{ZX}. Interlaminar normal stress σ_{ZZ} showed a similar behavior as in TL3 with a peak value of 0.0128 MPa at the tip of the middle dropped plies, 0.0344 MPa at the tip of the last dropped plies and 0.0259 MPa at the root of the taper. The maximum value of σ_{ZZ} was observed at the tip of the last dropped ply whereas the location for maximum σ_{ZZ} was at the tip of the middle dropped ply for configuration TL3. σ_{YZ} showed a similar behavior as in configurations TL1 and TL2 making a peak at the tip of the last dropped ply with a value of –0.115 MPa and remained approximately constant for the rest of the interply resin layer.

For TL4 configuration magnitudes of the stresses in the lower interply resin layer were considerably less than the stresses in the upper interply resin layer as in other configurations. At the tip of the middle dropped ply σ_{ZZ} slightly increased but remained compressive. At the same location also an increase in σ_{ZX} observed. At the tip of the last dropped ply, σ_{ZX} made a peak from positive to negative instantaneously and became positive again. σ_{ZZ} made a sharp3 fluctuation from compressive to tensile and became compressive again then increased gradually making a peak at the root of the taper. σ_{YZ}

remained positive through the lower interply layer. At the tip of the last dropped ply σ_{YZ} dropped suddenly from 0.0222 MPa to 0.00623 MPa then returned back to 0.0206 MPa. σ_{YZ} decreased gradually to a very small value just in front of the last dropped ply. The maximum stress was observed in σ_{ZX} between the last 3dropped ply and root of the taper with a value of 0.0581 MPa.

Equivalent von Mises stress for configuration TL4 is plotted for upper and lower interply resin at the tapered region layers in Figure 3.45.

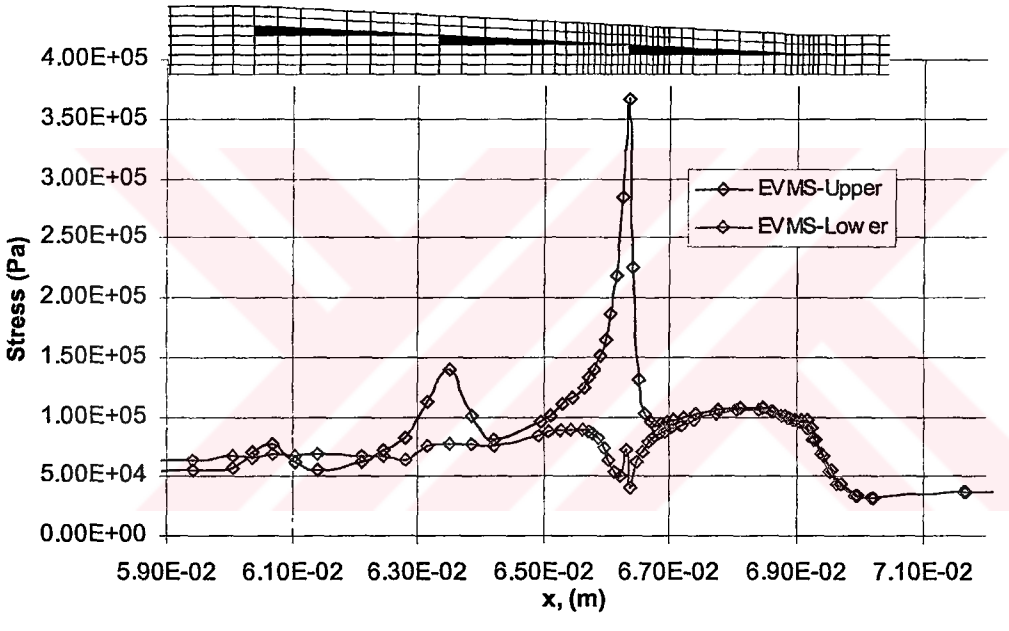

Figure 3.45: Equivalent von Mises Stresses in Upper and Lower Interply Resin Layers Over the Tapered Region

Maximum equivalent von Mises stress was attained as 0.367 MPa in the upper interply resin layer at x=0.0663 m. The location of delamination onset site for configuration TL4 was predicted at x=0.0663 m, in the upper interply resin layer, at the tip of the last dropped ply. The location is shown in Figure 3.46.

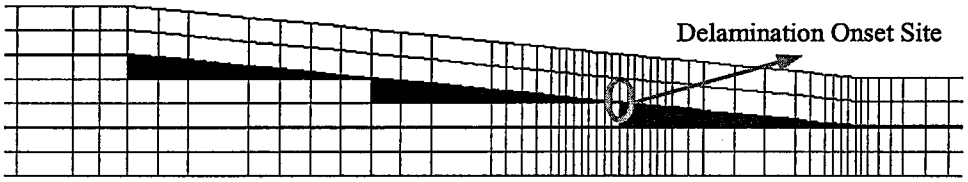

Figure 3.46: Predicted Delamination Onset Site for Configuration TL4

Delamination onset load was calculated using the interlaminar stresses at the predicted delamination onset site. Rescaled stress versus location plot is given in Figure 3.47.

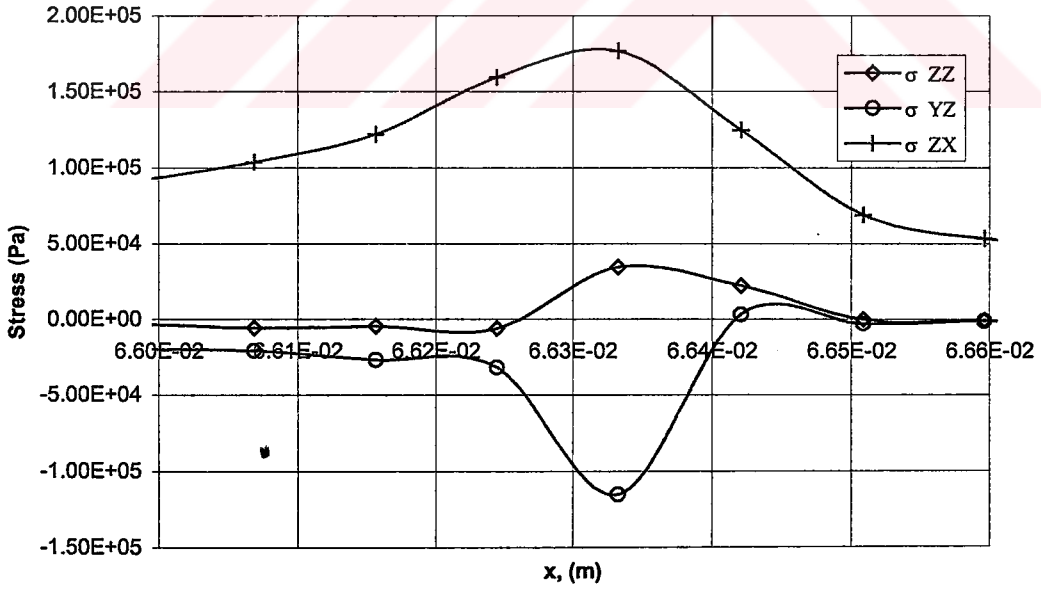

Figure 3.47: Interlaminar Stresses at the Predicted Delamination Onset Site

Average stress concept used with the modified Tsai-Wu delamination criterion and maximum stress criterion was applied to σ_{ZX}. The predicted delamination onset loads and stresses for configuration TL4 are given in Table 3.8.

Table 3.8: Results of FEA of Configuration TL4

Delamination Onset Location	In the upper interply resin layer At the end of last dropped ply	
Calculated Values	**Delamination Onset Load (kN)**	**Delamination Onset Stress based on thin section of the model (MPa)**
Delamination Failure Criterion	17.031	584
Maximum Stress Criterion	15.486	531

3.7.8 FEA of Configuration TL5

FEA results for configuration TL5 were studied to determine delamination onset site and delamination onset load. Equivalent von Mises stress and out-of-plane stresses are plotted in upper and lower interply resin layers in Figure 3.48 and 3.49.

For configuration TL5 interlaminar stresses at the tapered region were significantly greater then other regions. Figures 3.50 and 3.51 were plotted to investigate the stress state at the tapered region, between locations x=0.059 m and x=0.072 m.

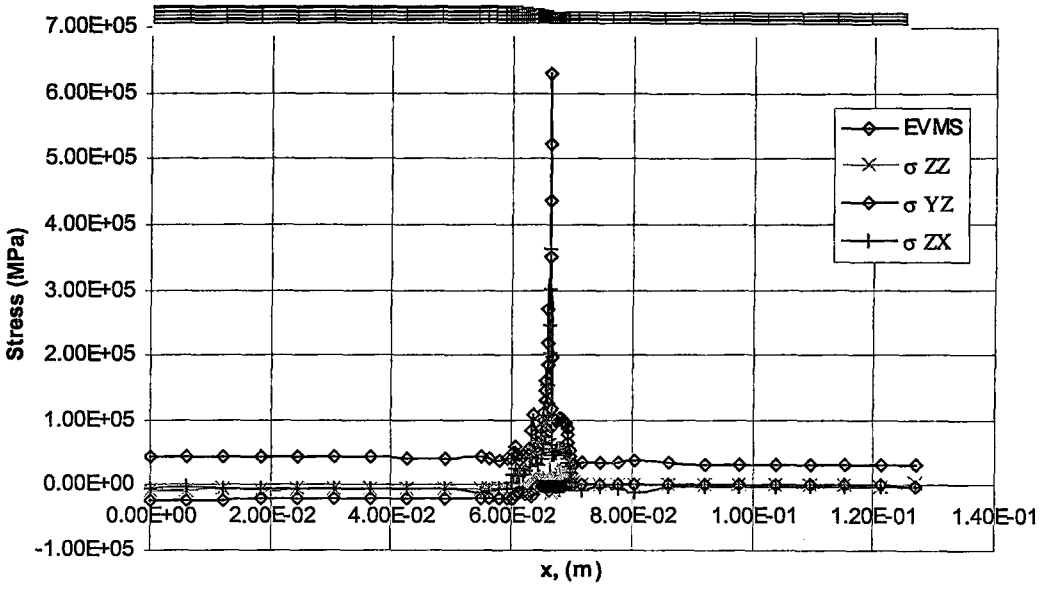

Figure 3.48: Equivalent Von Mises Stress and Interlaminar Stresses in Upper Interply Resin Layer Over the Entire Model

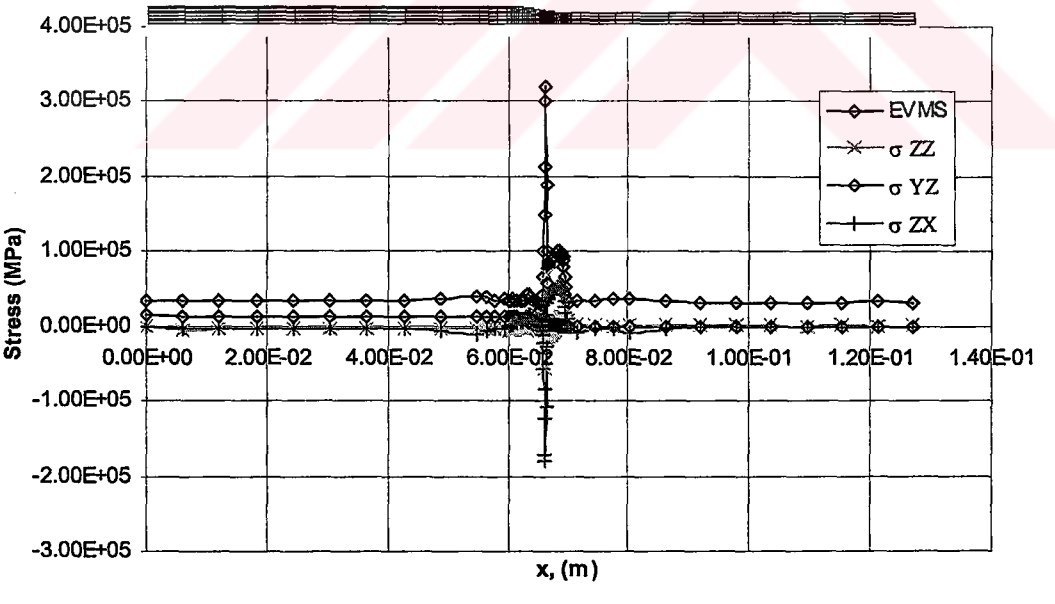

Figure 3.49: Equivalent von Mises Stress and Interlaminar Stresses in Lower Interply Resin Layer Over the Entire Model

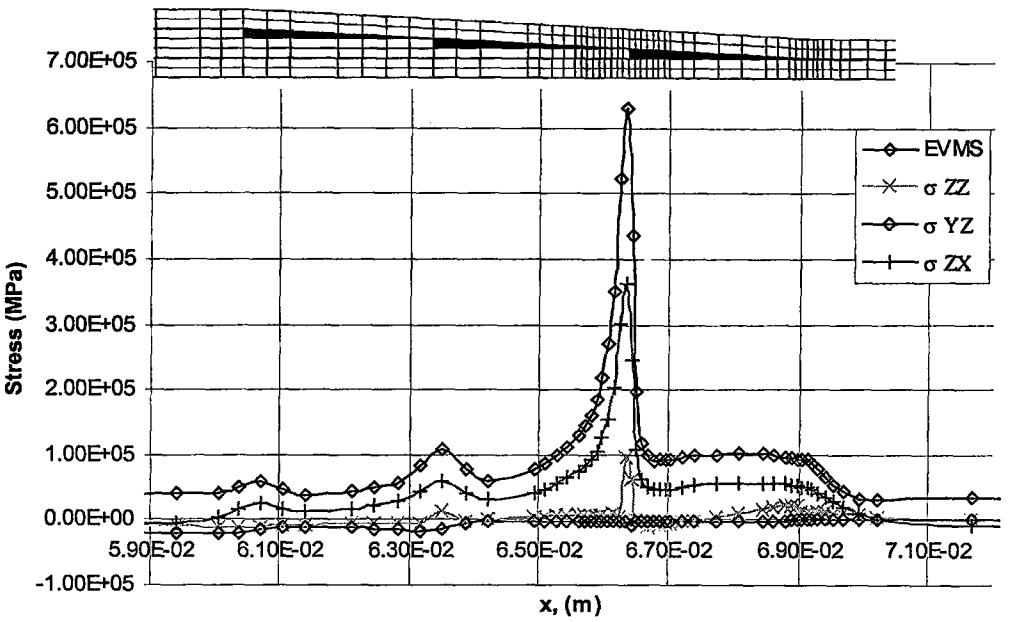

Figure 3.50: Equivalent von Mises Stress and Interlaminar Stresses in Upper Interply Resin Layer Over the Tapered Region

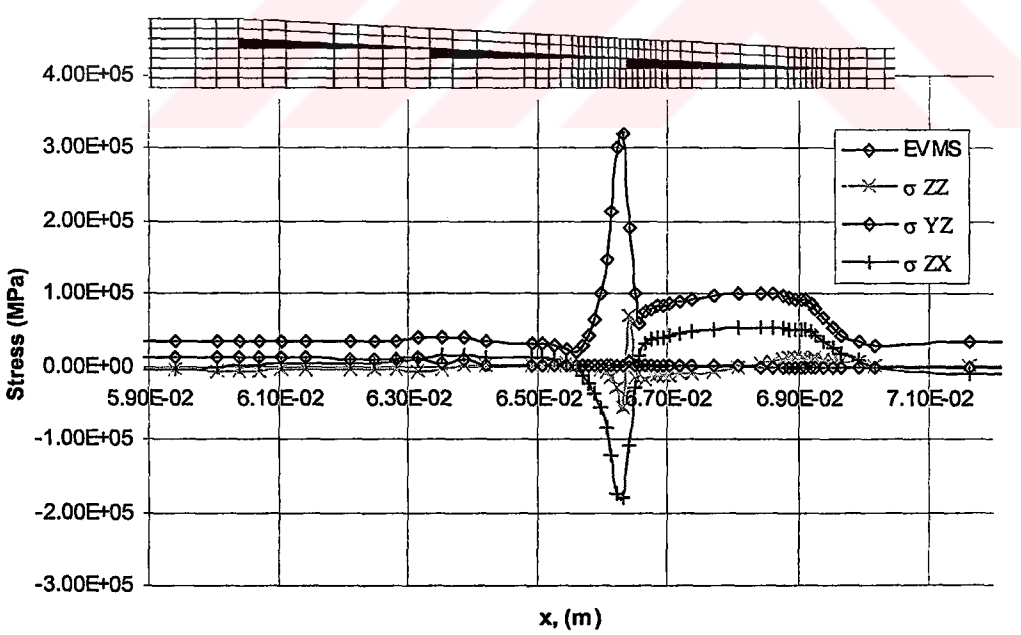

Figure 3.51: Equivalent von Mises Stress and Interlaminar Stresses in Lower Interply Resin Layer Over the Tapered Region

For the configuration TL5 the stress state in the upper interply resin layer was dominated by the interlaminar shear stress σ_{ZX} like other configurations. Interlaminar shear stress started to increase from the beginning of the taper from 0.00290 MPa and made two peaks at the tips of the dropped plies. The first peak was observed at the tip of the middle dropped plies with a value of 0.0607 MPa. The second peak was observed at the tip of the last dropped ply with a value of 0.362 MPa. The first peak was approximately 1/6 of the second one in magnitude. The maximum value of σ_{ZX} observed at the tip of last dropped ply. Interlaminar shear stress decreased to very small values at the root of the taper.

In the upper interply resin layer the magnitude σ_{ZX} was significantly higher than σ_{ZZ} and σ_{YZ} as in other configurations. Interlaminar normal stress σ_{ZZ} showed little variation through the tip of middle dropped ply. At this location, σ_{ZZ} increased instantaneously from –0.00345 MPa to 0.0128 MPa and then decreased to very small values. At the tip of the last ply drop σ_{ZZ} reached to its maximum value 0.0967 MPa and increased gradually through the root of the taper with a value of 0.0234 MPa at the root of the taper. The maximum value of σ_{ZZ} was observed at the tip of the last dropped ply. σ_{YZ} showed little variation through the interply resin layer. Different from other configurations σ_{YZ} remained approximately constant at the tip of last ply drop without making a peak towards a negative value.

Magnitudes of the stresses in the lower interply resin layer were less than the stresses in the upper interply resin layer as in other configurations. Stresses were approximately constant through the tip of the middle dropped ply. At this location σ_{ZZ} slightly increased from a compressive value –0.00474 MPa to a tensile value 0.00128 MPa. Starting from this location σ_{YZ} decreased to very small values just in front of the middle dropped ply and remained the same through the rest of the interply resin region. At the tip of the last dropped

ply, σ_{zx} decreased to a compressive value with a magnitude of –0.179 MPa quickly and came back to a tensile again. Then at the root of the taper σ_{zx} started to decrease, being very small at the root of the taper. σ_{zz} quickly decreased to –0.0556 MPa at the tip of the last ply drop and increased to 0.0700 MPa instantaneously, then became compressive again. σ_{zz} increased gradually through the root of the taper then decreased to very small values at a small distance from the root of the taper.

Equivalent von Mises stress for configuration TL5 is plotted for upper and lower interply resin at the tapered region layers in Figure 3.52.

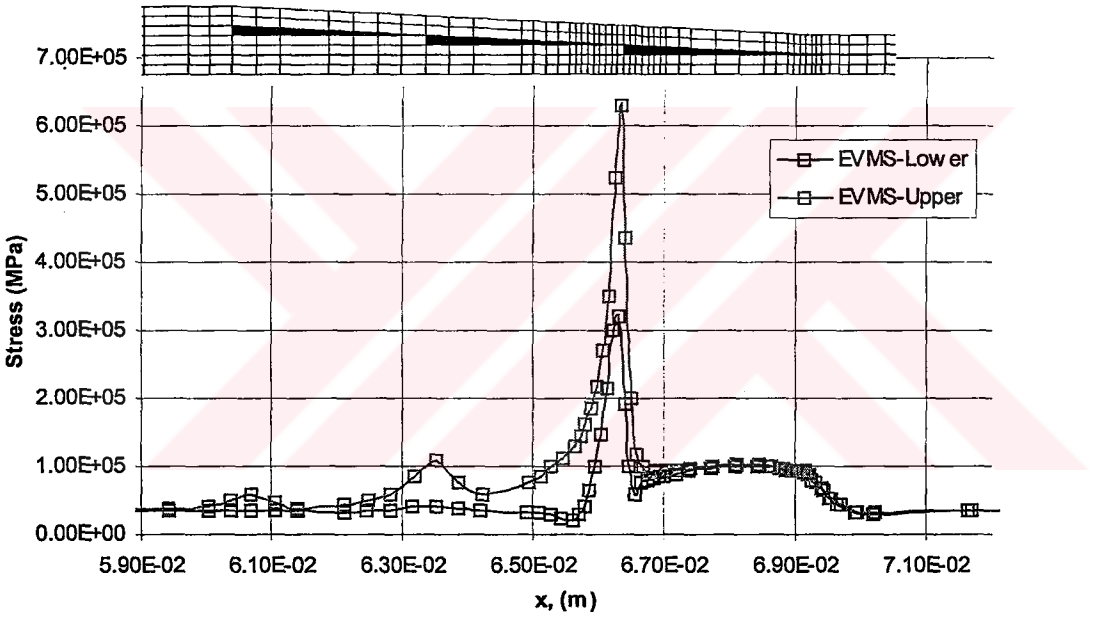

Figure 3.52: Equivalent von Mises Stresses in Upper and Lower Interply Resin Layers Over the Tapered Region

Maximum Equivalent Von Mises stress attained as 0.629 MPa in the upper interply resin layer at x=0.0663 m. The location of delamination onset site for configuration TL5 was predicted at x=0.0663 m, in the upper interply resin layer, at the tip of the last dropped ply. The location is shown in Figure 3.53.

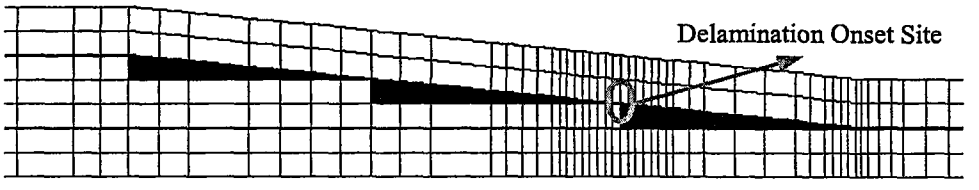

Figure 3.53: Predicted Delamination Onset Site for Configuration TL5

Delamination onset load was calculated using the interlaminar stresses at the predicted delamination onset site. Rescaled stress versus location plot is given in Figure 3.54.

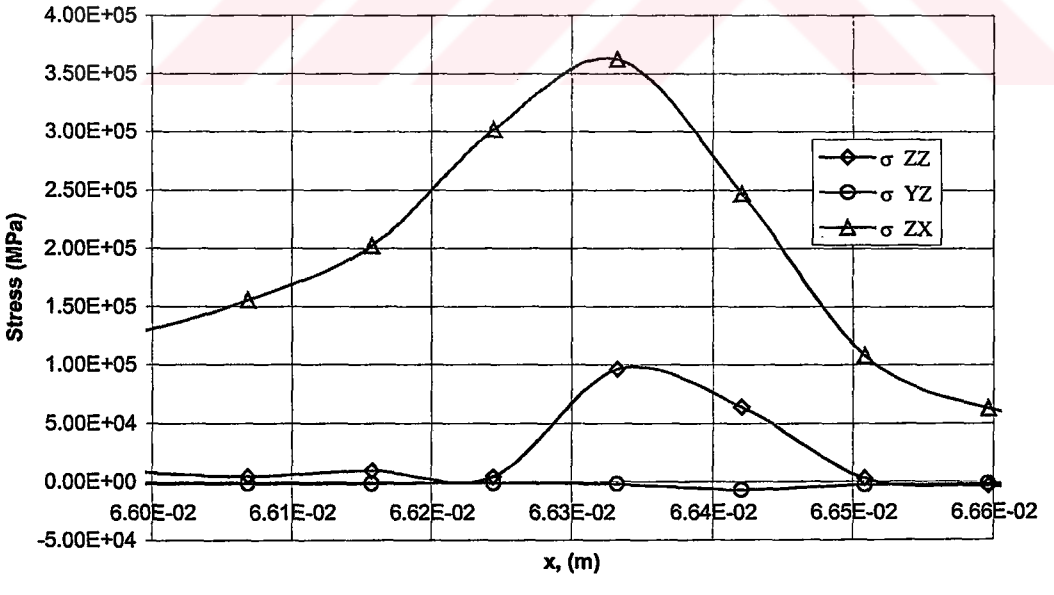

Figure 3.54: Interlaminar Stresses at the Predicted Delamination Onset Site

Average stress concept used with the modified Tsai-Wu delamination criterion and maximum stress criterion was applied to σ_{ZX}. The predicted delamination onset loads and stresses for configuration TL5 are given in Table 3.9.

Table 3.9: Results of FEA of Configuration TL5

Delamination Onset Location	In the upper interply resin layer At the end of last dropped ply	
Calculated Values	**Delamination Onset Load (kN)**	**Delamination Onset Stress based on thin section of the model (MPa)**
Delamination Failure Criterion	9.026	310
Maximum Stress Criterion	7.572	260

CHAPTER 4

EXPERIMENTAL STUDY

4.1 Determination of Material Properties

In the finite element analysis of composite parts, material properties were needed, also a 3D analysis requires additional material properties that was not given by manufacturer. Therefore, several tests were conducted to determine the material properties needed and to verify the material properties given by manufacturer.

All the tests were performed by using INSTRON 4481 (50 kN maximum load) and INSTRON 4506 (200 kN maximum load and equipped with extensometer) Universal Tensile Test Machines with suitable fixtures. The tests were conducted in a room maintained at 23±1 °C and 50±10 % relative humidity in accordance with Procedure A of ASTM D 618 [42]. Some specimens were equipped with HBM (Hottinger Baldwin Messtechnik) 6/350XY11 type, T-shape and HBM 6/350LY11 type, unidirectional strain gages. Photographs of specimens, testing machines and other equipments are given in Appendix D.

4.1.1 Material Description

The material used in experimental study was HYE E773FR/AS4 (flame retardent grade) carbon/epoxy prepreg tape of CYTEC FIBERITE INC. It is used extensively in helicopter blades and other structural components. The properties of the neat resin and unidirectional tape are given in Table 4.1 and Table 4.2.

Table 4.1: Neat Resin Properties

Typical Neat Resin Properties of E773FR Epoxy Resin	
Tensile Strength (MPa)	64
Tensile Modulus (GPa)	3.5
Flexural Strength (MPa)	94
Flexural Modulus (GPa)	3.8
Tg °C	155
Specific Gravity	1.28

Table 4.2: Unidirectional Tape Properties

Typical Unidirectional Carbon/Epoxy Prepreg Tape Properties		
	Room Temp. (RT)	**RT WET***
0° Tensile Strength (MPa)	2034-2137	1964-2137
0° Tensile Modulus (GPa)	131-145	131-145
0° Compression Strength (MPa)	1206-1344	1172-1310
0° Compression Modulus (GPa)	131-145	131-145
0° Interlaminar Shear Strength (MPa)	69-90	55-69
±45 In-Plane Shear Strength (MPa)	97-110	52-76
CPT (Cured Ply Thickness) (mm)	0.14	

* 1% moisture absorbed

4.1.2 Determination of Tensile Properties

Tensile properties of the material in 0° and 90° were determined according to the ASTM D 3039-76 (Standard Test Method for Tensile Properties of Fiber-Resin Composites). The recommended specimen width for 0° and 90° fiber orientations are 12.7mm and 25.4mm and the recommended specimen minimum gage length for 0° and 90° fiber orientations are 127mm and 38.1mm respectively. For the graphite reinforcement, recommended specimen thickness is between 0.508-2.54 mm.

For the tensile tests four specimens composed of 14 plies and five specimens composed of 8 plies were tested for 0° fiber orientation. The specimens with 8 plies were tested without an extension indicator where the test results were used to obtain strength properties.

Eight specimens composed of 14 plies were tested for 90° fiber orientation. Three specimens were tested without an extension indicator where the test results were used to obtain strength properties.

In order to determine strain, modulus and Poisson's ratio (ν_{LT}) strain-gauges were used. The geometry of tensile specimen is given in Figure 4.1.

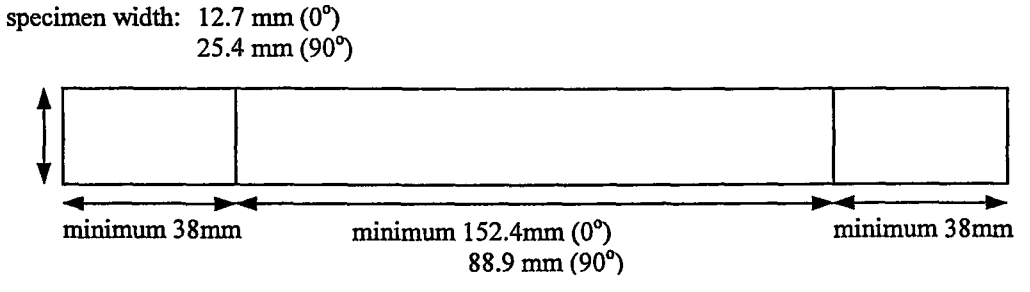

Figure 4.1: Tensile Specimen Geometry

L. J. Hart-Smith [38] recommends a uniformly wide untabbed all-0° laminate as the most cost-effective way of reliably measuring Young's Modulus along longitudinal direction. So, some specimens tested without using tab.

The tensile strength (S), elastic modulus (E) and Poisson's ratio were calculated by using the Equations 4.1 and 4.2 [39]. The tensile test results are given in Table 4.3, Table 4.4 and Table 4.5.

$$S = P/bd \tag{4.1}$$

$$E = (\Delta P/\Delta l)(l/bd) \tag{4.2}$$

where:

S= ultimate strength

P= maximum load

b= width

d= thickness

l= length

E= modulus of elasticity

$\Delta P/\Delta l$= slope of the plot of load as a function of deformation within the linear portion of the curve

where:

ν_{LT} = Poisson's ratio

$\nu_{LT} = -\Delta\varepsilon_T/\Delta\varepsilon_L$

$\Delta\varepsilon_T/\Delta\varepsilon_L$= Slope of strain-strain curve in the linear region, where $_T$ denotes the strain measured perpendicular to the applied load, and $_L$ denotes the strain measured parallel to applied load.

Table 4.3: Tensile Test Results for 8-ply Specimens with 0° Lay-up

Spec. No.	b (mm)	d (mm)	P (kN)	S (Mpa)
$T0^0$-1	14.34	1.12	30.54	1902
$T0^0$-2	14.02	1.03	25.81	1787
$T0^0$-3	14.45	1.10	34.38	2163
$T0^0$-4	14.07	1.10	26.27	1697
$T0^0$-5	14.20	1.06	25.09	1666
		Average		1843
		Std. Dev.		201

Table 4.4: Tensile Test Results for 14-ply Specimens with 0° Lay-up

Spec. No.	b (mm)	d (mm)	P (kN)	S (Mpa)	ε_{ult} (%)	E (Mpa)
$T0^0$-6**	14.33	1.9	-	-	-	142000
$T0^0$-7*	14.17	1.85	53.35	2043	1.100	145000
$T0^0$-8*	14.17	1.74	43.79	1777	1.234	144000
$T0^0$-9*	13.92	1.89	48.53	1845	1.157	139000
			Average	1888	1.163	142500
			Std. Dev.	138	0.067	3214

* Equipped with extensometer.

** Equipped with T-shape strain-gauge and loaded to 50 kN (No failure occurred)

Nine specimens tested totally to determine tensile properties with 0^o Lay-up. Test results show that the average tensile strength for the material is approximately 1865 MPa and the ultimate % strain value is approximately is 1.163. The average modulus value comes out to be approximately 142500 MPa.

Additionally one 14-ply specimen with 0^o Lay-up equipped with T-shape strain-gauge to determine the modulus along 0^o and Poisson's ratio (ν_{LT}). The results of strain-gauge measurements are given in "Strain-Gauge Measurements" topic.

Table 4.5: Tensile Test Results for 14-ply Laminate with 90^o Lay-up

Spec. No.	b (mm)	d (mm)	P (kN)	S (MPa)	ε_{ult} (%)	E (MPa)
$T90^0$-1	26.86	1.96	1.858	35.30	-	-
$T90^0$-2	27.30	2.03	1.517	27.73	-	-
$T90^0$-3	26.90	2.04	1.789	32.60		
$T90^0$-4*	25.21	2.07	1.644	31.51	0.393	7625
$T90^0$-5*	25.10	2.10	1.726	32.75	-	7449
$T90^0$-6*	25.02	2.10	1.600	30.46	0.407	7390
$T90^0$-7*	25.16	2.01	1.756	34.73	0.411	8094
$T90^0$-8**	25.32	2.11	1.921	35.96	0.458	7500
		Average		32.63	0.417	7611
		Std. Dev.		2.74	0.028	283

* Equipped with extensometer.

** Equipped with unidirectional strain-gauge

Tensile Test Results for 14-ply Laminate with 90° Lay-up show that the strength of the material in transverse direction is approximately 32 MPa.

Additionally one 14-ply specimen with 90° Lay-up equipped with unidirectional strain-gauge to determine the modulus along transverse direction. The results of strain-gauge measurements are given in Section 4.1.5.

4.1.3 Determination of In-Plane Shear Properties

In plane shear properties of the material is determined according to the AITM 1.0002 (Airbus Industrie Test Method). This practice is based on uniaxial tensile stress-strain response of balanced, symmetric laminate composed of only +45° and –45° plies (a ±45° laminate). The specimens were cut out of plates composed of 8 plies. For the tests, 4 specimens composed of 8 plies with ±45° layup were tested. One specimen instrumented with strain-gage in both longitudinal and lateral directions to determine shear modulus. The geometry of specimen is given in Figure 4.2.

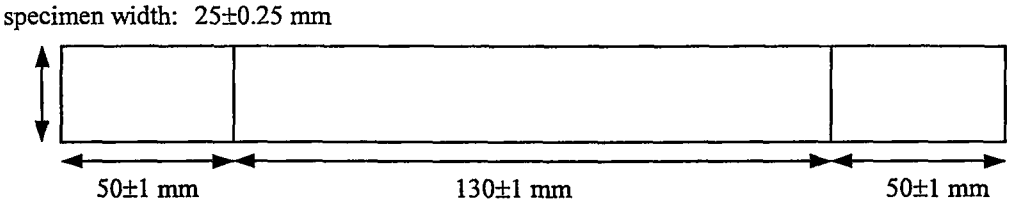

Figure 4.2: In-plane Shear Specimen Geometry

The shear strength (T) and shear modulus (G) were calculated by using the formulas given below [40]. The IPS (In-plane Shear) test results are given in Table 4.6.

$$T = 0.5P_{max}/wt \quad (4.3)$$

$$G = 0.5\Delta P/wt(\Delta\varepsilon_0 - \Delta\varepsilon_{90}) \quad (4.4)$$

where:

P_{max}= highest tensile load

w= width

t= thickness

ΔP= difference of tensile loads

$\Delta\varepsilon_0$= difference of longitudinal strains

$\Delta\varepsilon_{90}$= difference of transverse strains

Table 4.6: IPS Test Results for 8-ply Laminate with ±45° Lay-up

Spec. No.	w (mm)	t (mm)	P_{max} (kN)	T (Mpa)	$\varepsilon_{x\ ult}$ (%)
T±45°-1*	24.66	1.23	4.026	66.4	5.331
T±45°-2**	25.21	1.23	4.329	69.8	5.074
T±45°-3*	26.26	1.15	3.668	60.8	4.699
T±45°-4	21.86	1.09	2.873	60.3	-
			Average	64.3	5.034
			Std. Dev.	4.58	0.318

* Equipped with extensometer

** Equipped with T-shape strain-gauge

Tensile Test Results for 8-ply Laminate with ±45° Lay-up show that the in-plane shear strength of the material is approximately 64 MPa.

Additionally one 8-ply specimen with ±45° Lay-up equipped with T-shape strain-gauge to determine the in-plane shear modulus. The results of strain-gauge measurements are given in Section 4.1.5.

4.1.4 Determination of Apparent Interlaminar Shear Strength

Apparent interlaminar shear strength of the material is determined according to the A.E.C.M.A. prEN 2563. This standard defines a method for the determination of the apparent interlaminar shear by delamination of unidirectional carbon fibre reinforced thermosetting resin composites produced in sheet form for aerospace use. The shape and dimensions of test ILSS (Interlaminar Shear Strength) specimens are given in Figure 4.3. For the ILSS tests 9 specimens composed of 14 plies with 0^{o} lay-up were produced.

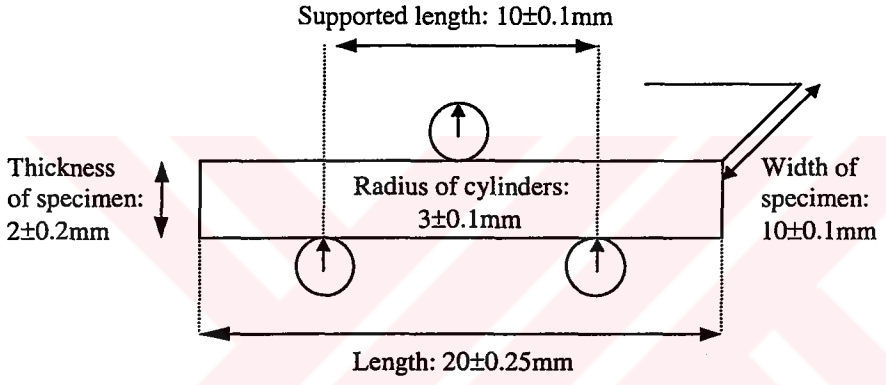

Figure 4.3: ILSS Test Specimen Geometry

The apparent interlaminar shear stress (τ) is calculated by using the Equation 4.5 [41]. The ILSS (Interlaminar Shear Strength) test results are given in Table 4.7.

$$\tau = 3\,P_R/4bh \qquad (4.5)$$

where:

τ= apparent interlaminar shear stress

P_R= maximum force at the moment of first failure

b= width

h= thickness

Table 4.7: ILSS Test Results for 14-ply Laminate with 0° Lay-up

Spec. No.	b (mm)	h (mm)	P_R (kN)	τ (Mpa)
ILSS-1	10.40	1.76	1.498	61.38
ILSS-2	10.42	1.87	1.542	59.35
ILSS-3	10.53	1.63	1.360	59.43
ILSS-4	10.83	1.50	1.283	59.23
ILSS-5	10.45	1.87	1.537	58.99
ILSS-6	10.50	1.70	1.477	62.06
ILSS-7	10.53	1.65	1.625	66.71
ILSS-8	10.38	1.68	1.483	63.78
ILSS-9	10.38	1.66	1.585	68.99
			Average	62.21
			Std. Dev.	3.61

Both, multiple shear mode of failure and single shear mode of failure seen in the ILSS test specimens in the test. The load vs. displacement plot shows that the test is acceptable.

From the results of the ILSS tests the Interlaminar shear strength of the material comes out to be approximately 62 MPa.

4.1.5 Strain Gauge Results

Specimens $T0^0$-6, $T90^0$-8 and T±45°-2 were equipped with HBM 6/350XY11 350Ω T-shape and HBM 6/350LY11 350Ω unidirectional strain gauges and HP (Hewlett-Packard) 7500B Series Data Acquisition System used

for collecting data. The time vs. load data were taken from Instron test machine and the time vs. strain data were taken from HP Data Acquisition System.

The stress vs. % strain and load vs. % strain curves plotted using obtained data and by using the previously given formulations [39], [40] Poisson's ratio and modulus values calculated. The curves are given in Figure 4.4, Figure 4.5 and Figure 4.6. The calculated values are given in Table 4.8.

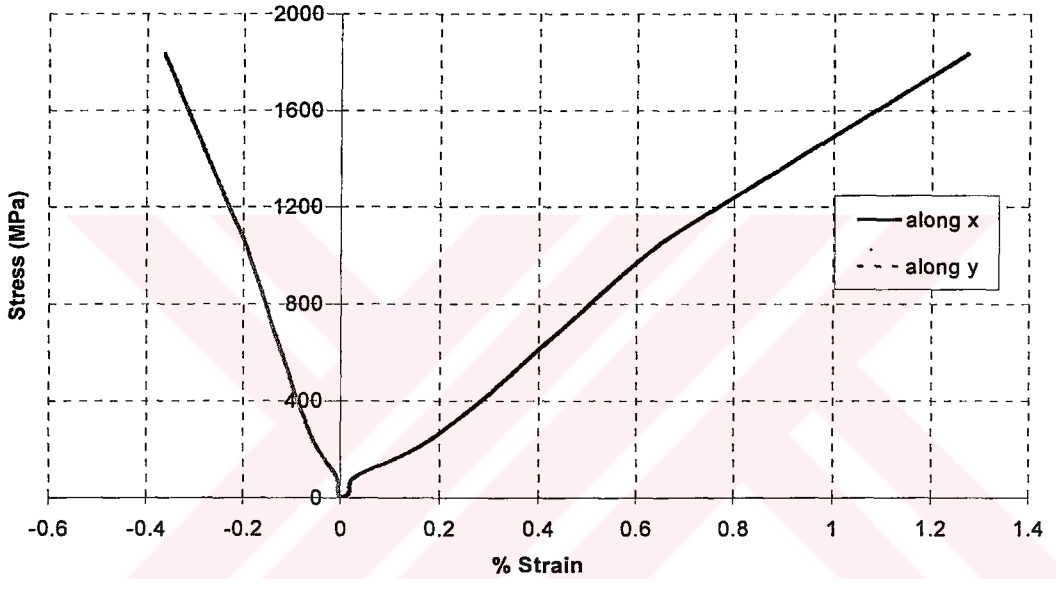

Figure 4.4: Stress vs. % Strain Curve of the Test Specimen $T0^0$-6

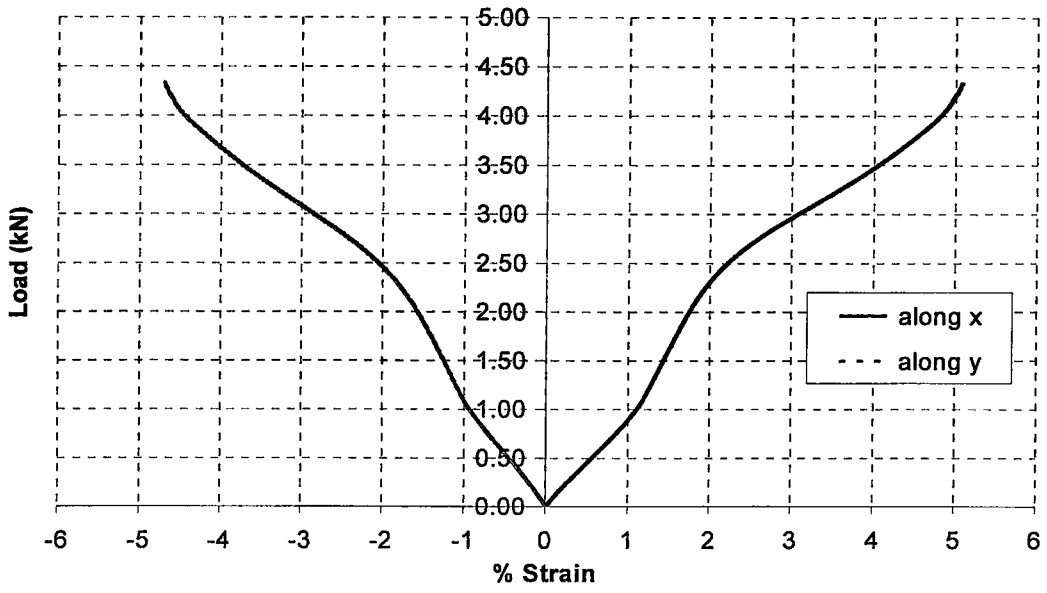

Figure 4.5: Load vs. % Strain Curve of the Test Specimen T±45°-2

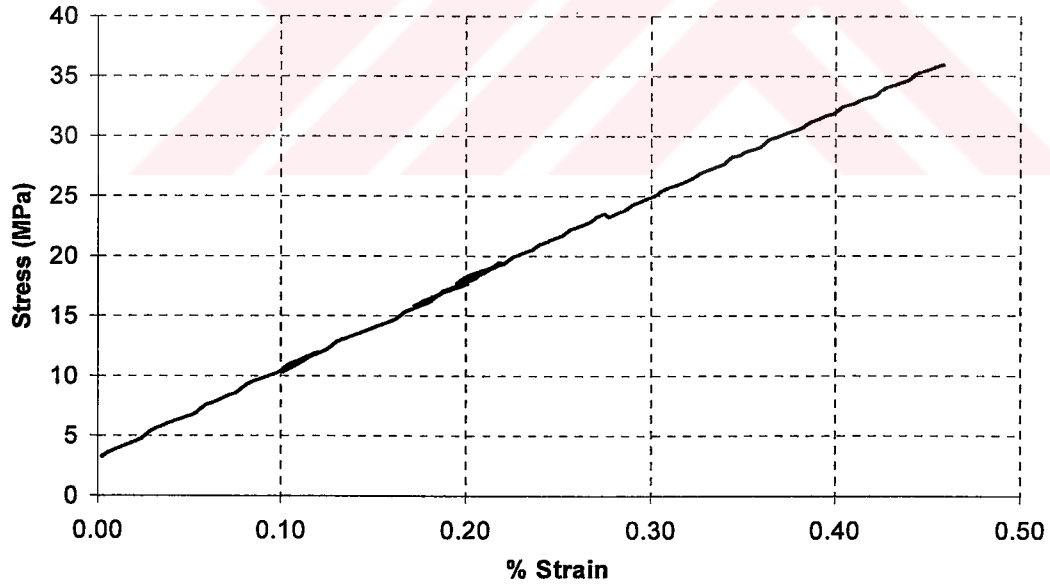

Figure 4.6: Stress vs. % Strain Curve of the Test Specimen T90°-8

Table 4.8: Material Properties calculated by Using Strain-gauge Data

	Longitudinal	**Transverse**	**In-Plane**
Young's Modulus (MPa)	142000	7500	-
Shear Modulus (MPa)	-	-	4250
ε_{ult} (%)	-	0.458	-
Poisson's Ratio (ν_{LT})	0.3		

4.1.6 Material Properties Used in Finite Element Analysis

Various tests conducted to determine the material properties for the material HYE E773FR unidirectional prepreg tape. Some of the properties do not match with the manufacturers data sheet. This may be due to aging of the material. The material was produced in 10.7.1998 and shelf life of the material was two years at 4 °C.

Approximating the test results, the values given in Table 4.9 were used for the finite Element analysis. No tests were conducted to determine neat resin properties because of absence of neat resin of the material. So, Neat resin properties directly taken from manufacturers data sheet.

Table 4.9: Material Properties Used in Finite Element Analysis

Longitudinal Modulus, E_L (GPa)		142.5
Tensile Strength (MPa)		1865
Tranverse Modulus, E_T (GPa)		7.6
Transverse Strength (MPa)		32
In-plane Shear Modulus, G_{LT} (GPa)		4.25
In-plane Shear Strength, S_{LT} (MPa)		64
Interlaminar Shear Strenght (MPa)		62
Poisson's Ratio, ν_{LT}		0.3
Neat Resin	**Tensile Modulus (GPa)**	3.5
	Tensile Strength (MPa)	64
	Flexural Strength (MPa)	94

4.2 Manufacturing of Test Specimens

In this section, manufacturing of flat test specimens for determining material properties and manufacturing of tapered specimens for experimental study are discussed. Also introductory level information is given on unidirectional tape manufacturing and molding.

4.2.1 General Remarks on Manufacturing of Unidirectional Tapes

Unidirectional tape manufacturing processes fall into three major categories: hand layup, where the operator cuts lengths of the tape and places them on the tool surface in the desired ply orientation, machine-cut patterns that are laid-up by hand, and automatic machine layup, where numerically controlled automatic tape laying machines programmed to lay down plies of tape in the quasi-isotropic patterns required by most design applications.

Autoclave molding is the standard aerospace industry process for fabrication with prepreg tapes. The autoclave is simply a heated pressure vessel into which the mold (with lay-up) is placed and subjected to the required temperature and pressure for curing. The mold and lay-up are often covered with release fabric, a bleeder cloth, and a vacuum bag. A vacuum line is then attached to the mold for the evacuation of volatile gasses during the cure process.

The materials used in preparing the layup for autoclave curing are release film, peel ply, bleeder, breather, caul plate, vacuum vane, vacuum bag and sealant. Figure 4.7 represents the most common layup used for autoclave curing.

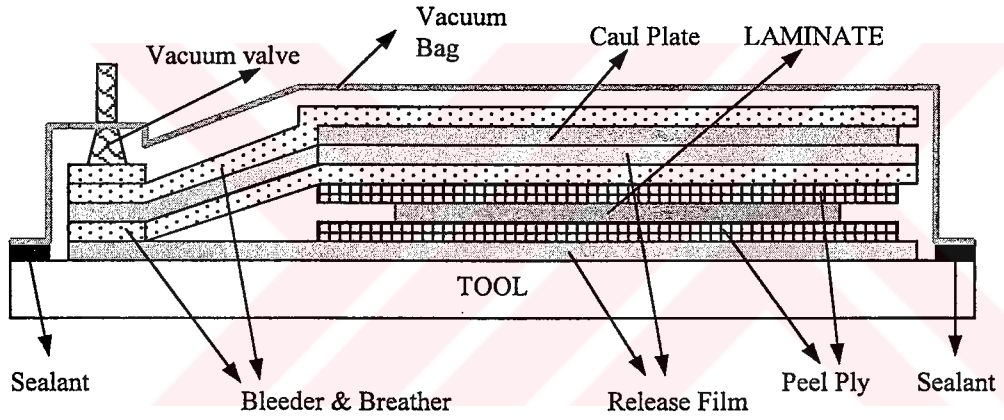

Figure 4.7: Layup for Autoclave Curing

Release film is placed top and under the peel ply to avoid adhesion of laminate to caul plate and tool. Usage of peel ply in autoclave curing process is optional but to prevent entrapped volatiles and porosity in laminate and to get a clean bondable surface, peel ply is placed top and under the laminate. Caul plate provides a more uniform pressure distribution on the laminate. Breather and bleeder absorb excess resin from the layup during cure and provide uniform application of vacuum pressure and removal of entrapped air or

volatiles during cure. The vacuum bag is used to contain any vacuum pressure applied to the layup before and during cure and to transmit external autoclave pressure to the part. It prevents any gaseous pressurizing medium used in the autoclave (inert gas) from permeating the part end causing porosity and poor or unacceptable part quality. Two vacuum vanes used, one for vacuum and one for vacuum pressure measurement in the vacuum bag.

4.2.2 Test Specimen Manufacturing

Several tests specimens were manufactured for determining the material properties and for experimental study of tapered laminates. All the specimens were manufactured from the same batch of HYE773FR/AS4 unidirectional prepreg tape. The prepreg tapes are hand laid up. As hand lay-up technique is an operator dependent technique, extreme care was taken. The material was cut with razor blades with the help of steel rulers and square to the specified dimensions. A magnifier (x8) with scale was used to control the orientation and distance between the dropped plies while preparing the tapered specimens. All the cured materials were cut into specimen dimensions by using a high rpm cutting machine with a diamond cutting wheel.

Layup for autoclave curing of flat test specimens is given in Figure 4.7. The material was cured with the recommended cure cycle supplied from the manufacturer. A conventional room type autoclave, product of SCHOLTZ GMBH, was used with all the materials discussed above, products of AIRTECH INC, for autoclave curing.

Manufacturing of flat specimens were straight forward. No additional tooling was used apart from the layup given in Figure 4.7. But incase of manufacturing of tapered specimens some difficulties appeared. Considering these difficulties a preliminary study was conducted to determine a proper layup method for autoclave cure of tapered specimens.

4.2.3 Preliminary Study for Manufacturing of Tapered Specimens

Controlling the exact geometry of the tapered laminates was difficult although the distances between the dropped plies and length of the dropped plies were controlled precisely before curing. If the specimen is cured without using any additional apparatus, the vacuum and cure pressures change the shape of the resin rich pockets formed in front of the dropped plies. This is illustrated in Figure 4.8. The dotted lines refer to the uniform taper angle.

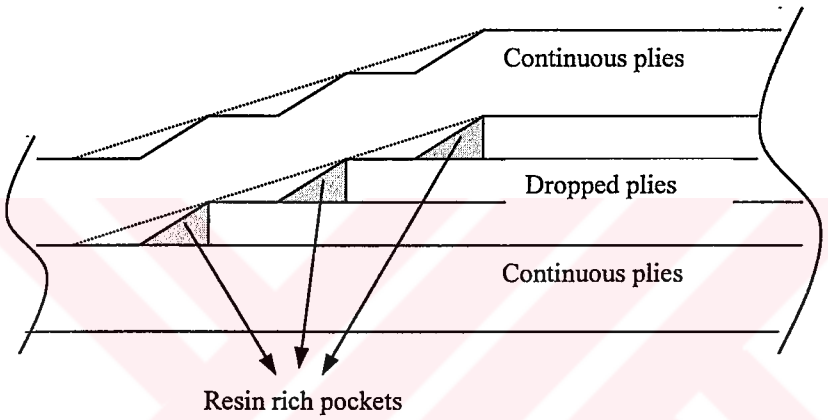

Figure 4.8: Shape Change Due to Curing

In most of the previous studies [3, 13, 15] specially machined jig plates to the desired taper angle were used during the cure process. This method is useful for manufacturing of thick parts but in case of thin laminates, machining jig plates for a constant taper angle became expensive and time consuming. Another technique is the usage of fill-in plies [8] and an upper caul plate where fill in plies are separated from the laminate by a release film. Fill-in plies have the same number of plies as the dropped section and caul plate provides a uniform pressure distribution. In this method the geometry of the taper is not controlled so precisely and due to the fill-in plies lots of scrap material is produced. Also in some studies no additional apparatus was used [6] to control the geometry. This method is the least expensive method but due to the

geometric differences of the tapered laminates different experimental results can be obtained.

A preliminary study was conducted to determine a suitable manufacturing technique for the tapered laminate specimens. Three methods were studied to find the most effective solution to manufacture tapered specimens. The number of continuous and discontinuous plies and dimensions were kept the same with the tapered specimen. The layup was chosen to be all 0 degree not to scrap material and for ease of production. These methods are given below.

1) The tapered laminates were cured free standing. No additional apparatus was used. The vacuum and cure pressure affected the geometry of the taper. As expected, the geometry of the taper was far away from the ideal case that was shown in Figure 4.8. The cured geometry of the taper could not be controlled accurately by this method.

2) A new method was developed to control the geometry of the taper. Using a metal shim with a suitable thickness is a good way to control the taper angle. A flat metal shim with the same in-plane dimensions of the laminate was fixed on the laminate before curing. Vacuum and cure pressure made the shim to get the shape of the tapered laminate without distorting the shape of the resin pockets and taper angle. This approach is shown in Figure 4.9.

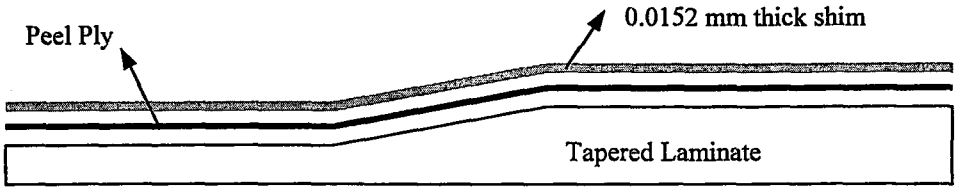

Figure 4.9: Layup of Method 2

3) The third method investigated was the combination of the method 2 and method of fill-in plies [8]. Fill-in plies were used additionally with an upper caul plate. This layup is given Figure 4.10.

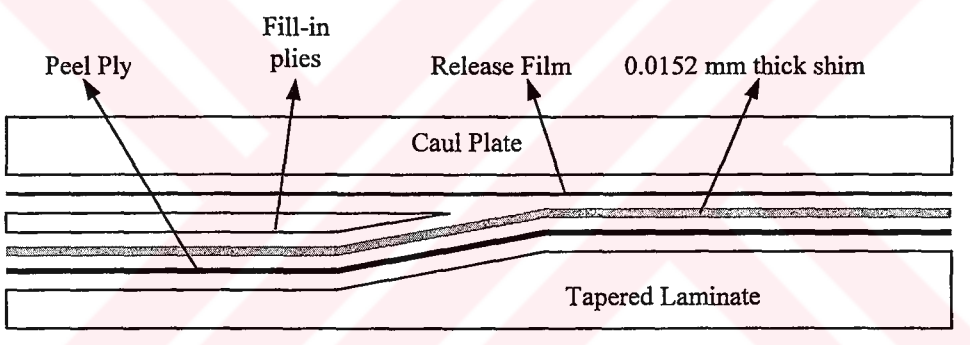

Figure 4.10: Layup of Method 3

Examining the geometries of the cured tapered laminates under a video microscope, it was seen that unwanted geometric distortions occurred in specimens manufactured with layup method 1. As shown in Figure 4.7, the taper angle has changed and a stair-like geometry was formed.

The geometries of the tapered laminates manufactured with layup methods 2 and 3 were very similar and satisfactory. No stair like geometric distortions formed. The geometry of the taper was close to an ideal case for both specimens manufactured with layup method 2 and 3.

Comparing the above mentioned layup methods for manufacturing, layup method 2 was found to be the most effective manufacturing method due to ease of production and low scrap ratio. Thus, all of the tapered specimens were manufactured with method 2.

4.2.4 Recommended Cure Cycle

The recommended autoclave cure cycle supplied from the manufacturer is given in Figure 4.11. All the specimens were cured with this cycle under inert nitrogen gas pressure.

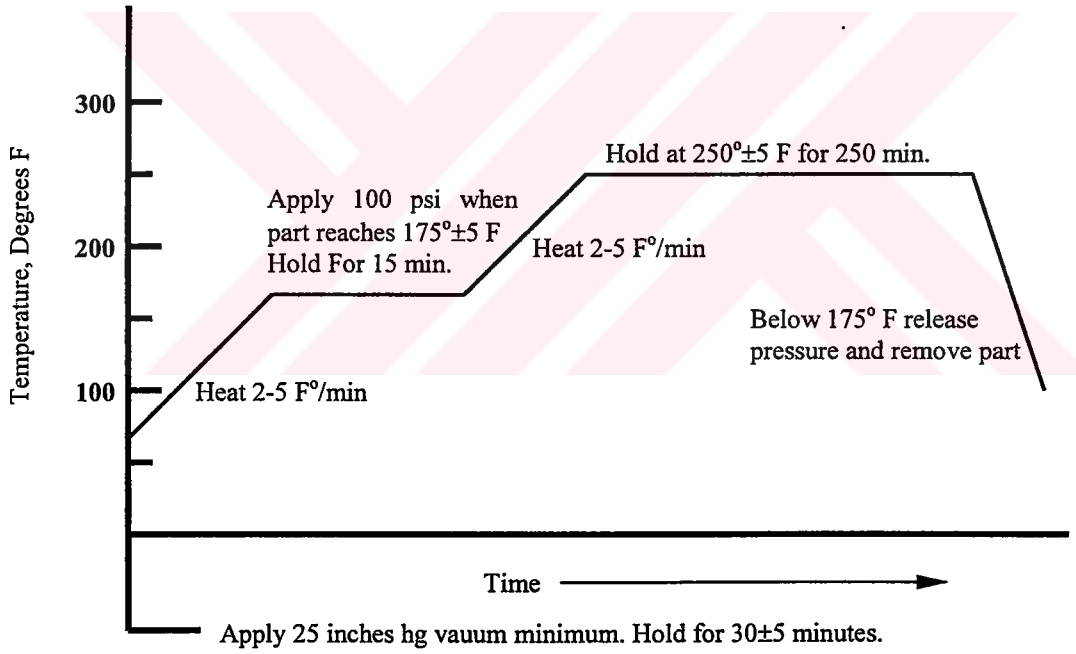

Figure 4.11: Recommended Cure Cycle

4.3 Experimental Study on Tapered Laminates

The validation of the finite element results was carried out with experiments on tapered specimens. Critical load for delamination onset was determined by tension tests.

The tapered specimens were 220 mm long, 25.4 mm wide with a gage length of 127 mm and were tapered from 14 plies to 8 plies through a taper angle of approximately 5.7°. Three pairs of symmetric two-ply steps were used to produce the taper by keeping the distance between the discontinuous plies approximately 2.8 mm (as shown in Figure 4.12). As there is no standard test method for tapered laminates the dimensions of the test specimen were taken from ASTM D 3039-76 [39]. The dimensions of the tapered specimens are given in Figure 4.12.

All of the discontinuities were introduced into the specimens by removing material of the designated plies during the layup. Care was taken to line up the ends of the discontinuous plies. The positions of dropped plies were controlled by using a 8x magnifier. The specimens were machined to the desired dimensions with a cutting machine equipped with diamond-grit cutting wheel.

Samples were taken from the cured laminates, grinded and polished by using BUEHLER-METASERV Grinder-Polisher Machine. These samples were investigated with an optical microscope OLYMPUS PME 3. Photographs of the samples were taken with a Polaroid camera mounted in the microscope. The optical microscope photos of the samples, at the tapered region are given in Appendix C.

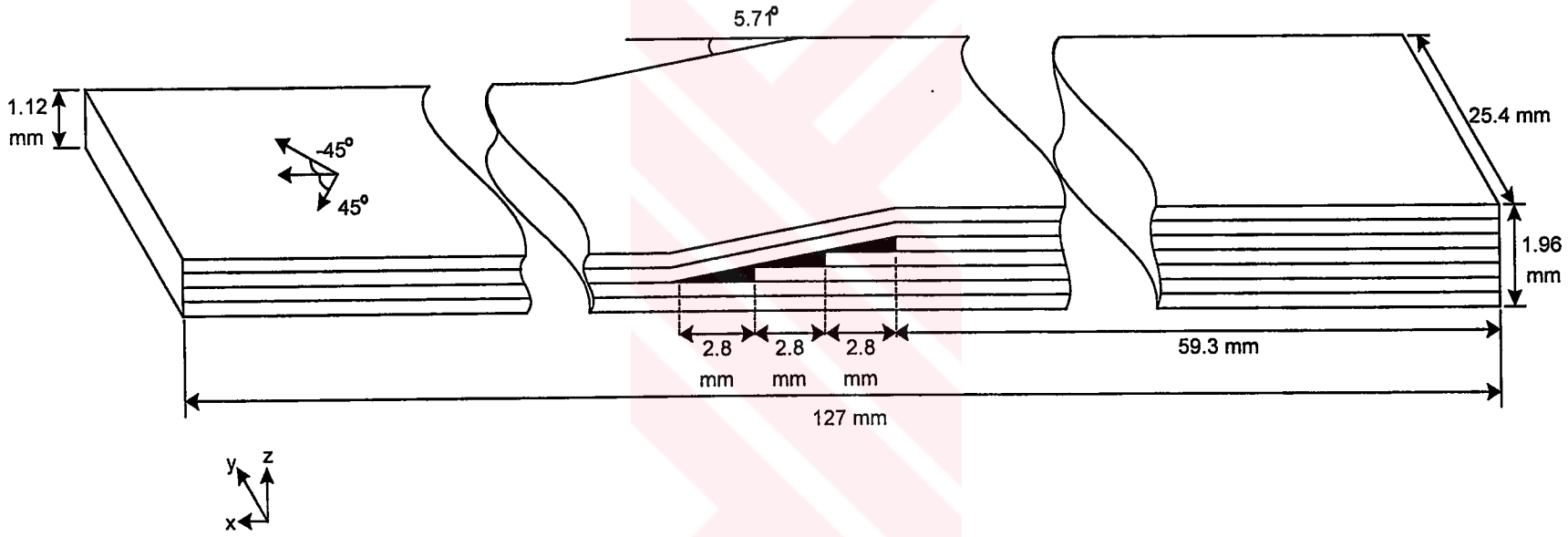

Figure 4.12: Tapered Specimen

In addition to the tapered specimens, flat coupons representing the thin sections of the tapered specimens were tested. The in-plane dimensions of the flat coupons were identical to those of the tapered specimens.

Carbon/epoxy tabs with 1.1 mm thick were adhesively bonded by using LOCTITE 307 Engineering Adhesive and LOCTITE 7471 Activator to the ends of all test specimens to prevent grip damage during tests.

4.3.1 Set-up and Tests

The tensile tests were performed with an INSTRON 4506 Tensile Testing Machine. Load and displacement were continuously monitored with the cross-head speed 1 mm/min.

Three tapered specimens were tested to failure and delamination onset and growth observed visually by using a magnifier. Two specimens were loaded until the onset of delamination and then unloaded for inspection with optical microscope.

The delamination initiation stress and failure stress were determined by dividing the load by the measured cross-sectional area of the thin section of the specimens.

4.3.2 Experimental Results of Flat Laminates

Flat coupons representing the thin sections of the tapered specimens were tested. Failure stresses were determined by dividing the load by the measured cross-sectional area of the thin section of the specimen. The dimensions of the flat specimens were kept the same with the dimensions of the tapered specimens except for the thickness. The specimen dimensions are given in Fig. 4.13. The photos of the flat specimens are given in Appendix D.

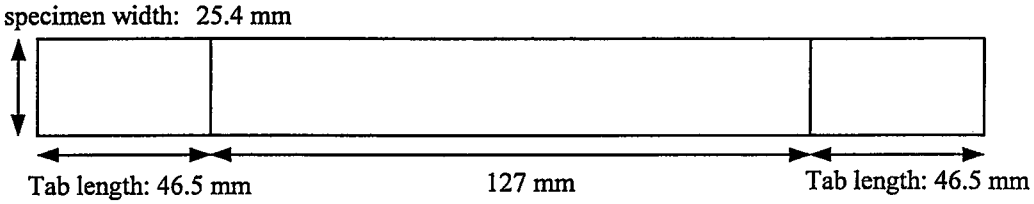

Figure 4.13: Specimen Dimensions for Flat Laminates

Three samples of each of two configurations identified as RL1 and RL2 were tested. RL1 configuration represents the thin section of the configurations TL1, TL2, and RL2 configuration represents the thin sections of configurations TL3, TL4, TL5.

The tests of flat laminates were carried out with the same experimental set-up and procedure of tapered laminates. The results of the tests are given in Table 4.10 and 4.11 where w is the width, t is the thickness, P is the failure load and S is the failure stress.

Table 4.10: Experimental Test Results for Configuration RL1

Spec. No.	w (mm)	t (mm)	P (kN)	S (Mpa)
RL1-1	25.32	1.14	30.700	1063
RL1-2	25.34	1.18	31.770	1062
RL1-3	25.34	1.16	29.730	1011
	Average		30.733	1045
	Std. Dev.		1.02	30

Table 4.11: Experimental Test Results for Configuration RL2

Spec. No.	w (mm)	t (mm)	P (kN)	S (Mpa)
RL2-1	25.26	1.10	35.02	1260
RL2-2	25.38	1.16	44.60	1515
RL2-3	25.20	1.18	43.45	1461
	Average		41.023	1412
	Std. Dev.		5.23	134

4.3.3 Experimental Results of Tapered Laminates

Tapered laminates were tested under quasi-static tension. Five specimens were tested. Two of the tests halted just after the determination of delamination onset. Remaining three were tested to failure.

In many of the previous studies acoustic emission data, strain-gage response and visual inspection technique were used to detect delamination onset [7, 11, 13, 26, 30, 43, 44, 54, 55, 58]. Visual inspection technique was used for only semi transparent glass/epoxy specimens by using a light source and black ink. For the experimental study of the tapered laminates, none of these detection techniques could be used. The visual inspection was impossible because of non-transparent carbon/epoxy material. Additionally acoustic emission and strain-gage systems were unavailable. Thus delamination onset was detected by investigating the load versus displacement plots of the samples.

The specimens were investigated during the tests for the onset and growth of delamination. Delamination was detected audibly during the loading of the specimens. A corresponding drop in load also occurred at the time when

delamination was detected audibly. The mechanism of failure is illustrated in Figure 4.14 and 4.15 on the Load vs. displacement graph of specimen 3 of configuration TL1. The data taken from INSTRON were plotted by using MS EXCEL program. Two original sample plots belong to configurations TL1 and TL2 are given in Appendix E.

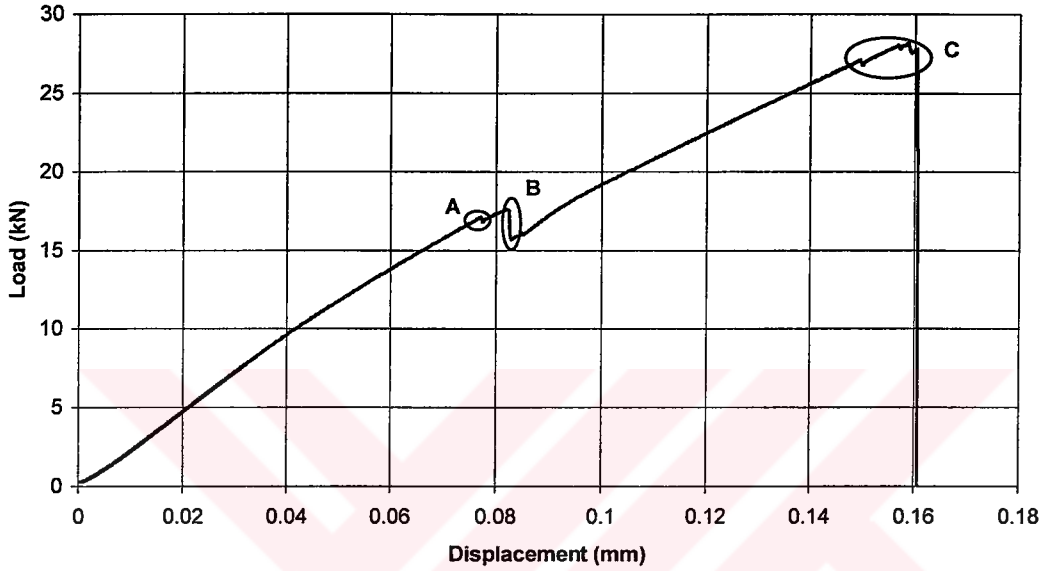

Figure 4.14: Load vs. Displacement Graph of Specimen 3 of Configuration TL1

The onset of delamination was detected at point A with an approximately 200 N drop in load. Then, delamination grew through the width and at point B specimen delaminated through the whole width with a larger drop in load. Delamination grew slowly along the longitudinal axis of the specimen to the point of failure C. Figure 4.14 is rescaled to illustrate delamination initiation event in Figure 4.15.

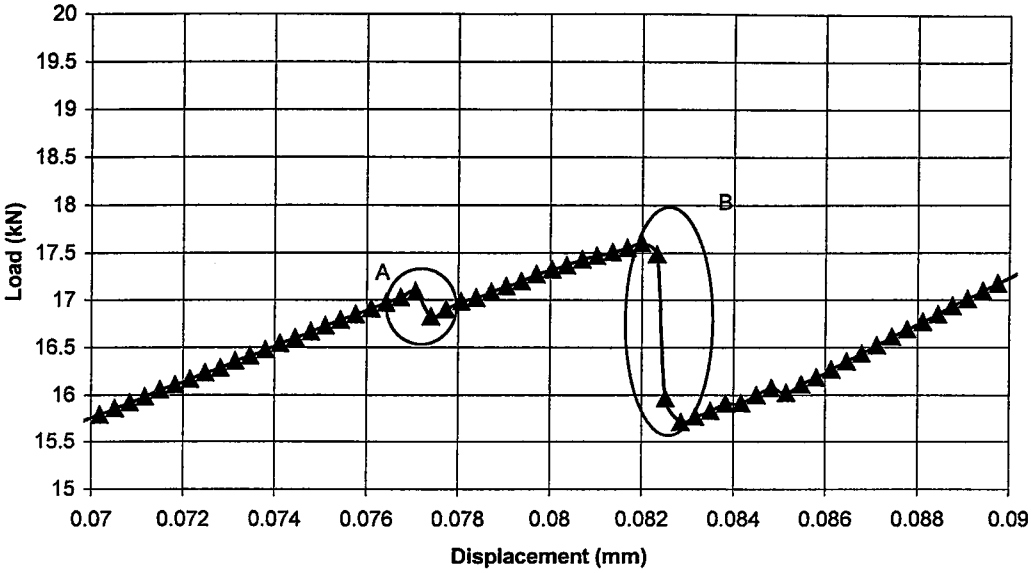

Figure 4.15: Delamination Onset of Specimen TL1-3

In this study, delamination onset load for tapered specimens were detected by investigating the load versus displacement data exported from the INSTRON testing machine. A load drop higher than 100 N was judged as delamination onset.

Test results for different tapered laminate configurations are given separately. Also the visual observations on specimens are illustrated. The specimens which were tested until delamination onset, examined under optical microscope and also optical microscope photos of the delaminated site are given in Appendix C.

4.3.3.1 Experimental Results of TL1

Delamination onset easily detected by a high cracking sound and a corresponding drop in load. But it was hard to locate delamination onset site. Although the test was halted just in a second after the detection of audible indication it was seen that delamination was followed by matrix cracking of

90° plies. However the observed delamination path includes the predicted delamination onset site by FEA.

Visual observation of delamination onset and growth examined by a magnifier and illustrated in Figure 4.16. The sequence of events observed during the tests are listed below. All TL1 specimens showed similar delamination behaviour.

1) Delamination onset at one edge. (Continuous lines)
2) Delamination growth through the width.
3) Delamination along the width.
4) Delamination growth through the longitudinal axis of specimen. (Dotted arrows)

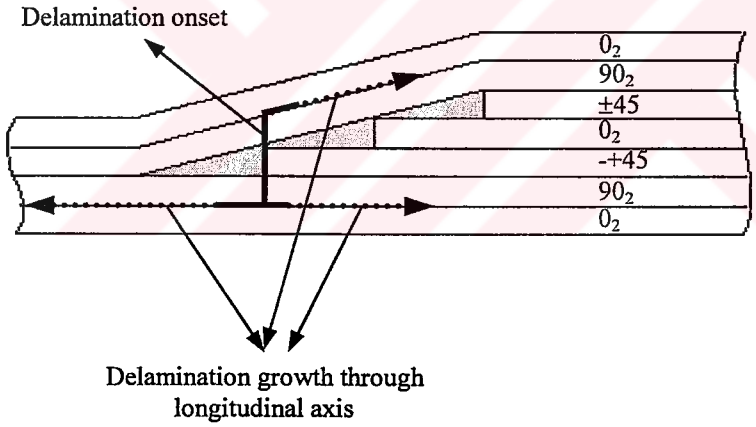

Figure 4.16: Delamination Onset and Delamination Growth in TL1

Tensile test results for configuration TL1 are given in Table 4.12.

Table 4.12: Test Results for Configuration TL1

Spec. No.	w (mm)	t (mm)	Delamination Onset		Failure	
			P(kN)	S(Mpa)	P(kN)	S(Mpa)
TL1-1	25.34	1.08	15.348	560	27.320	998
TL1-2	25.30	1.08	16.731	612	23.030	843
TL1-3	25.28	1.10	17.087	614	26.890	967
TL1-4*	25.16	1.10	15.671	566	-	-
TL1-5*	25.24	1.08	17.510	642	-	-
	Average		16.469	599	25.747	936
	Std. Dev.		0.926	35	2.362	82

* Examined for delamination onset site under optical microscope

4.3.3.2 Experimental Results of TL2

Similar delamination onset behaviour was seen in configuration TL2 as in configuration TL1. The sequence of events were the same as given in Figure 4.16. Tensile test results for configuration TL2 are given in Table 4.13.

Table 4.13: Test Results for Configuration TL2

Spec. No.	w (mm)	t (mm)	Delamination Onset		Failure	
			P(kN)	S(Mpa)	P(kN)	S(Mpa)
TL2-1*	25.26	1.08	17.026	624	-	-
TL2-2*	25.18	1.10	18.100	653	-	-
TL2-3	25.18	1.08	18.604	684	25.300	930
TL2-4	25.22	1.07	18.892	700	28.280	1048
TL2-5	25.10	1.06	19.644	738	22.340	839
	Average		18.453	680	25.306	939
	Std. Dev.		0.974	44	2.907	104

* Examined for delamination onset site under optical microscope

4.3.3.3 Experimental Results of TL3

The tests conducted using the same experimental set-up and conditions. However, the delamination onset could not have been seen for any of the specimens. Although some small audible signs occurred there was no drop in load. Specimens delaminated through the width suddenly at higher loads with a significant load drop. Investigating the load versus displacement plot, only one load drop was seen which indicate the delamination along the width. The load versus displacement plot of TL3-1 specimen is given in Figure 4.17.

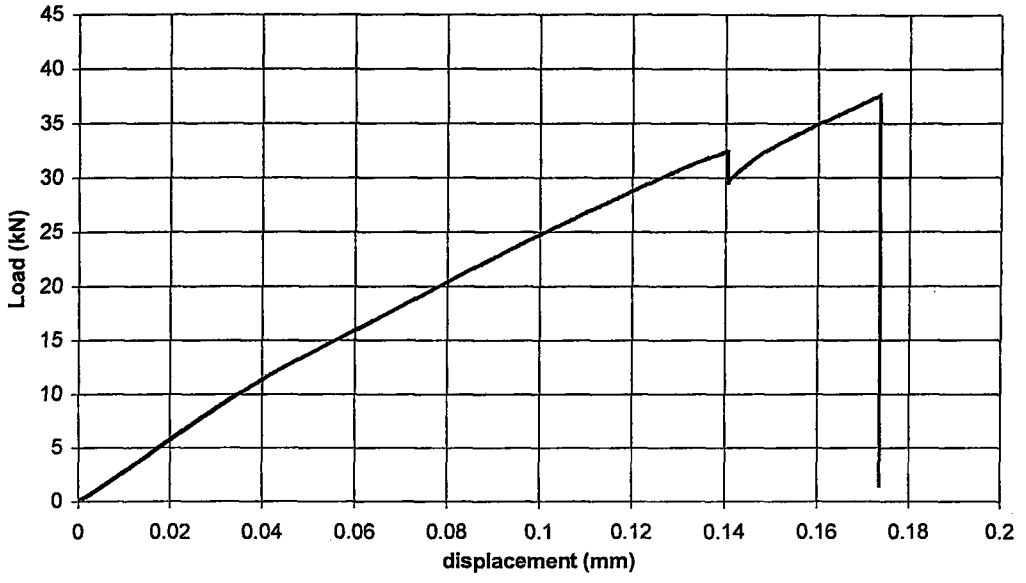

Figure 4.17: Delamination of Specimen TL3-1

For the configuration TL3, three specimens were tested to failure and two specimens were tested to delamination through width. The test results are given in Table 4.14. Delamination path is illustrated in Figure 4.18.

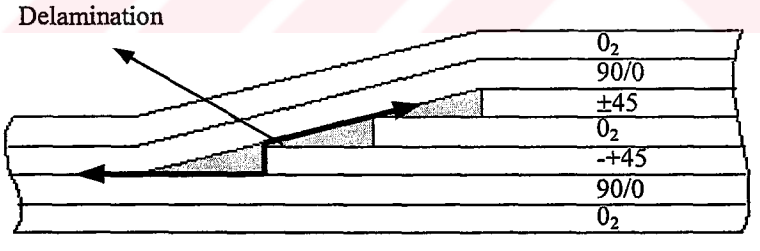

Figure 4.18: Delamination Path in TL3

Table 4.14: Test Results for Configuration TL3

Spec. No.	w (mm)	t (mm)	Delamination		Failure	
			P(kN)	S(Mpa)	P(kN)	S(Mpa)
TL3-1	25.30	1.11	32.415	1154	37.543	1337
TL3-2*	25.20	1.13	30.200	1061	-	-
TL3-3*	25.14	1.14	33.520	1170	-	-
TL3-4	25.04	1.14	32.617	1143	36.230	1269
TL3-5	25.16	1.12	32.415	1150	37.400	1327
	Average		32.233	1135	37.057	1311
	Std. Dev.		1.225	43	0.720	37

* Examined for delamination onset site under optical microscope

4.3.3.4 Experimental Results of TL4

In experiments, although audible signs heard, delamination onset could not have been detected by the described method. Moreover there was no load drop, indicating any delamination. Investigating the failed specimens, it was observed that delamination must have been occurred. Specimens failed in tensile failure mode but it was seen that discontinuous plies were separated from continuous plies from below and above. But during the tests this event could not been captured. Thus, test results for TL4 is given in Table 4.15 without any result about delamination.

Table 4.15: Test Results for Configuration TL4

Spec. No.	w (mm)	t (mm)	Failure	
			P(kN)	S(Mpa)
TL4-1	25.38	1.12	43.310	1524
TL4-2	25.24	1.14	42.870	1490
TL4-3	25.22	1.13	44.560	1563
TL4-4	25.13	1.12	45.460	1615
TL4-5	25.16	1.11	43.880	1571
	Average		44.016	1553
	Std. Dev.		1.026	47

4.3.3.5 Experimental Results of TL5

TL5 specimens showed a similar behaviour as TL4. Delamination occurred instantaneously along the width. Delamination onset could not have been detected. Sudden delamination along width observed by a drop in load. The load versus displacement plot of specimen TL5-4 is given in Figure 4.19.

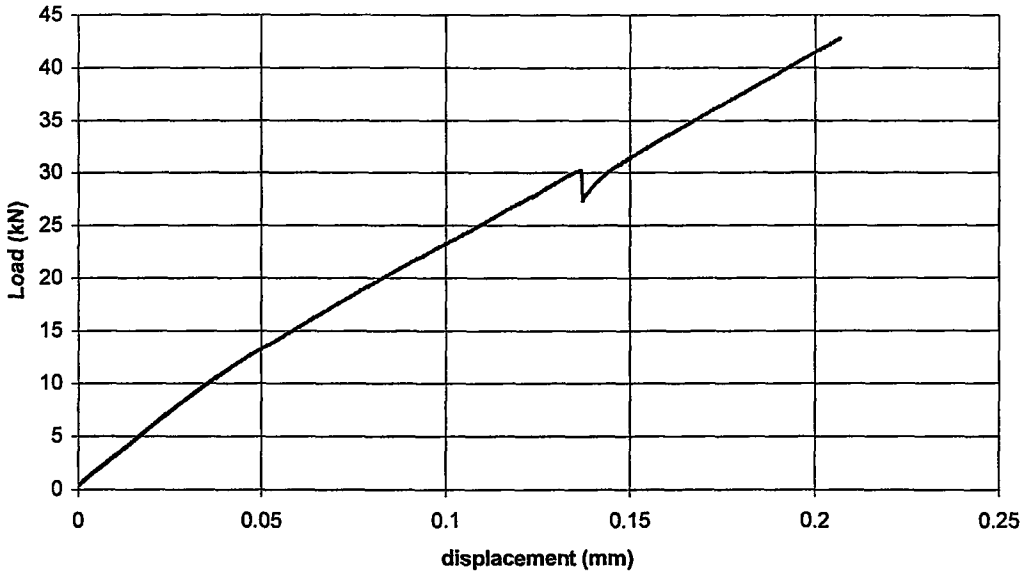

Figure 4.19: Delamination of Specimen TL5-4

Specimens delaminated from the upper interface of the discontinuous plies. Delamination path is given in Figure 4.20. Test results are given in Table 4.16.

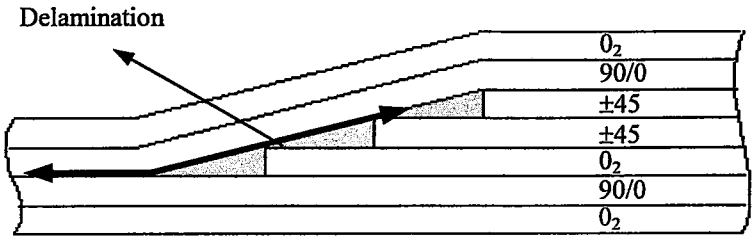

Figure 4.20: Delamination Path in TL5

Table 4.16: Test Results for Configuration TL5

Spec. No.	w (mm)	t (mm)	Delamination		Failure	
			P(kN)	S(Mpa)	P(kN)	S(Mpa)
TL5-1	25.30	1.10	28.939	1040	39.341	1414
TL5-2*	25.31	1.10	28.872	1037	-	-
TL5-3*	25.32	1.10	27.140	974	-	-
TL5-4	25.24	1.14	30.200	1050	42.750	1486
TL5-5	25.21	1.10	28.603	1031	37.247	1343
	Average		28.750	1026	37.779	1414
	Std. Dev.		1.091	30	2.777	71

* Examined for delamination onset site under optical microscope

CHAPTER 5

DISCUSSION AND COMPARISON

A tapered laminate with ply drops analyzed for various configurations by using the finite element method and several tests were conducted to verify the analysis. Five different configurations were investigated numerically and experimentally by changing the orientation of plies. Additionally two configurations were reanalyzed with FEM to take into account the migration of fibers in 90° plies.

In this chapter numerical results and experimental results are discussed and compared.

5.1 Finite Element Analysis of Tapered Laminates

Tapered laminates with configurations TL1, TL2, TL1-M, TL2-M, TL3, TL4, TL5 were analyzed with the FEM. The boundary conditions were employed so that they approximated the restrains of the experimental set-up. Finite element mesh size was determined by preliminary studies.

In preliminary studies, a simple basic model with different element sizes corresponding to different aspect ratios was investigated. The behavior of out-of-plane stresses was compared qualitatively with a previous study [59]. It was seen that in-plane stresses were not affected by changing the element

aspect ratio whereas out-of-plane stresses were increased by decreasing aspect ratio. This was expected because of free-edge effect. Poisson's ratio mismatch between the plies gave rise to very high stresses or even singularities at the free-edge. Also it was seen that to capture the free–edge effect in FEA, three-dimensional modeling is required or special elements must be used to take into account the out-of-plane stresses.

The smallest aspect ratio investigated in the preliminary study was 2.5. For the basic model it was possible to decrease the element sizes to that ratio but for the tapered laminates using such a small aspect ratio for elements was prevented by hardware capabilities. However, the aspect ratio value of 5 used for the FE analysis of tapered laminates was acceptable since the results were not far from the FE results for aspect ratio value of 2.5. Thus, for the aspect ratio a value of 5 was chosen for the FEA of tapered laminates.

Including interply resin layer in the model is a common approach in literature [3, 13, 30, 43]. The effect of including this layer in the FE model was investigated in preliminary studies. It was seen that in-plane stresses were not affected by inclusion of interply resin layers whereas out-of-plane stresses were significantly affected. The preliminary study was verified by comparing qualitatively with a previous study [59]. Also in an actual case these interply resin layers are likely to be formed. Investigation of the manufactured tapered laminates under optical microscope revealed these interply resin layers and a photomicrograph showing the interply resin layer is given in Appendix C.

As a result of preliminary studies, tapered laminates were modeled with resin rich pockets and interply resin regions. These resin rich pockets and interply resin layers are formed as a result of the manufacture and cure process. Tapered laminates were modeled with ideal geometry with constant ply thickness, constant taper angle and perfect placement of plies in a tapered lamina.

The material properties were obtained from the manufacturer's specifications when possible. But for the three-dimensional analysis of the laminates, additional material constants were required. Therefore, some tests were conducted to find the needed material properties. However, neat resin of the material could not be tested due to the lack of neat resin. Thus, the material properties used in the FEA were the combination of the manufacturer data and test results.

The analyses were performed using MARC package program with a SGI-OCTANE workstation, which took about 15-20 minutes run time per analysis.

Interlaminar stresses and equivalent von Mises stress were used to characterize the stress state in tapered laminates. As the interply resin is the weak link, it was assumed that critical stresses occurred in the lower and upper interply resin layers. Analyzing the stresses in the interply resin layers, it was seen that stresses away from the tapered region were approximately constant. It can be said that the effect of taper and dropped plies gets diminished as one moves away from the tapered region and becomes negligible. The stresses far away from the tapered region represent the stresses that exist in untapered laminates of the same thickness as the thick and thin sections respectively.

FEA shows that critical stresses occur at the tapered region. Stresses start to increase from the beginning of the taper and decrease at the root of the taper. Thus it is obvious that failure will initiate at the tapered region for a laminate with taper.

In Chapter 3 the stress versus location plots for the interply resin layers were given for various configurations. It was seen that in all of the configurations stresses in the upper interply resin layer were more critical than

stresses in the lower interply resin layer. So, upper interply resin layer was found to be the probable failure site according to the FEA.

An isotropic failure criterion was used to predict the location of delamination onset. Equivalent von Mises stress distribution was plotted for upper and lower interply resin layer for each configuration. The location of maximum equivalent von Mises stress was taken as delamination onset site. For all of the configurations delamination onset site was predicted to be at the end of the last ply drop in the upper interply resin layer.

The configurations were chosen to find out the effect of orientations of plies. In all of the configurations orientation of plies were arranged to construct symmetrical laminates for both the thick and thin sections. However in some of the configurations the thick sections were not symmetrical but very close to a symmetrical one because of +-45° plies used for the middle dropped ply. Also in configuration TL5 an unsymmetrical layup was chosen for the thick section. In configurations TL1, TL2, TL1-M, TL2-M and TL3, TL4, TL5 the orientations of continuous plies were the same. Keeping the lay-up of the continuous plies the same decreased the parameters to be investigated at a time. To discuss the effect of orientation of plies, configurations are investigated in groups.

The original FEM models of TL1 and TL2 were modified to model migrated fibers of 90° plies and these models were designated as TL1-M and TL2-M. Migrated fibers filling the resin pockets decreased the stresses in the interply resin layers at the tapered region. σ_{ZX} decreased about 3% at the end of the last ply drop where maximum interlaminar shear stress was attained. Also magnitude of σ_{YZ} decreased 16% at the same location. At the root of the taper the value of σ_{ZZ} decreased by 2.4%. The reduction percentages are approximately the same in both configurations.

Examining the specimens under optical microscope, it was seen that fibers of 90° plies indeed migrate. It is clear that fibers migrated to the resin pockets, leaving very small, dispersed resin rich regions. This event can be seen from photomicrographs, given in Appendix C. Thus, it is more appropriate to discuss the configurations TL1-M and TL2-M in detail which considers the effects of migrated fibers of 90° plies.

Configurations TL1-M and TL2-M have the same orientation of continuous plies. The middle dropped ply changed from 0_2 in TL1-M to +-45 in configuration TL2-M. As the dominant stress came out to be σ_{ZX} in the upper interply resin layer for all configurations, interlaminar shear stresses will be compared first. The plots for interlaminar shear stresses at the tapered region are given in Figure 5.1.

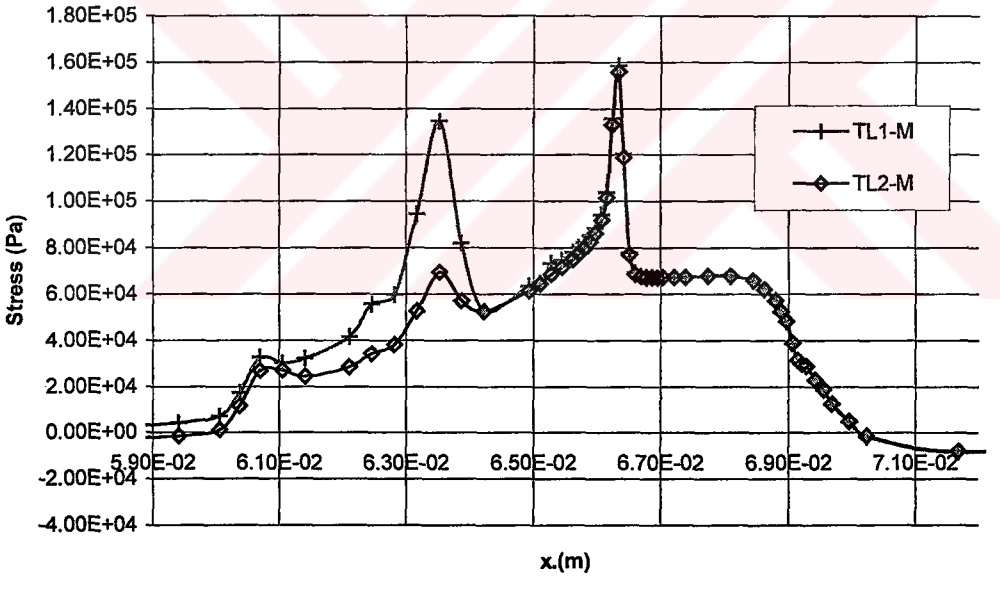

Figure 5.1: Interlaminar Shear Stresses in the Upper Interply Resin Region for TL1-M and TL2-M

Interlaminar shear stresses showed peaks at the tips of the dropped plies. Thus dropped plies were found to act as stress risers. The magnitudes of peaks may change but these stress concentrations at the tips of the dropped plies are mainly responsible for onset of delamination.

The stacking sequences of the configurations are different at the thick section and same at the thin section for TL1-M and TL2-M. This difference can be seen from Figure 5.1, stresses in TL2-M are 48% smaller at the thick section and approximately the same at the thin section. This is the expected variation of interlaminar shear stress as tapered laminates behave like flat laminates far from the tapered region.

It was found that maximum interlaminar shear stresses occur at the end of the last ply drop. Investigating Figure 5.1, it is observed that stresses at that location are so close to each other; σ_{ZX} in TL2-M is approximately 2% smaller in magnitude.

At the location where middle dropped plies end, there is a large difference between interlaminar shear stresses. When a ply which is stiffer along the longitudinal direction than in the lateral direction, is introduced in the laminate, the interlaminar shear stress roughly doubles. As there is a stress concentration at that point, introducing 0° plies doubles the effect of this concentration.

The same effect is also valid for σ_{YZ} and σ_{ZZ}. As interlaminar shear stress is mainly responsible for delamination onset, the effects of dropped plies on other stress components are not discussed in detail.

If we compare the predicted delamination onset stresses for configurations TL1-M and TL2-M, we see that the maximum delamination onset stress was found for configuration TL2-M. According to the maximum

stress criterion, delamination onset increased by 1.83 % and 1.98% according to the delamination failure criterion by replacing the middle dropped plies. Delamination onset stress increased very little in going from configuration TL1-M to TL2-M.

Interlaminar stresses in the lower interply resin layer came out to be small compared to the upper one. Also in the lower interply resin layer, the locations where ply drops end are critical. σ_{ZX} and σ_{YZ} suddenly become compressive from tensile and return back to tensile again and sharp fluctuations occur in σ_{ZZ} at this location.

Comparing TL3, TL4 and TL5 would give a better understanding of the effects of dropped plies on the stress states. These three configurations have the same lay-up of continuous plies. The interlaminar stress distributions in the upper interply resin layer are given in Figure 5.2.

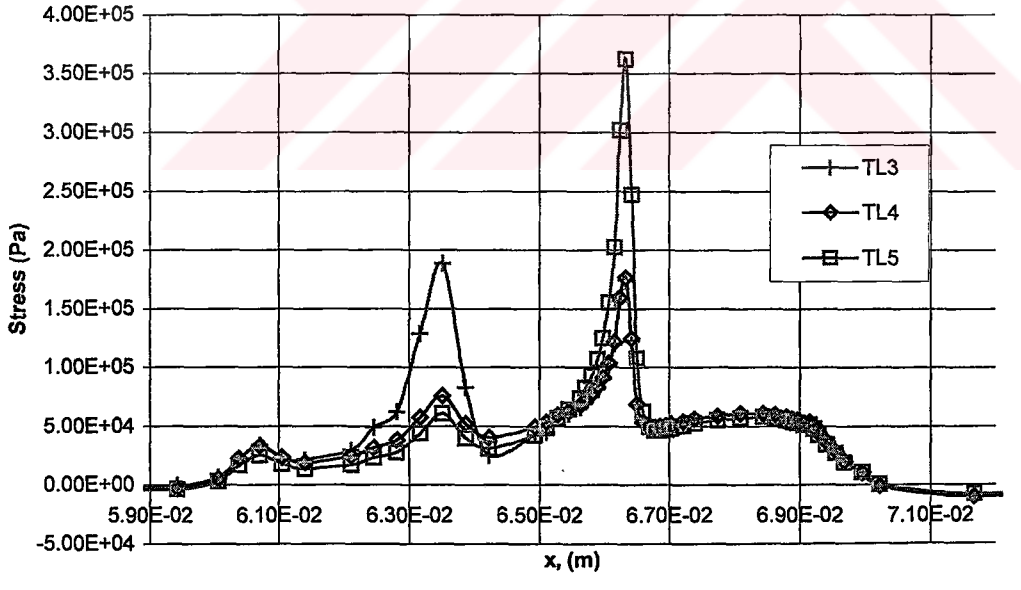

Figure 5.2: Interlaminar Shear Stresses in the Upper Interply Resin Region for TL3, TL4, and TL5

It is clear that using 0^{o} plies multiplies the magnitude of stress concentration. At the end of the first ply drop, σ_{ZX} in TL3 and TL4 are very close to each other and approximately 23% smaller than TL5. At the end of the middle dropped plies, the effect of replacing 0^{o} plies with $+\text{-}45^{o}$ plies in configuration TL3 can be seen by an increase in magnitude of stress about 2.5 times. Although, maximum σ_{ZX} was seen at the end of the last ply drop in other configurations, in TL3 the location of maximum σ_{ZX} came out to be at the end of the middle dropped plies. At the end of last dropped plies, σ_{ZX} doubled by replacing $+\text{-}45^{o}$ plies with 0^{o} plies in configuration TL5. Also σ_{ZZ} was tripled at the end of the middle dropped ply in configuration TL3 and at the end of the last dropped ply in configuration TL5. However the magnitude of σ_{YZ} decreased 20 times in configuration TL5 at the end of the last dropped ply. Thus, we can say that introducing a ply which is stiffer in longitudinal direction decreases σ_{YZ}.

In the lower interply resin the same doubling effect is valid for σ_{ZX}. Interlaminar shear stress increased 9.5 times at the end of the last ply drop in configuration TL5. Also the fluctuation band of σ_{ZZ} increased 43% in magnitude for configuration TL5 at the same location.

If we investigate the delamination onset stresses according to the maximum stress criterion, the minimum delamination onset stress was found to be 51% smaller for configuration TL5 than configuration TL4 and 52% smaller than configuration TL3. Delamination onset stress in configuration TL3 is 1.6% higher than in configuration TL4. According to the delamination failure criterion, delamination onset stress in TL4 was reduced 47% in configuration TL5 and also delamination onset stress of configuration TL3 is 1.7% less than that of TL4.

Comparison of the interlaminar shear stresses shows that, the most critical stress concentrations arise at the end of the last ply drop. It is possible to increase the delamination onset stress by changing the orientation of the last dropped ply. Introducing a ply which is stiffer in longitudinal direction decreases the delamination onset stress.

The effect of orientation of dropped plies on the stress state and delamination onset stress is clear. Investigating the configurations which have the same orientation of dropped plies further, gives a better understanding of the effect of continuous plies covering the dropped plies. Figures 5.3 and 5.4 show the dominant stress (σ_{ZX}) distributions in the upper interply resin layer for TL1, TL3 and TL2, TL4 respectively. Configurations TL1-M and TL2-M are not included in the figures to have the same basis for comparing the configurations.

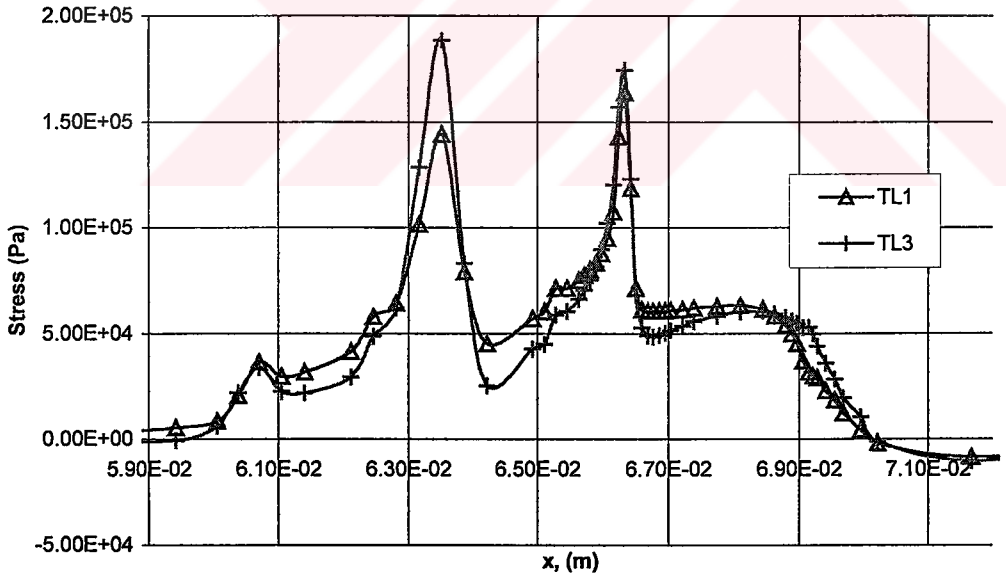

Figure 5.3: Interlaminar Shear Stresses in the Upper Interply Resin Region for TL1 and TL3

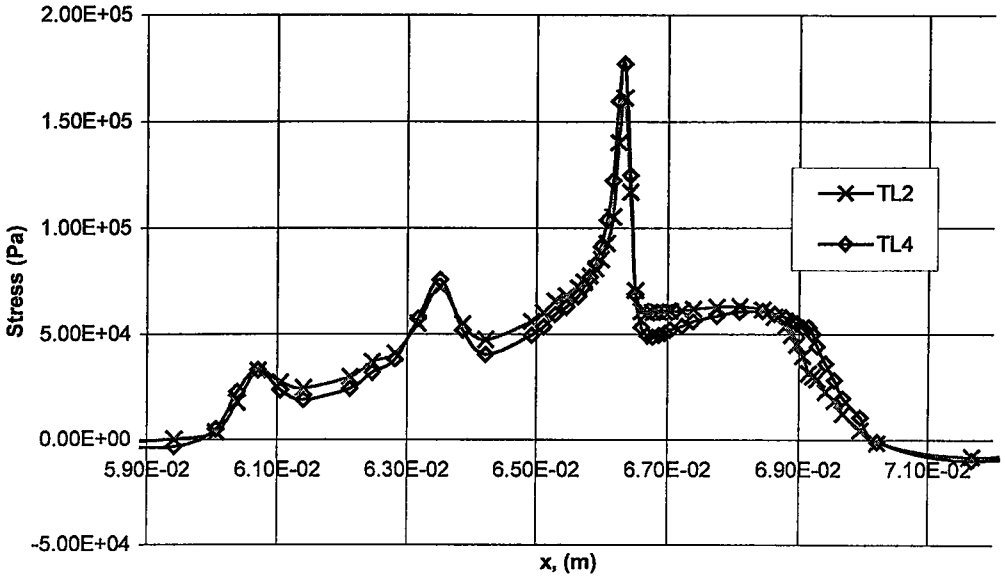

Figure 5.4: Interlaminar Shear Stresses in the Upper Interply Resin Region for TL2 and TL4

Investigating Figure 5.4 alone, it seems to have little effect to change the covering ply from 90° to 0°. This replacement increased maximum stress by 10 %. But from Figure 5.3 it is observed that if this replacement is done with the presence of 0° dropped plies, interlaminar shear stress increases significantly. This effect can be seen at the end of the middle dropped plies in Figure 5.3. Configurations TL1 and TL2 have 0° middle dropped plies and at that location, replacing the 90° cover ply with a 0° ply increased the interlaminar shear stress by 30%.

From previous observations we know that if longitudinally stiffer plies are used as dropped plies, interlaminar shear stresses in the upper interply resin layer increase. Moreover, from Figures 5.3 and 5.4 it is clear that if longitudinally stiffer covering plies are used with the presence of longitudinally stiffer dropped plies interlaminar shear stress increases more. The same result is also valid for interlaminar normal stress whereas it is the opposite for σ_{YZ}.

The effect of dropped plies on the stress state of tapered laminates was studied with Finite Element Analysis. The results of the analysis can be summarized as follows

- Significant interlaminar stresses arise at the tapered region.
- Dropped plies act as a stress riser.
- Interlaminar shear stress in the upper interply resin layer is the dominant stress state and mainly responsible for the onset of delamination
- The end of the last ply-drop is the critical location for delamination onset
- Delamination onset stress can be altered by changing the orientation of dropped plies or covering plies.

The cause for delamination can be explained as follows.

In the tapered region, the load carried by the discontinuous plies is transferred to the continuous plies through interply resin layers surrounding the ply drops. The transfer of the axial load to dropped plies is by interlaminar shear. Significant interlaminar stresses arise in these interply resin layers and these stresses promote delamination. The interply resin layers are the weak link in the component and will fail first. Fracture of the resin layers will result in delamination in the taper region.

Generally, geometric discontinuities result in stress concentrations. In the problem statement of this study, geometric discontinuity was introduced by dropping plies to produce the taper. Although the taper angle is uniform, the ends of the dropped plies are sharp corners and bring additional increase in stresses in the tapered region at the end of the dropped plies.

Tensile loading was applied to the model. As the geometry is not symmetrical, bending moments are created due to the tensile loading. So the loading was bending-tension coupled loading. Bending moment increases interlaminar shear stress but decreases interlaminar normal stress. When a tensile load is applied to the thin end of the structure, the continuous plies try to become straight along longitudinal direction and interlaminar normal stresses build up. But as the model is free to move along the normal direction the interlaminar normal stresses are not so severe as the interlaminar shear stresses. This tendency significantly increases interlaminar shear stresses. If the boundary conditions are modified to a symmetrically tapered laminate (i.e. taper on both sides), the interlaminar shear stresses will decrease whereas the interlaminar normal stresses will increase.

5.2 Experimental Results

Several tests were conducted to verify the finite element results. Five specimens for each tapered configuration were tested. Totally 31 specimens were tested including the reference untapered laminates.

Delamination event was observed visually during tests. Some delaminated specimens were taken out from the test fixture before failure and were investigated under an optical microscope. The photos of the specimens are given in Appendix D.

When observed under an optical microscope with a magnification factor of 50, it was seen that the fibers of 90^{o} cover plies migrated into the resin pockets in specimens of configurations TL1 and TL2.

Specimens TL1 and TL2 delaminated similarly. Specimens of these configurations first delaminated at the end of the last ply drop and followed by matrix cracking of 90^{o} plies from the lower interface between 0^{o} and 90^{o} to the

upper interface. Then delamination grew through the width of the laminate. Further loading of specimens enlarged delamination through the thin section at the lower interface and through the thick section at the upper interface. These sequences of events were evident in load-displacement response by a small decrease of load at the onset of delamination and a larger drop in load at the delamination through the whole width. Delamination onset stresses were found by investigating the load versus displacement plots and calculated by dividing the load with the area of the thin section.

Delamination onset stress of configuration TL2 was found to be 13% higher than that of TL1. Replacing 0° middle dropped plies with $+-45^{\circ}$ plies increased the delamination onset stress. Failure stresses for both configurations are approximately the same. Comparing the failure stresses with the reference flat laminate RL1, it is observed that the failure stress is decreased by 10.5% in tapered laminates. Thus, tapering decreased the failure stress below the failure stress of thin section in configurations TL1 and TL2.

For configurations TL3, TL4 and TL5 the same approach was used to detect the delamination onset stress. However there was no drop in the load indicating the onset of delamination. For these three configurations delamination onset stress could not be found. At higher loads a load drop was observed in configurations TL4 and TL5 indicating the delamination through the width.

The detection of delamination onset load for configurations TL1 and TL2 was easy by examining the load-displacement response. As delamination onset followed by matrix cracking of 90° plies, the failed surface was larger than other configurations. Thus the load drop could be detected with relative ease. But in configurations TL3, TL4 and TL5 delamination was restricted by 0° covering plies. It is probable that delamination initiation occurred at the thin interply resin and grew through the width slowly without any remarkable

indication. As the failed surface is so small compared with other configurations, there was no effect of delamination onset in the load-displacement response of the specimens. Thus, for configurations TL3 and TL5 delamination stresses and failure stress are reported rather than the delamination onset.

In configuration TL4 there was no evidence of delamination in the load-displacement curves. Because of the reason discussed above the onset of delamination could not be detected. Moreover, TL4 specimens did not delaminate through the complete width. It is probable that delamination initiated in the thin interply resin layer and grew along the longitudinal axis of the laminate, without a remarkable drop in the load. Thus, only the failure stresses are reported for configuration TL4.

Detection of the delamination onset load was proved to be a difficult task, requiring special measuring systems. Acoustic emission systems are mostly used to detect delamination in literature. As delamination occurs with the cracking of thin interply resin layers, the noises generated by the cracking resin layers are good indications of a delamination onset. Also in some of the previous studies strain gauges were used for the detection of delamination onset in tapered laminates. However neither of these systems was available during the testing of tapered laminates.

Delamination through the whole width stress in configuration TL3 is found to be 10.6% greater than TL5. Comparing failure stresses with flat laminate RL2, it is found that failure stress of TL3 is 7.15% smaller, TL4 is 9.1% higher and TL5 is approximately equal to as that of RL2.

Delamination was restricted by the covering plies in specimens TL3 and TL5. In TL3 specimens, delamination occurred at the end of last ply drop going through the lower and upper interply resin layer. It then grew from the

lower interply resin layer to the mid-plane of the thin section and along the upper interply resin layer through the end of the thick section. TL5 specimens delaminated from the upper interply resin layer and grew through the tips of the specimens by further loading.

Delamination onset location was difficult to detect. Delamination occurs very fast. Even if the test is stopped after the detection of damage for some specimens, the failure surface grows rapidly making the onset location indistinguishable. However the predicted locations of delamination onset by FEA came out to be within the first observed failure surfaces.

The results of the experimental study show that the tensile strength may be significantly reduced by the presence of a thickness discontinuity and delamination is mainly responsible for this reduction. By changing the orientation of plies the tensile strength may be increased by delaying the delamination onset. As explained by Vizzini [11], the reduction in strength is directly related to the increase in the axial stiffness of the thick section relative to the thin section. Thus, the greater the change in stiffness between the thick section and the thin section at the dropped ply location, the greater is the reduction in strength. Also in this study it was observed that the location of the last dropped ply is critical and changes in stiffness of the last dropped ply is the primary reason for the change in tensile strength.

The failure stresses of the tapered laminates were lower then the failure stresses of the reference flat laminates except for configuration TL4. The increase in the failure stress may be explained by the words of Fish and Lee [7]: " The increase in failure stress may be due to a beneficial stress state created by taper or, more likely, to greater end effects on the thin section of the tapered laminate."

5.3 Comparison of Numerical and Experimental Results

In the numerical studies, delamination onset stresses were found for seven different configurations. In the experimental study, delamination onset stresses could be detected for only two of the configurations.

Delamination onset stresses for configurations TL1-M and TL2-M, were found by using the maximum stress and delamination failure criteria. Delamination onset stresses were detected for configurations TL1 and TL2 experimentally. The results are given in Table 5.1.

Table 5.1: Delamination onset stresses

	TL1-M	**TL2-M**
Max. Stress (MPa)	591	602
Delamination Fail. Crit. (MPa)	642	655
Experimental (MPa)	599	680

Delamination onset stress is underestimated with maximum stress criterion by 1.33%, overestimated with delamination failure criterion by 7% for configuration TL1. Delamination onset stress is underestimated with maximum stress criterion by 11.5% and underestimated with delamination failure criterion by 3.7% for configuration TL2.

Thus, it can be said that the results of Finite element analysis by using both failure criteria agree well with experimental results. Delamination onset stresses predicted by numerical analysis are close to experimentally determined values.

In finite element analysis of tapered laminates the geometry of the taper has been idealized. However, variations due to manufacturing are common. These variations may affect delamination onset stresses. So, to be more accurate these geometric variations must be included in the model. Because of this reason it is probable that accuracy of the finite element analysis changes from one configuration to another. The effects of realistic geometries in tapered laminates on the finite element model were investigated by Vizzini [57]. In his study, geometries such as ill-formed pockets, unsymmetric or offset ply drops, and voids were modeled. He concluded that an ill-formed resin pocket increases the stress state by increasing the local taper angle at the ply drop and the site of damage onset is dependent on the geometry of the resin pocket.

Damage detection schemes often require sufficient damage to occur. Whereas the analytical model indicates the onset of damage, experimental data indicate the point at which the damage is detected. Measuring systems like acoustic emission or strain gauge systems must be used to detect the real delamination onset value accurately in experiments.

CHAPTER 6

CONCLUSION

The effects of ply-drops on the stress-state of tapered laminates have been investigated with finite element method and verified with experiments. A three-dimensional finite element model, including resin rich pockets and interply resin layers, was constructed and solved. Equivalent von Mises stress was used to predict delamination onset location. Maximum stress criterion and delamination failure criterion, which is the modification of Tsai-Wu criterion, were used to predict delamination onset stress. Tapered specimens with different stacking sequences were manufactured and tested under uniaxial tension.

Based on the results of the experimental and Finite Element analyses, the following conclusions can be made:

- Presence of ply-drops increases interlaminar stresses in a tapered laminate. For an unsymmetric tapered laminate the stress-state is dominated by the interlaminar shear stress. Thus, the failure of the tapered laminates is due to the interlaminar shear stress, σ_{ZX} and occurs in the upper interply resin layer at the last ply-drop step.

- Primary failure mode for tapered laminates with ply-drops is delamination. Changing the orientation of plies can alter delamination onset stress but does not affect the location of delamination onset. The orientation of the last dropped ply is the most important factor for the delamination onset. Also the orientation of adjacent cover ply has a significant effect on delamination onset.

- The actual geometry of tapered laminates is different from ideal geometry. Migration of fibers in 90° plies probable if they are used as covering plies. This migration was found to cause an increase in delamination onset stress.

- Experimentally detecting delamination onset requires special measuring systems. Delamination initiation cannot be detected for all configurations by monitoring load-displacement response of the specimens.

- The finite element results for delamination onset stress values agree well with the experimentally determined delamination onset stress values. Delamination onset stress is underestimated with maximum stress criterion by 1.33% and overestimated with delamination failure criterion by 7% for configuration TL1. Delamination onset stress is underestimated with maximum stress criterion by 11.5% and underestimated with delamination failure criterion by 3.7% for configuration TL2.

REFERENCES

[1] B.L. Kemp and E. R. Johnson, "Response and Failure Analysis of a Graphite-Epoxy Laminate Containing Terminating Internal Plies", Proceedings of the 2nd Annual Review of the Center for Composite Materials and Structures, pp. 42-84, 1985, (AIAA Paper 85-0608).

[2] Anthony J. Vizzini, "Strength of Laminated Composites with Longitudinal Discontinuities", AIAA/ASME/ASCE/AHS/ASC Structures, Structural Dynamics and Materials Conference, AIAA, pp. 1260-1269, 1990, (AIAA Paper 90-1065).

[3] Antonio S. Llanos, Sung W. Lee and Anthony J. Vizzini, "Delamination Prevention in Tapered Composite Structures Under Uniaxial Tensile Loads", AIAA/ASME/ASCE/AHS/ASC Structures, Structural Dynamics and Materials Conference, AIAA, pp. 1242-1252, 1990, (AIAA Paper 90-1063).

[4] C. Y. Poon, C. Ruiz and C. B. Allen, "Finite E22lement Analysis of a Tapered Laminate", Composites Science and Technology, Vol. 51, pp. 429-440, 1994.

[5] J. Daoust and S. V. Hoa., "Parameters Affecting Failure of Tapered Laminates Under Static Loading Conditions", Polymer Composites, Vol. 10, No. 5, pp. 374-383, 1989.

[6] Raymond K.Cannon and Paul A. Lagace, "The Effects of Ply Dropoffs on the Tensile Behavior of Graphite/Epoxy Laminates", TELAC Report 87-12, MIT, Cambridge, MA, pp. 242-252, 1987.

[7] John C. Fish and Sung W. Lee, "Tensile Strength of Tapered Composite Structures", Proceedings of the AIAA/ASME/ASCE/ AHS/ASC 29th Structures, Structural Dynamics, and Materials Conference, Part 1 (VA), AIAA, Washington DC, pp. 324-333, 1988, (AIAA Paper 88-2252).

[8] Michael R. Wisnom, M. I. Jones and Weicheng Cui, "Failure of Tapered Composites Under Static and Fatigue Tension Loading", AIAA Journal, Vol. 33, No. 5, pp. 911-918, 1995.

[9] Carlos G. Dávila and Eric R. Johnson, "Analysis of Delamination Initiation in Postbuckled Dropped-ply Laminates", AIAA Journal, Vol. 31, No. 4, pp. 721-727, 1993.

[10] R. Y. Kim and S. R. Soni, "Experimental and Analytical studies On the Onset of Delamination in Laminated Composites", Journal of Composites, Vol.18, pp. 70-80, 1984.

[11] JAMES M. Curry, Eric R. Johnson and James H. Starnes, "Effect of Dropped Plies on the Strength of Graphite-Epoxy Laminates", Proceedings of the AIAA/ASME/ASCE/ AHS/ASC 28th Structures, Structural Dynamics, and Materials Conference, Monterey, CA, pp. 449-456, 1987, (AIAA Paper 87-0874).

[12] D. S. Cairns, J. F. Mandell, M. E. Scott and J. Z. Maccagnano, "Design and Manufacturing Considerations for Ply Drops in Composite Structures", Composites, Part B 30, pp. 523-534, 1999.

[13] Anthony D. Botting, Anthony J. Vizzini and Sung W. Lee, "Effect of Ply-Drop Configuration on Delamination Strength of Tapered Composite Structures", AIAA Journal, Vol. 34, No. 8, pp. 1650-1656, 1996.

[14] B.R. Trethewey, J.W. Gillespie and D.J. Wilkins, "Interlaminar Performance of Tapered Composite Laminates", Proceedings of the American Society for Composites, 5th Technical Conference, East Lansing, Michigan, pp. 361-372, 1990.

[15] O. O. Ochoa, W. S. Chan, "Tapered Laminates: A study on Delamination Characterization", Journal of Composite Materials, Composite Structure Design and Analysis, pp. 633-641, 1991.

[16] P99hilippe M. Manne and Stephen W. Tsai, "Design Optimization of Composite Plates: Part II-Structural Optimization by Ply drop Tapering", Journal of Composite Materials, Vol. 32, No. 6, pp. 572-598, 1998.

[17] Jianxin Tao and C. T. Sun, "Influence of Ply Orientation on Delamination in Composite Laminates", Journal of Composite Materials, Vol. 32, No. 21, pp. 1933-1949, 1998.

[18] Weicheng Cui, Michael R. Wisnom and Mike Jones, "New model to Predict Static strength of Tapered Laminates", Composites, Vol. 26, No. 2, pp. 141-146, 1995.

[19] E. A. Aramanios, and L. Parnas, "Delamination Analysis of Tapered Laminated Composites Under Tensile Loading", Composite Materials: Fatigue and Fracture, ASTM STP 1110, American Society for Testing and Materials, PA, pp. 340-358, 1991.

[20] C. M. L. Wu, and J. P. H. Webber, "Analysis of Tapered (in steps) Laminated Plates Under Uniform Inplane Load", Composite Structures, Vol. 5, pp. 87-100, 1986.

[21] J. M. Whitney and R. J. Nuismer, "Stress Fracture Criteria for Laminated Composites Containing Stress Concentrations", Journal of Composite Materials, Vol. 8, pp. 253-265, 1974.

[22] R. Y. Kim and S. R. Soni, "Experimental and Analytical studies On the Onset of Delamination in Laminated Composites", Journal of Composites, Vol.18, pp. 70-80, 1984.

[23] S. V. Hoa, J. Daoust, B. L. Du and T. Vu-Khanh, "Interlaminar Stresses in Tapered Laminates", Polymer Composites, Vol. 9, pp.227-244, 1988.

[24] M. R. Wisnom, "Prediction of Delamination in Tpaered Unidirectional Glass Fiber-Epoxy with Dropped Plies under Ststic Tension and Compression", AGARD CP 530, Vol. 25, pp. 1-7, 1992.

[25] A.D. Botting, A.J. Vizzini and S.W. Lee, "The Effect of Ply drop Configuration on the Delamination Strength of Tapered Composite Structures", in Proceedings of AIAA/ASME/ASCE/ AHS 33rd Structures, Structural Dynamics and Materials Conference, Dallas, Texas, pp. 40-47, 1992, (AIAA Paper 92-2227).

[26] Anthony J. Vizzini, "Strength of Laminated Composites with Internal Discontinuities Parallel to the Applied load", AIAA Journal, Vol. 30, No. 6, pp. 1515-1520, 1992.

[27] B.R. Trethewey, J.W. Gillespie and D.J. Wilkins, "Interlaminar Performance of Tapered Composite Laminates", Proceedings of the American Society for Composites, 5th Technical Conference, East Lansing, Michigan, pp. 361-372, 1990.

[28] Weicheng Cui, Michael R. Wisnom and Mike Jones, "An Experimental and Analytical Study of Delamination of 3Unidirectional Specimens with Cut central Plies", Journal of Reinforced Plastics and Composites, Vol. 13, pp. 722-739, 1994.

[29] M. R. Wisnom, "Delamination in Tapered Unidirectional Glass Fibre-Epoxy Under Static Tension Loading", Proceedings of the AIAA/ASME/ASCE/AHS/ASC 32nd Structures, Structural Dynamics and Materials Conference, Part 2 (Baltimore, MD), AIAA, Washington, DC, pp. 1162-1172, April 1991 (AIAA Paper 91-1142-CP).

[30] John C. Fish and Sung W. Lee, "Delamination of Tapered Composite Structures", Engineering Fracture Mechanics, Vol. 34, No. 1, pp. 43-54, 1989.

[31] Som R. Soni and Ran Y. Kim, "Delamination of Composite Laminates Stimulated by Interlaminar Shear", Composite Materials: Testing and design (7^{th} Conference), ASTM STP 893, pp.286-307, 1986.

[32] T. K. O'Brien, "Characterization of Delamination onset and Growth in a Composite Laminate", Damage in Composite Materials, ASTM STP 775, American Society for Testing and Materials, pp. 140-167, 1982.

[33] R. J. Nuismer and J. M. Whitney, "Uniaxial Failure of Composite Laminates Containing Stress Concentrations", Fracture Mechanics of Composites, ASTM STP 593, American Society for Testing and Materials, pp. 117-142, 1975.

[34] R. Byron Pipes and N. J. Pagano, "Interlaminar Stresses in Composite Laminates Under Uniform Axial Extension", Journal of Composite Materials, Vol. 4, pp. 538-549, 1970.

[35] John C. Brewer and Paul A. Lagace, "Interlaminar Shear in Laminated Composites Under Generalized Plane Stress", Journal of Composite Materials, Vol. 22, pp. 1141-1155, 1988.

[36] A. H. Puppo and H. A. Evensen, "Interlaminar Shear in Laminated Composites Under Generalized Plane Stress", Journal of Composite Materials, Vol. 4, pp. 204-220, 1970.

[37] Stephen W. Tsai and Edward M. Wu, "A General Theory of Strength for Anisotropic Materials", Journal of Composite Materials, Vol. 5, pp. 58-80, 1971.

[38] L. J. Hart-Smith, "Some Observations About Test Specimens and Structural Analysis for Fibrous Composites", Composite Materials: Testing and Design (9th Volume), ASTM STP 1059, American Society for Testing and Materials, pp. 86-120, 1990.

[39] ASTM D3039-76, "Standard Test method for Tensile Properties of Fiber Composites", Annual Book of ASTM Standards, Vol 08.01, pp. 118-122, 1976.

[40] AITM 1.0002, Airbus Industrie Test Method, "Determination of In-Plane Shear Properties for Fiber Reinforced Plastics", AITM, pp.1-10, 1994.

[41] PrEN 2563, "Unidirectional Laminates Carbon-Thermosetting Resin Test Method – Determination of Apparent Interlaminar Shear Strength", A.E.C.M.A. Standard, pp. 1-10, 1989.

[42] ASTM D618, "Standard Methods of Conditioning Plastics and Electrical Insulating Materials for Testing", Annual Book of ASTM Standards, Vol 10.02, pp. 94-96, 1981.

[43] J.C. Fish, and S. W. Lee, "Edge Effects in Tapered Composite Structures," Proceedings of the AHS National Technical Specialists Meeting on advanced Rotorcraft Structures, Williamsburg, V.A., pp.1-16, 1988.

[44] Antonio Miravete, "Strain and Stress Analysis in Tapered Laminated Composite Structures", Composite Structures, Vol. 16, pp. 65-84, 1990.

[45] M. R. Wisnom and J. W. Atkinson, "Reduction in Tensile and Flexural Strength of Uni-Directional Glass Fiber-Epoxy with Increasing Specimen Size", Composite Structures, Vol. 38, No. 1-4, pp. 405-411, 1997.

[46] Micheal R. Wisnom, Rachael Dixon and Graham Hill, "Delamination in Axisymmetrically Tapered Composites Loaded in Tension", Composite Structures, Vol. 35, pp. 309-332, 1996.

[47] G. B. Murri, S. A. Salpekar and T. K. O'Brien, "Fatigue Delamination Onset Prediction in Unidirectional Laminates." Composite Materials: Fatigue and Fracture (3rd Volume), ASTM STP 1110, American Society for Testing and Materials, pp. 312-339, 1991.

[48] Engineered Materials handbook, 2nd Edition, Vol. 1, "Composites", ASM International, Ohio, US, pp. 783-785, 1988.

[49] O. O. Ochoa and J. N. Reddy, " Finite Element Analysis of Composite Laminates", Solid Mechanics and Its Applications, pp. 37-41, 1992.

[50] S. W. Tsai, "A Survey of Macroscopic Failure Criteria for Composite Materials", Technical Report, AFWAL-TR-84-4025.

[51] R. Y. Kim and S. R. Soni, "Experimental and Analytical Studies on the Onset of Delamination in Laminated Composites", Journal of Composite Materials, Vol. 18, pp. 70-80, 1984.

[52] J. C. Brewer and P. A. Lagace, "Quadratic Stress Criterion for Initiation of Delamination", Journal of Composite Materials, Vol. 8, pp. 253-265, 1974.

[53] B. R. Trethewey, J. W. Gillespie, and D. J. Wilkins, "Delamination in Thickness Tapered Composite Laminates", Journal of Engineering Materials and Technology, Vol. 115, pp. 193-199, 1993.

[54] W. S. Chan, C. Rogers, J. D. Cronkhite and J. Martin, "Delamination Control of Composite Rotor Hubs," Journal of the American Helicopter Society, Vol. 31, No. 3, pp. 60-69, 1986.

[55] J. A. Vizzini, S. W. Lee, "Damage analysis of Composite Tapered Beams", Journal of the American Helicopter Society, Vol. 29, pp. 1-28, 1985.

[56] J. Rhim, J. A. Vizzini, "Analysis of Interlaminar Stresses in an Internally-Dropped Ply Region", Textile Composites and Characterization, Vol. 5, pp. 652-661, 1997.

[57] A. J. Vizzini, "Influence of Realistic Ply Drop Geometries on Interlaminar Stresses in Tapered Laminates", Composite Materials: Fatigue and Fracture (5^{th} Volume), ASTM STP 1230, American Society for Testing and Materials, pp. 467-485, 1995.

[58] J. C. Fish and A. J. Vizzini, "Delamination of Ply Drop Configurations", Composite Materials: Testing and Design (11th Volume), ASTM STP 1206, American Society for Testing and Materials, pp. 323-332, 1993

[59] J. D. Whitcomb and I. S. Raju, "Analysis of Interlaminar Stresses in Thick Composite Laminates With and Without Edge Delamination", Delamination and Debonding of Materials, ASTM STP 876, American Society for Testing and Materials, pp.69-94, 1985.

APPENDIX A

TRANSFORMATION OF STRESS COMPONENTS IN 3-D SPACE

Finite element analysis of the tapered laminate requires transformation of cartesian tensors of second order. The stresses taken from the solution of the finite element analysis are in global coordinate system and are needed to be transformed to element coordinate system. As shown in Figure A.1, the elements at the tapered region of the finite element model have a rotation of 5.71° about y axis.

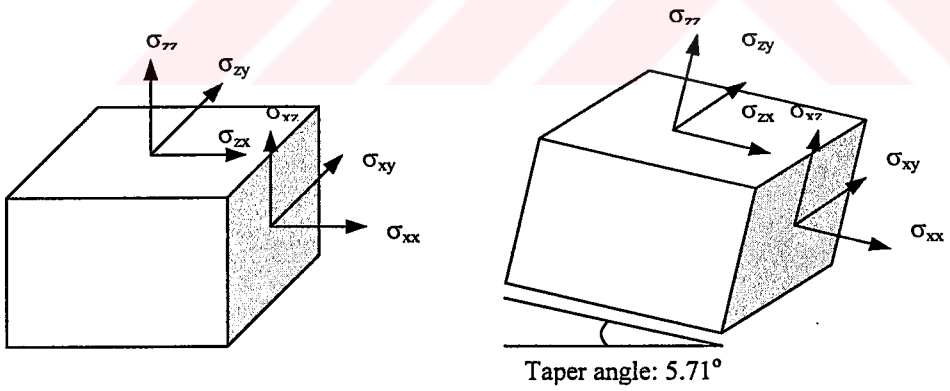

Figure A.1: Rotation of Element Stress Resultants

Transformation of the stress resultants were accomplished by rotation of the global coordinate system to element coordinate system. In Figure A.2, global coordinates x, y, z are rotated about y axis and new element coordinates are obtained as x', y', z'. Rotation angle is represented by θ, where θ is the taper angle 5.71°.

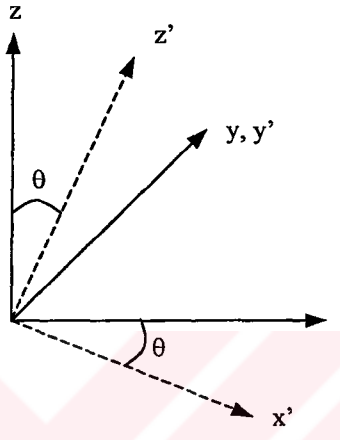

Figure A.2: Rotation of Coordinates

Without giving the derivation of this transformation, the transformation matrix is obtained as:

$$[T]=\begin{bmatrix} m^2 & 0 & n^2 & 0 & 0 & -2mn \\ 0 & 1 & 0 & 0 & 0 & 0 \\ n^2 & 0 & m^2 & 0 & 0 & 2mn \\ 0 & 0 & 0 & m & -n & 0 \\ 0 & 0 & 0 & n & m & 0 \\ mn & 0 & -mn & 0 & 0 & m^2-n^2 \end{bmatrix}$$

where,

m=Cos(θ) and n=Sin(θ).

The stress resultants were transformed by using the transformation matrix obtained and the expression is given below. Primes refer to the transformed stresses.

$$\begin{bmatrix} \sigma'_{xx} \\ \sigma'_{yy} \\ \sigma'_{zz} \\ \sigma'_{xy} \\ \sigma'_{yz} \\ \sigma'_{zx} \end{bmatrix} = \begin{bmatrix} m^2 & 0 & n^2 & 0 & 0 & -2mn \\ 0 & 1 & 0 & 0 & 0 & 0 \\ n^2 & 0 & m^2 & 0 & 0 & 2mn \\ 0 & 0 & 0 & m & -n & 0 \\ 0 & 0 & 0 & n & m & 0 \\ mn & 0 & -mn & 0 & 0 & m^2 - n^2 \end{bmatrix} \cdot \begin{bmatrix} \sigma_{xx} \\ \sigma_{yy} \\ \sigma_{zz} \\ \sigma_{xy} \\ \sigma_{yz} \\ \sigma_{zx} \end{bmatrix}$$

APPENDIX B

DELAMINATION FAILURE CRITERION

Delamination is an out-of-plane failure mode and out-of-plane stresses are the primary contributors to any delamination strength criteria. Therefore Tsai-Wu failure criterion may be modified and developed to predict the delamination strength of composite structures.

The basic assumption of the Tsai-Wu strength criterion is that there exists a surface in the stress-space which can be expressed in scalar form as

$$F_i \sigma_i + F_{ij} \sigma_i \sigma_j = 1$$

Where F_i and F_{ij} (i,j = 1, 2, 3.....,6) are strength tensors and σ_i and σ_j are stress tensors equivalent to σ_{xx}, σ_{yy}, σ_{zz},..., σ_{xy}, respectively. If delamination is considered an out-of-plane failure mode, independent of the inplane stress state, the inplane stresses can be uncoupled from the out-of-plane stresses, reducing the failure criteria to

$$F_3 \sigma_3 + F_4 \sigma_4 + F_5 \sigma_5 + F_{33} \sigma_3^2 + 2 F_{34} \sigma_3 \sigma_4 + 2 F_{35} \sigma_3 \sigma_5 + F_{44} \sigma_4^2 + 2 F_{45} \sigma_4 \sigma_5 + F_{55} \sigma_5^2 = 1$$

Furthermore, if strength is considered to be independent of the sign of the shear stress, all components containing a linear stress term may be excluded, leaving

$$F_3\,\sigma_3 + F_{33}\,\sigma_3^2 + F_{44}\,\sigma_4^2 + F_{55}\,\sigma_5^2 = 1$$

Finally if the two out of plane shear strengths are assumed to be equal (F_{44}=F_{55}), the failure criterion can be expressed as

$$F_3\,\sigma_3 + F_{33}\,\sigma_3^2 + F_{44}\,[\,\sigma_4^2 + \sigma_5^2\,] = 1$$

The strength parameters can be obtained in terms of the out-of-plane strengths. Thus, the modified Tsai-Wu failure criterion for predicting delamination strength can be represented by

$$\frac{ZC - ZT}{ZC * ZT}\sigma_{ZZ} + \frac{1}{ZC * ZT}\sigma_{ZZ}^2 + \frac{1}{S}\left[\sigma_{YZ}^2 + \sigma_{ZX}^2\right] = 1$$

where ZT, ZC and S are the through the thickness tensile, compressive and shear strengths, respectively.

APPENDIX C

PHOTOMICROGRAPHS OF SPECIMENS

- Magnification factor is 50x, if not specified.
- The actual length of the scale is 10/Magnification Factor (mm).

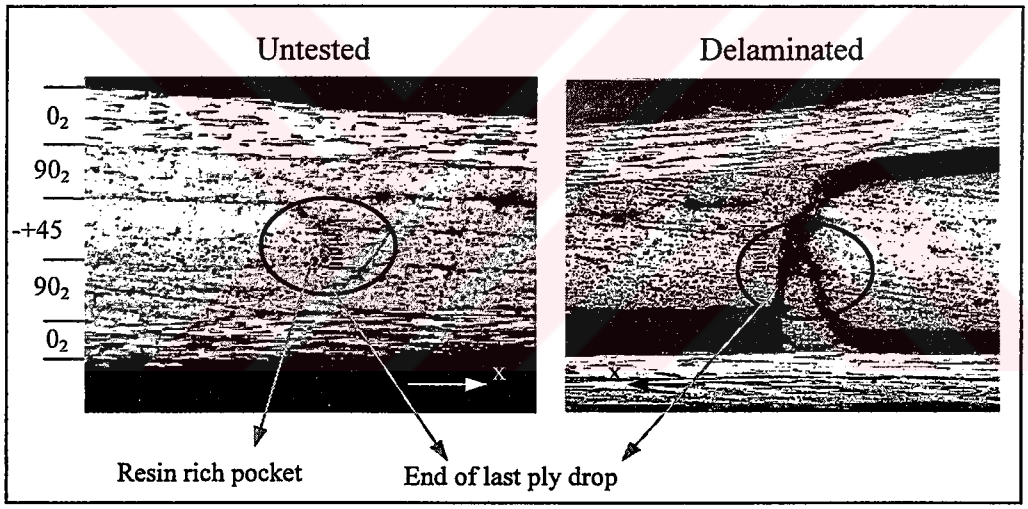

Figure C.1: Photomicrographs of configuration TL1

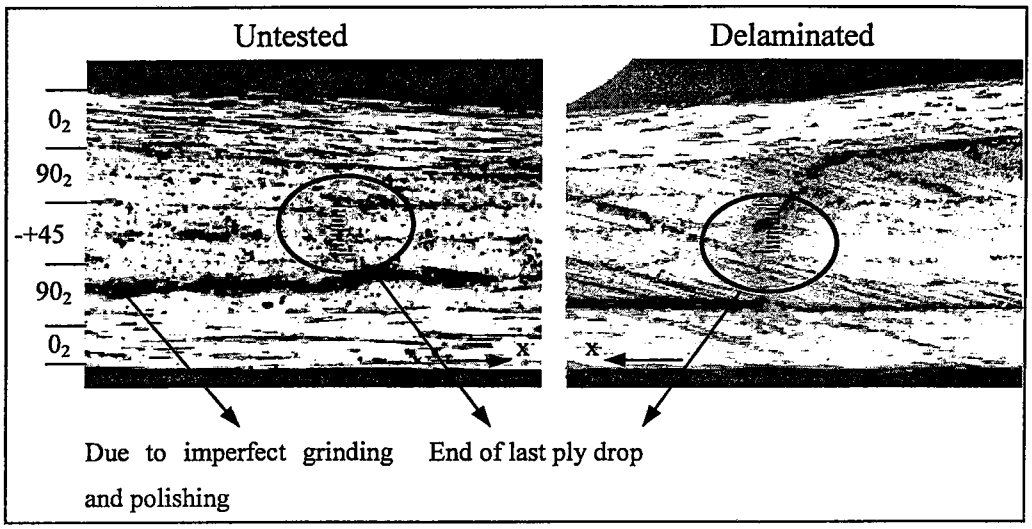

Figure C.2: Photomicrographs of configuration TL2

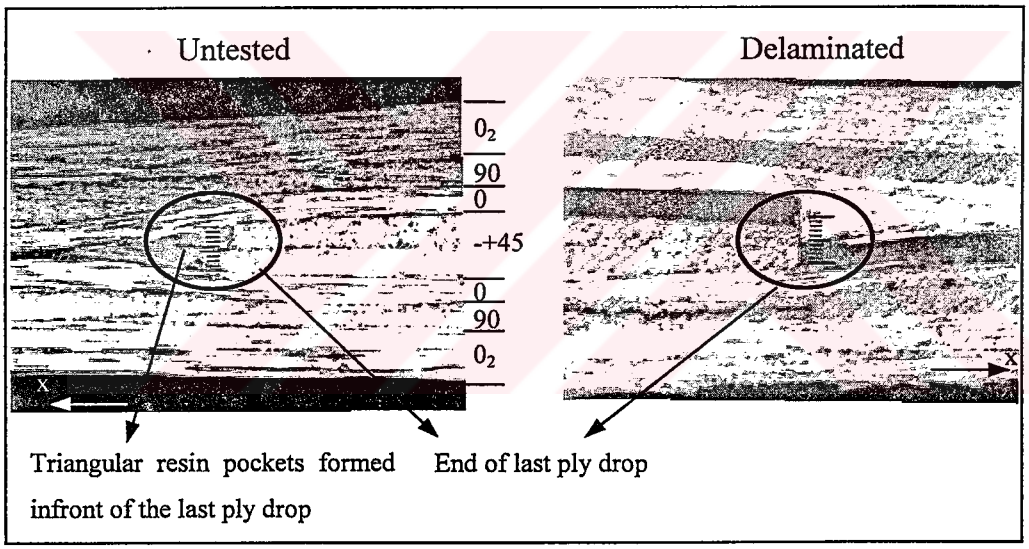

Figure C.3: Photomicrographs of configuration TL3

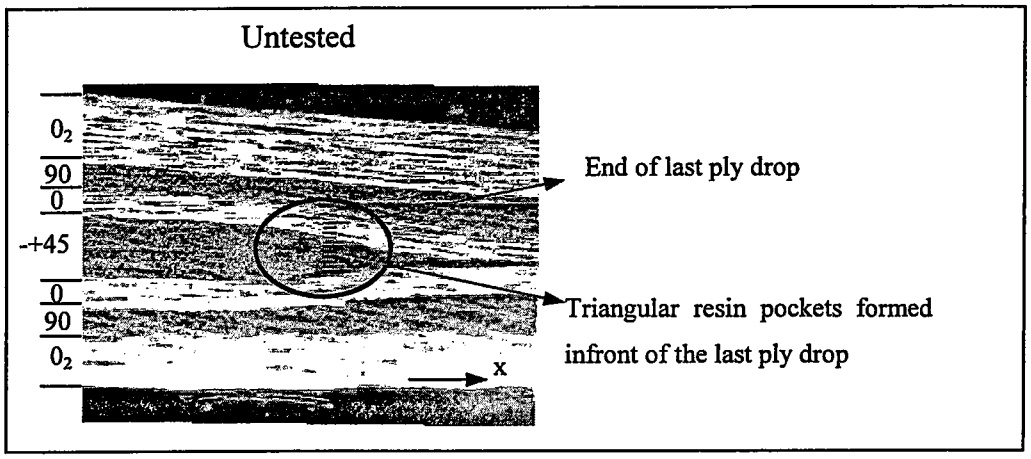

Figure C.4: Photomicrographs of configuration TL4

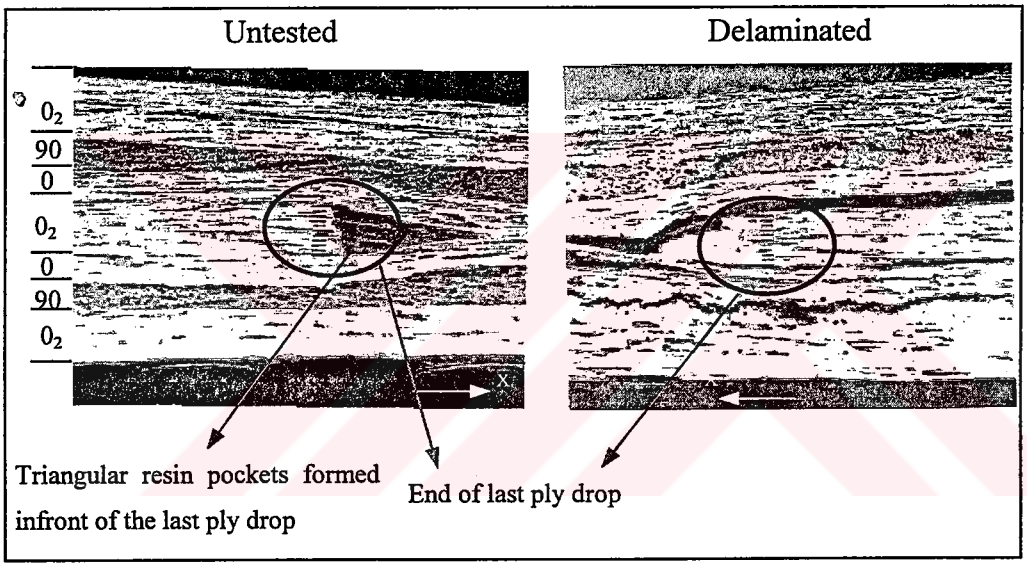

Figure C.5: Photomicrographs of configuration TL5

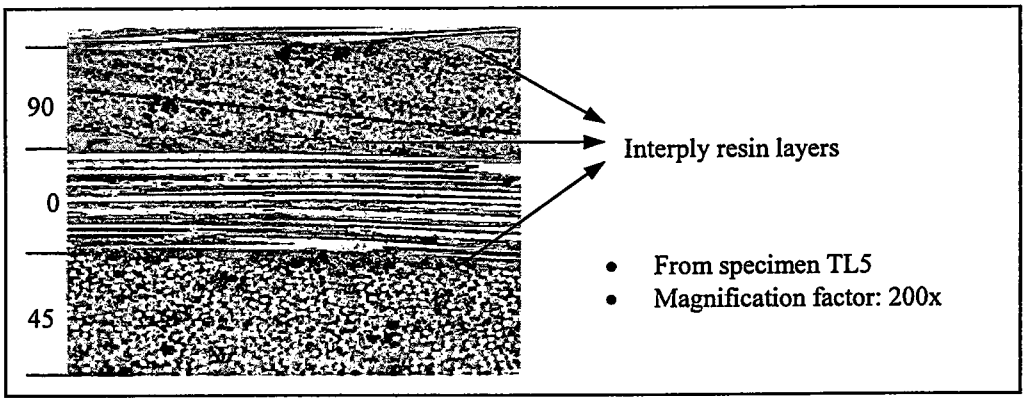

Figure C.6: Interply resin layers in configuration TL5

APPENDIX D

TEST EQUIPMENTS AND TEST SPECIMENS

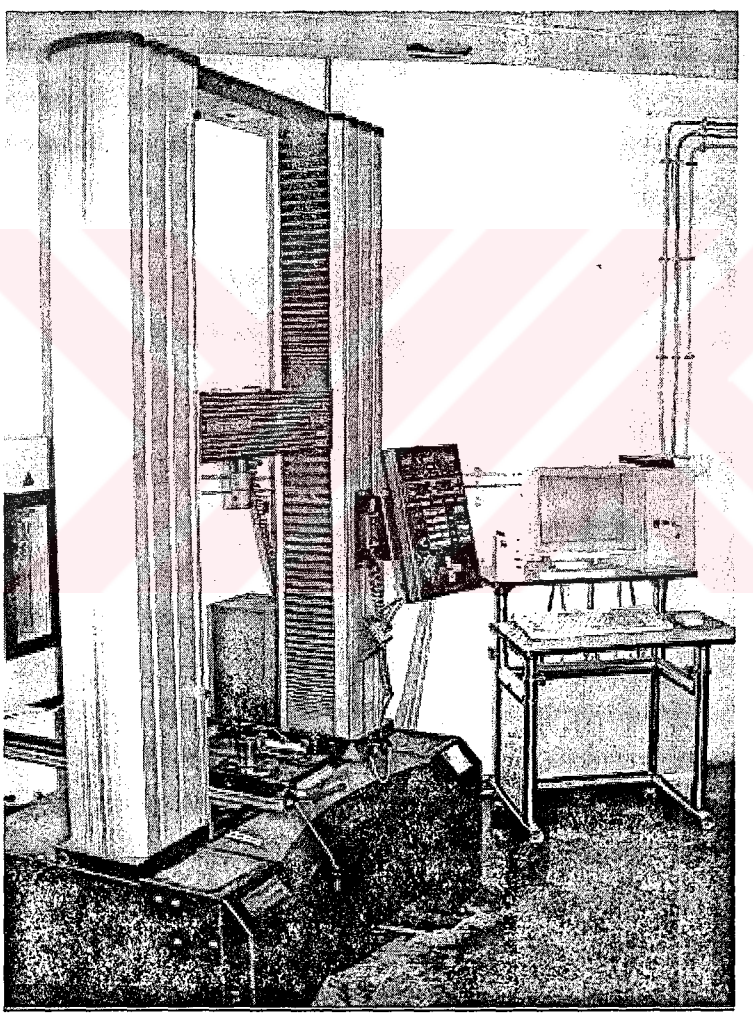

Figure D.1: Instron 4481 Universal Tensile Test Machine

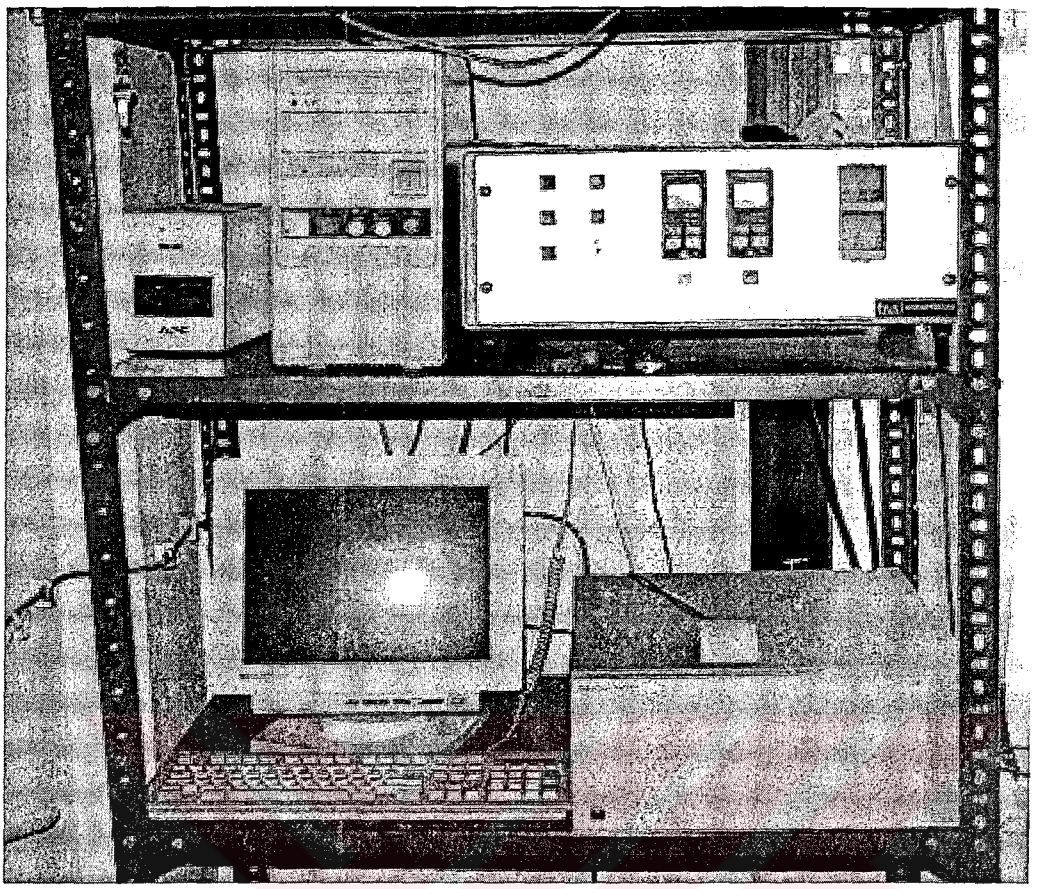

Figure D.2: HP 7500B Data Acquisition System Used for Strain-gage Measurements

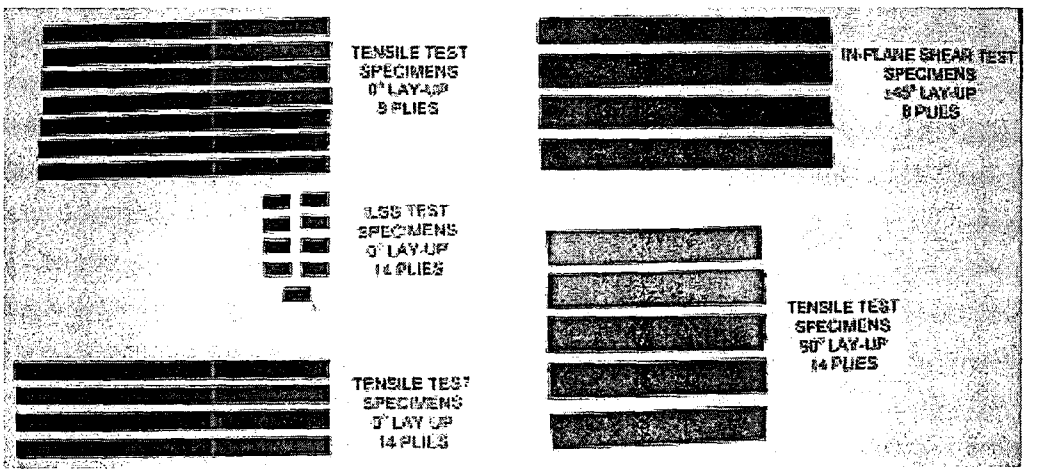

Figure D.3: Specimens Used for Material Property Determination

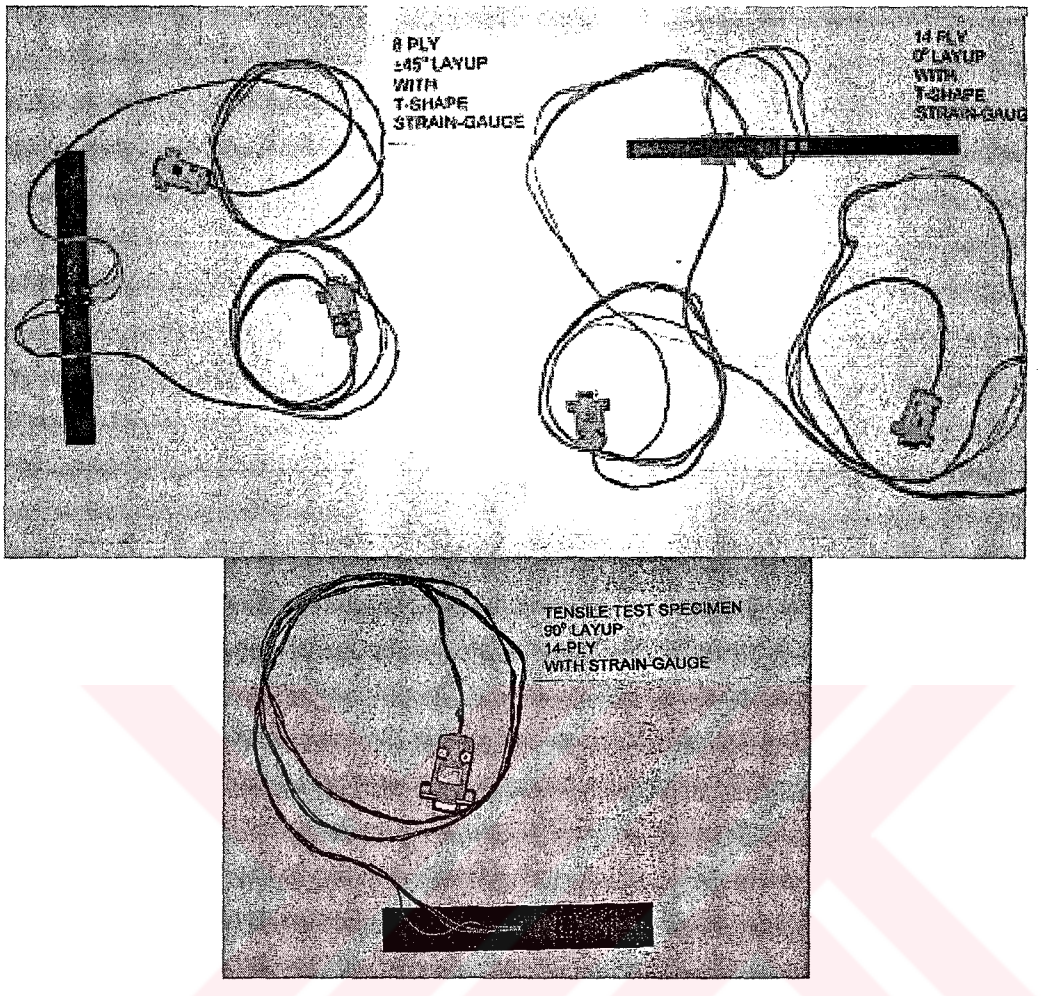

Figure D.4: Specimens with Strain-gages for Material Property Determination

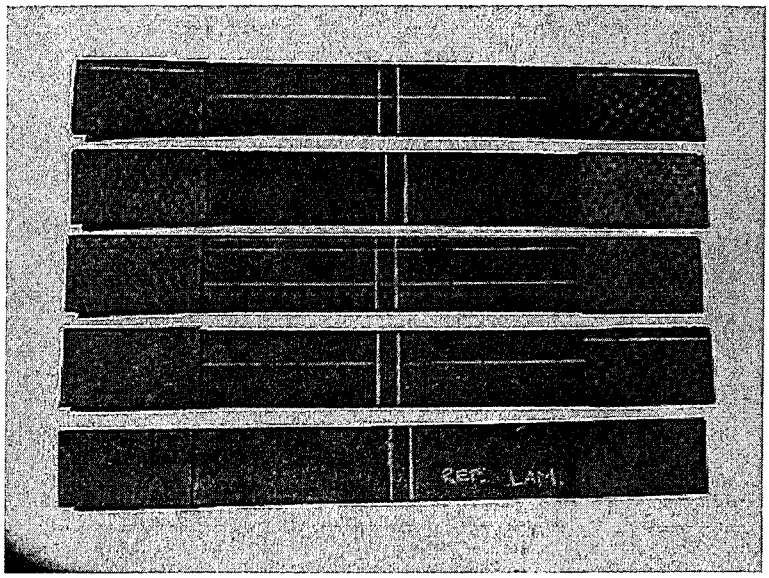

Figure D.5: RL-1 Flat Specimens

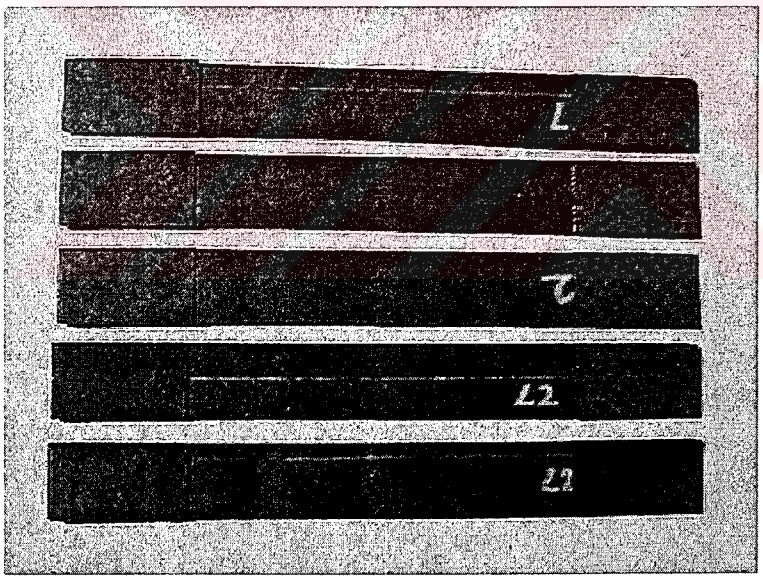

Figure D.6: TL-1 Flat Specimens

APPENDIX E

SAMPLE OUTPUTS FROM INSTRON TESTING MACHINE

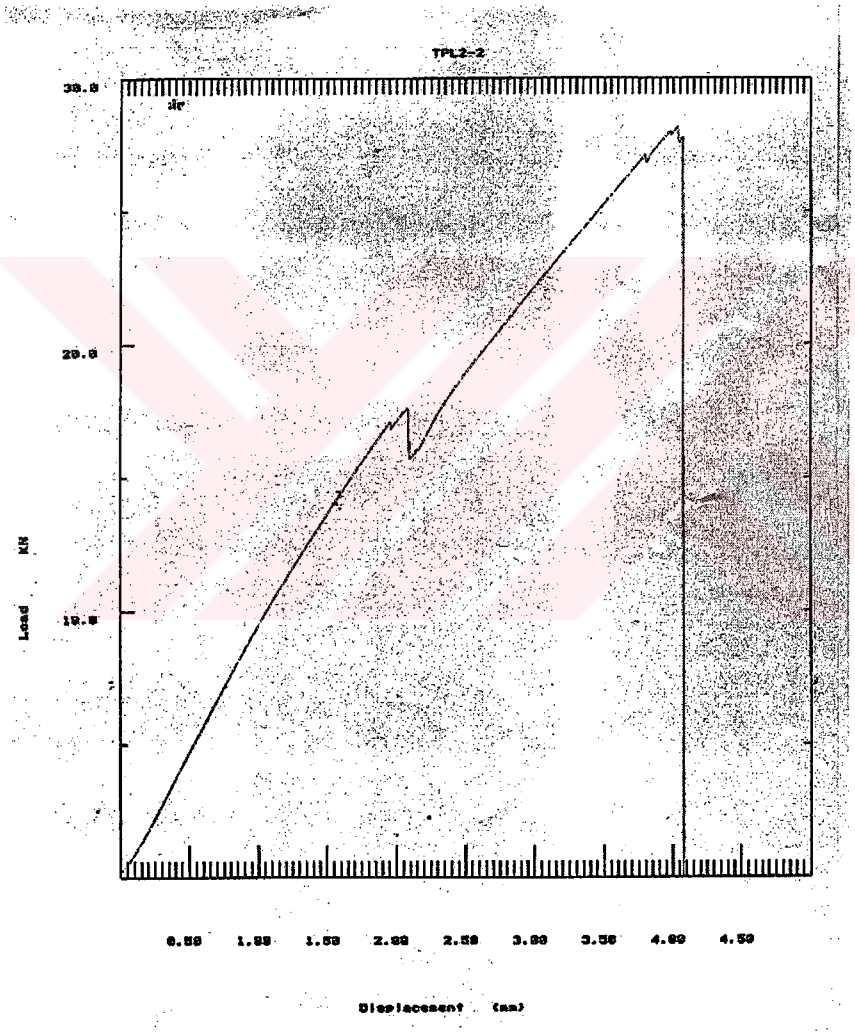

Figure E.1: Load vs. Displacement Curve of Specimen TL1-3

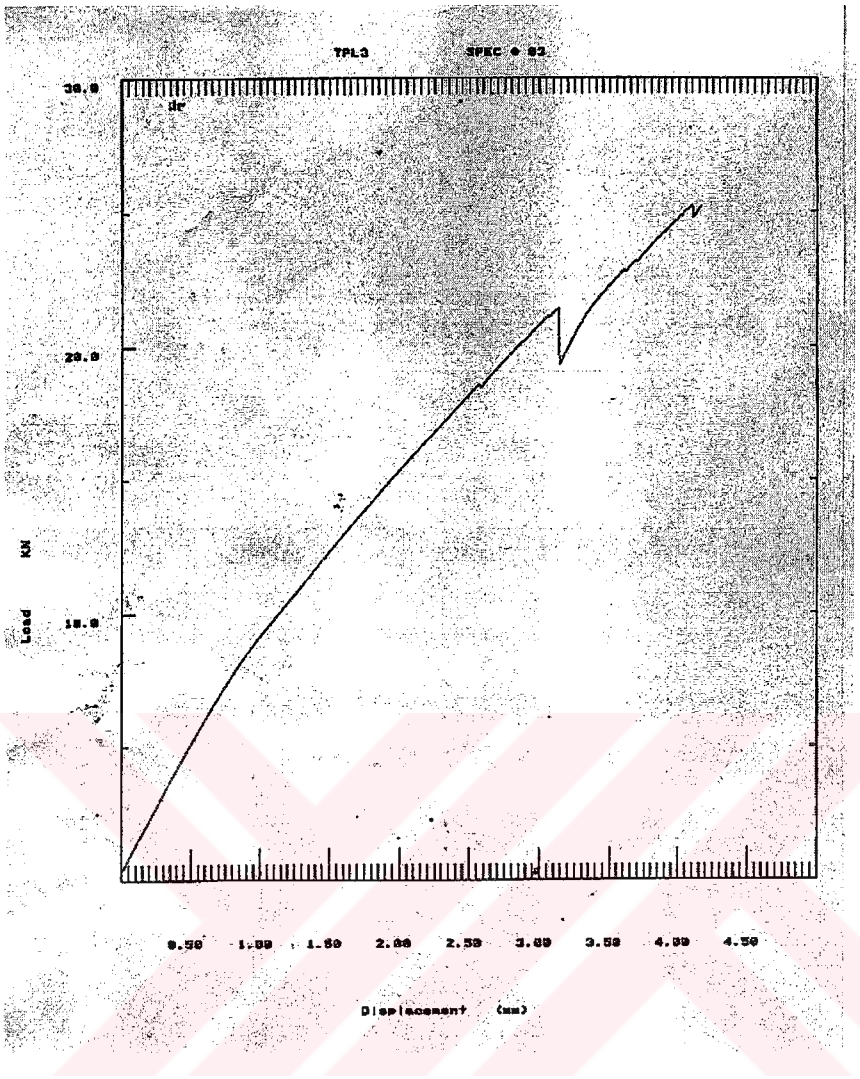

Figure E.1: Load vs. Displacement Curve of Specimen TL2-3